AN ABSTRACT OF THE DISSERTATION OF

Jeffrey Barber for the degree of Doctor of Philosophy in Chemistry presented on April 28, 2003.

Title: High Resolution Spectroscopic Studies of $^{32}S^{16}O_3$ and $^{34}S^{16}O_3$.

Redacted for Privacy

Abstract approved: _____

Joseph W. Nibler

The two sulfur isotopomers of sulfur trioxide, $^{32}S^{16}O_3$ and $^{34}S^{16}O_3$, have been studied via high resolution infrared and Coherent anti-Stokes Raman (CARS) spectroscopy. The ν_1 symmetric SO stretching Q-branches observed by the latter are quite different, being especially complex for $^{32}S^{16}O_3$. Understanding this band structure required analysis of infrared-active hot bands originating from the ν_2 and ν_4 bending mode levels to the states $2\nu_2$ (l=0), $\nu_2 + \nu_4$ (l=±1), and $2\nu_4$ (l=0, ±2). These upper states are strongly coupled to the ν_1 symmetric stretching mode levels via Fermi resonance and indirect Coriolis interactions, causing the CARS spectra of these two molecules to be highly perturbed and quite different in appearance.

From the analysis of 11 000 $^{32}S^{16}O_3$ and 7000 $^{34}S^{16}O_3$ infrared transitions, accurate rovibrational constants have been determined for these mixed states, leading to respective values for ν_1, α_1^B, and α_1^C of 1064.924(11), 0.000 840 93(64), and 0.000 418 19(58) cm^{-1} for $^{32}S^{16}O_3$ and 1064.920(84), 0.000 834 5(54), and 0.000 410(11) cm^{-1} for $^{34}S^{16}O_3$. These parameters reproduce the respective CARS spectra very well and permit determination of accurate rotational constants for the equilibrium structure of SO_3. The results are B_e values of 0.349 763 96(64) and 0.349 760 61(334) cm^{-1} and r_e values of 141.734 027(130) and 141.734 704(677) pm for $^{32}S^{16}O_3$ and $^{34}S^{16}O_3$ respectively, values that agree within the uncertainties of the measurements. The structure of SO_3 is thus one of the best determined configurations of any nonlinear polyatomic molecules.

As part of the analysis, the infrared-active ν_2 and ν_4 bending modes were found to be strongly coupled via Coriolis and *l*-resonance interactions. These interactions cause noticeable wavenumber and intensity perturbations in the ν_2, ν_4 spectra. Although the emphasis of this work was to fit the transitions, an accompanying analysis of the intensities yielded an average value of $\pm 0.62(8)$ for the dipole derivative ratio $(\partial\mu^x/\partial Q_{4x})/(\partial\mu^z/\partial Q_2)$ and a positive sign for the product of this ratio with the ζ^y_{24} Coriolis constant, for which experiment gives $\pm 0.5940(15)$. The sign of individual terms are not determinable from experiment but *ab initio* calculations were done which indicate that the signs of $\partial\mu^x/\partial Q_{4x}$ and $\partial\mu^z/\partial Q_2$ are both positive and hence ζ^y_{24} is also positive.

High Resolution Spectroscopic Studies of $^{32}S^{16}O_3$ and $^{34}S^{16}O_3$

by
Jeffrey Barber

A DISSERTATION

submitted to

Oregon State University

in partial fulfillment of
the requirements for the
degree of

Doctor of Philosophy

Presented April 28, 2003

Commencement June 2003

Doctor of Philosophy dissertation of Jeffrey Barber presented on April 28, 2003

APPROVED:

Redacted for Privacy

Major Professor, representing Chemistry

Redacted for Privacy

Chair of the Department of Chemistry

Redacted for Privacy

Dean of the Graduate School

I understand that my dissertation will become part of the permanent collection of Oregon State University libraries. My signature below authorizes release of my dissertation to any reader upon request.

Redacted for Privacy

Jeffrey Barber, Author

ACKNOWLEDGEMENTS

My first acknowledgement goes to Joseph Nibler. Joe, I can't begin to express how much I have enjoyed working for you for these past years. Who would have ever thought that I would end up learning how to water-ski and wakeboard! I appreciate how you have managed to take the right approach with me and my frustrations, and didn't fire me for all those times you caught me goofing off either on the internet or playing games. I have truly become a better thinker thanks to your way of solving a problem and thinking about situations. I am privileged to have worked under your tutelage.

To the members of the Nibler group, you are also a big part of what I've been able to accomplish at OSU. Engs, you have taught me not only spectroscopy, but also the importance of tact and professionalism. Tony, what would my time here be without Chang's trips with Ben, wrestling PPVs, and drinking at the Junction? Stéphanie, you were a joy to work with. Thanks for not taking the French jokes too personally. Last, but most certainly not least, I must thank Nicu. You have taught me to live and to appreciate every day that goes by. I'll never forget how you always had a smile no matter how bad you were feeling. I hope I get to see you again some day and hear more stories about the gypsies.

Thanks also to Art, Alfons, Tom, and Bob. Art and Alfons, I appreciate all your help, especially the letters of recommendation to Los Alamos. It's good to have such big names on your résumé. Tom and Bob, thanks for all of your help as well, as I wouldn't be anywhere if it wasn't for all of the data that I've been analyzing for the last four years. I'm looking forward to being able to continue our working relationship in the future. Feel free to ship me some beautiful spectra anytime!

Thanks also to my committee members, Glenn Evans, Mike Schuyler, Doug Keszler, and John Wager. You have taken a big role in my studies here at OSU, from steering me to working with Joe, to giving me opportunities for research, to not drilling me too badly in my orals.

An important group I need to thank is my family. It hasn't been easy for me to be so far away from home. Everyone has been supportive, and kept my head above water financially. I wish that I could be home more often and see you. It's good to know that I have anything I need just a phone call away. I hope that I have made you all proud with my accomplishments and can continue to be a big part of everyone's lives, no matter where I am in this world.

Others I wish to thank are my friends from OSU, like Ben and Sara, Jennifer, Tom, George, Rebecca, Korf, and Sundaram, among others, for keeping me sane, my tag-team partner Broz for Killer B plaguings and Christmas cards, and Houser for keeping in touch over the years and letting us crash at his place in Meadville. I would also like to thank the following corporate sponsors: Rolling Rock, The Savage Nation, The Simpsons, Fox News, Towelie, Hot Pockets, Lipton, Principal Onyx Blackman, Togo's #9 combo with the plastic drink cups, and The Cantina.

Finally, I have to thank Megan. You have changed my life for the better. You have been both the needed distraction and the needed reminder in regards to work. It's nice to come home to a smile and a warm meal. I love you and appreciate everything that you do for me. Start packing for Los Alamos.

CONTRIBUTION OF AUTHORS

Engelene t.H. Chrysostom collected the CARS spectra of SO_3 and assisted in the analysis of the CARS and FTIR spectra. Tony Masiello assisted in the collection and analysis of the FTIR spectra and the synthesis of SO_3. Joseph W. Nibler contributed to the writing of all chapters and the analysis of the spectra. Arthur Maki assisted in the writing of Chapters 2, 3, and 4 and the analysis of the FTIR spectra. Alfons Weber contributed to the writing of Chapters 2, 3, and 4, the analysis of the FTIR spectra, and provided the sample of ^{34}S. Thomas A. Blake assisted in the collection and analysis of the FTIR spectra. Robert L. Sams assisted in the collection of the FTIR spectra.

TABLE OF CONTENTS

TABLE OF CONTENTS (Continued)

TABLE OF CONTENTS (Continued)

LIST OF FIGURES

LIST OF FIGURES (Continued)

LIST OF TABLES

HIGH RESOLUTION SPECTROSCOPIC STUDIES OF $^{32}S^{16}O_3$ AND $^{34}S^{16}O_3$

1. INTRODUCTION

1.1. HISTORICAL BACKGROUND

Sulfur trioxide, SO_3, is an important and interesting molecule. Combustion of sulfur in the presence of air or pure oxygen leads mainly to the formation of sulfur dioxide, SO_2. However, further oxidation in the presence of a catalyst, such as platinum (Contact Process), enables the formation of SO_3. Once present, it reacts readily with water to form sulfuric acid, one of the most important chemicals in the world, with many industrial uses, and environmentally, a major contributor to acid rain. SO_3 is also of astronomical interest since it is believed to be present in the atmosphere of Venus.

The spectroscopy of sulfur trioxide has been the focus of our research group for the past several years. Several properties of sulfur trioxide make this an outstanding molecule for spectroscopic experimentation. It is a planar, oblate symmetric top with D_{3h} symmetry, leading to a simplified spectrum as a result of its nuclear spin statistics. Due to its extreme reactivity, the spectroscopy of SO_3 was surprisingly incomplete. Additionally, no experimental data involving the various ^{34}S and ^{18}O isotopomers was available. Finally, the best previously known Raman spectrum of the ν_1 symmetric stretching mode of SO_3 was performed at 8 cm^{-1} resolution (*1*), whereas our CARS (coherent anti-Stokes Raman scattering) system at Oregon State University is able to achieve a resolution of 0.001 cm^{-1} (*2*). All of these factors combined to spur our interest in this molecule.

1.2. THEORY – VIBRATION-ROTATION ENERGY LEVELS OF SO_3

1.2.1. Initial development of the Hamiltonian

The following theoretical background is a summary of the work found in References (*3-7*). In general, the properties of a molecule such as SO_3 are determined by the wavefunction, which is a function of both time and the coordinates of the electrons and nuclei. It is possible to separate the time-dependent and time-independent parts of the wavefunction from one another. High resolution vibrational-rotational spectroscopy, be it infrared or Raman, is a study of transitions between time-independent, or stationary energy states, so this work will concentrate on the time-independent Schrödinger equation

$$\mathbf{H}\Psi = \mathrm{E}\Psi. \qquad [1]$$

Here, **H** is the time-independent Hamiltonian operator for a vibrating-rotating system, Ψ is the molecular wavefunction, and E is the stationary state energies of the system, the eigenvalues of the Schrödinger equation.

While one can write down the Schrödinger equation in an exact form, it is a more difficult task to solve the Schrödinger equation exactly. It is commonplace to begin with a first-order approximation, and successively add higher and higher order corrections to the form of the Hamiltonian. It should be noted here that the molecular wavefunction consists of three parts, a vibrational piece, a rotational piece, and an electronic piece

$$\mathbf{H}\Psi(r,Q,\theta,\phi,\chi) = \mathrm{E}\Psi(r,Q,\theta,\phi,\chi). \qquad [2]$$

The wavefunction is defined using r for the position of the electrons, Q for the internal vibrational coordinates for the molecule, and θ, ϕ, and χ for the rotational coordinates of the molecule. Using the Born-Oppenheimer approximation, it is possible to separate the electronic part of the Schrödinger equation from the vibration-rotation part, leaving

$$\mathbf{H}_{\mathrm{vr}}\psi_{\mathrm{vr}}(Q,\theta,\phi,\chi) = \mathrm{E}_{\mathrm{vr}}\psi_{\mathrm{vr}}(Q,\theta,\phi,\chi). \qquad [3]$$

Developing the wavefunction in terms of classical mechanics allows for the wavefunction to be expressed as a product of separate vibrational and rotational wavefunctions

$$\psi_{vr}(Q,\theta,\phi,\chi) = \psi_{v}(Q)\psi_{r}(\theta,\phi,\chi). \quad [4]$$

The Hamiltonian can also be separated into its vibrational and rotational pieces,

$$\mathbf{H}_{vr} = \mathbf{H}_{rot} + \mathbf{H}_{vib}, \quad [5]$$

allowing one to solve the Schrödinger equation using the rigid rotor and harmonic oscillator models.

1.2.2. Rigid rotor model

Ignoring the vibrational motion of the molecule, the rotational Hamiltonian in the rigid rotor approximation is defined as

$$\mathbf{H}_{rot} = \frac{1}{2hc}\left(\frac{\mathbf{J}_x^2}{I_x} + \frac{\mathbf{J}_y^2}{I_y} + \frac{\mathbf{J}_z^2}{I_z}\right) \quad [6]$$

where $\mathbf{J}_x$, $\mathbf{J}_y$ and $\mathbf{J}_z$ are angular momentum operators, and I_x, I_y, and I_z are the moments of inertia around the molecule-fixed axes x, y, and z. A factor of $1/hc$ has been added because traditionally, spectroscopy expresses energy in units of cm^{-1}. The angular momentum operators are related to the total angular momentum operator, $\mathbf{J}$, through

$$\mathbf{J}^2 = \mathbf{J}_x^2 + \mathbf{J}_y^2 + \mathbf{J}_z^2. \quad [7]$$

The rotational wavefunction is a common eigenfunction of the angular momentum operators, and it has been shown (*4*) that for a symmetric top, the wavefunction can be denoted as $|J,k\rangle$, where J is a measure of the total angular momentum of the molecule, and k is its projection upon the molecular symmetry axis. The restrictions on the quantum numbers J and k are such that $J \geq 0,1,2,3\ldots$ and $k = -J, -J+1,\ldots,+J$. The eigenvalues for the operators $\mathbf{J}^2$ and $\mathbf{J}_z$ are

$$\mathbf{J}^2|J,k\rangle = \hbar^2 J(J+1)|J,k\rangle \quad [8]$$

$$\mathbf{J}_z^2|J,k\rangle = \hbar^2 k^2|J,k\rangle. \quad [9]$$

For the case of SO_3, a planar oblate top, $I_x = I_y < I_z$. Equation [6] can now be rewritten as

$$\mathbf{H}_{\text{rot}} = \frac{1}{2hc}\left(\frac{\mathbf{J}_x^2}{I_x} + \frac{\mathbf{J}_y^2}{I_y} + \frac{\mathbf{J}_z^2}{I_z}\right) = \frac{1}{2hc}\left(\frac{\mathbf{J}^2 - \mathbf{J}_z^2}{I_x} + \frac{\mathbf{J}_z^2}{I_z}\right) \quad [10]$$

or

$$\mathbf{H}_{\text{rot}} = \frac{1}{\hbar^2}\left[B\left(\mathbf{J}^2 - \mathbf{J}_z^2\right) + C\mathbf{J}_z^2\right] \quad [11]$$

where the rotational constants, B and C, are given by

$$B = h/(8\pi^2 c I_x),\ C = h/(8\pi^2 c I_z). \quad [12]$$

By operating on the wavefunction with the rigid rotor Hamiltonian, the eigenvalues are given by

$$E_{\text{rot}} = \langle J,k|\mathbf{H}_{\text{rot}}|J,k\rangle = BJ(J+1) + (C-B)k^2 \quad [13]$$

and E_{rot}, B, and C are expressed in cm^{-1}.

1.2.3. Harmonic oscillator model

By choosing the molecule fixed axis system, pure rotational motion of the molecule can be ignored, allowing for the development of theory involving the pure vibrational motion of the molecule. For a nonlinear molecule, there are $3N$–6 normal vibrational modes, where N denotes the number of atoms. The Hamiltonian for a harmonic oscillator is given by

$$\mathbf{H}_{\text{vib}} = \frac{1}{2}\sum_{k=1}^{3N-6}\mathbf{P}_k^2 + \frac{1}{2}\sum_{k=1}^{3N-6}\lambda_k Q_k^2 \quad [14]$$

where Q_k is the normal coordinate of the k-th mode with frequency $\nu_k = \lambda_k^{1/2}/2\pi$ and $\mathbf{P}_k$ is the conjugate momentum operator defined as $-i\hbar\partial/\partial Q_k$. When operating on the vibrational wavefunction, the harmonic oscillator Hamiltonian yields

$$E_{\text{vib}} = \sum_{k=1}^{3N-6} h\nu_k\left(\nu_k + \frac{1}{2}\right) \quad [15]$$

where ν_k is the vibrational quantum number with values 0,1,2,...

In certain molecules, such as SO_3, it is possible to have degenerate vibrations. This is the case where two independent vibrations have the same frequencies. In such a case, it is possible to

take a linear combination of the operators for these normal modes. Equation [14] can now be rewritten to be

$$\mathbf{H}_{\mathrm{vib}} = \frac{1}{2}\sum_{s}\left(\mathbf{P}_s^2 + \lambda_s Q_s^2\right) + \frac{1}{2}\sum_{t}\left(\mathbf{P}_{t1}^2 + \mathbf{P}_{t2}^2 + \lambda_t\left[Q_{t1}^2 + Q_{t2}^2\right]\right) \qquad [16]$$

where s indicates a nondegenerate vibration and t1 and t2 are the two normal modes of a doubly degenerate vibration. It is often convenient to write the degenerate coordinates Q_{t1} and Q_{t2} in polar coordinates of the form $Q_{t1} = \rho \cos \varphi$, $Q_{t2} = \rho \sin \varphi$, introducing a phase factor φ, ranging from zero to 2π, and a radial piece ranging from zero to infinity.

The solution to the Schrödinger equation for a doubly degenerate normal vibration yields the wavefunction as a product of radial and angular wavefunctions, for which the angular piece takes the form of $\exp(il\varphi)$. This factor indicates the presence of vibrational angular momentum due to the superposition of the two normal modes. l is therefore termed the vibrational angular momentum quantum number, with a range of $l = \mathrm{v}_t, \mathrm{v}_t - 2, \ldots, -\mathrm{v}_t + 2, -\mathrm{v}_t$. The radial portion of the wavefunction involves a Laguerre polynomial and a normalization factor. As an illustration, Figure 1.1 shows how it is possible to achieve circular motion of the sulfur atom by taking linear combinations of the two normal modes of ν_4 with a phase factor of $\varphi = \pm 90^\circ$. Elliptical and linear motion of the atoms is also possible if a different phase is present.

1.2.4. Higher order rigid rotor – harmonic oscillator terms

Using the convention of Papoušek and Aliev (*3*), the total Hamiltonian is given by

$$\mathbf{H} = \sum_{m,n} \mathbf{H}_{mn} \qquad [17]$$

where m defines the degree of the vibrational operators and n is the degree (power) of the total angular momentum operator **J**. With this convention, the Hamiltonian for the rigid rotor approximation, $\mathbf{H}_{\mathrm{rot}}$, is $\mathbf{H}_{02}$. For high resolution work, higher order centrifugal distortion terms are needed to accurately describe the rotational parameters of the molecule. Quartic and sextic corrections are necessary, such that the purely rotational Hamiltonian becomes

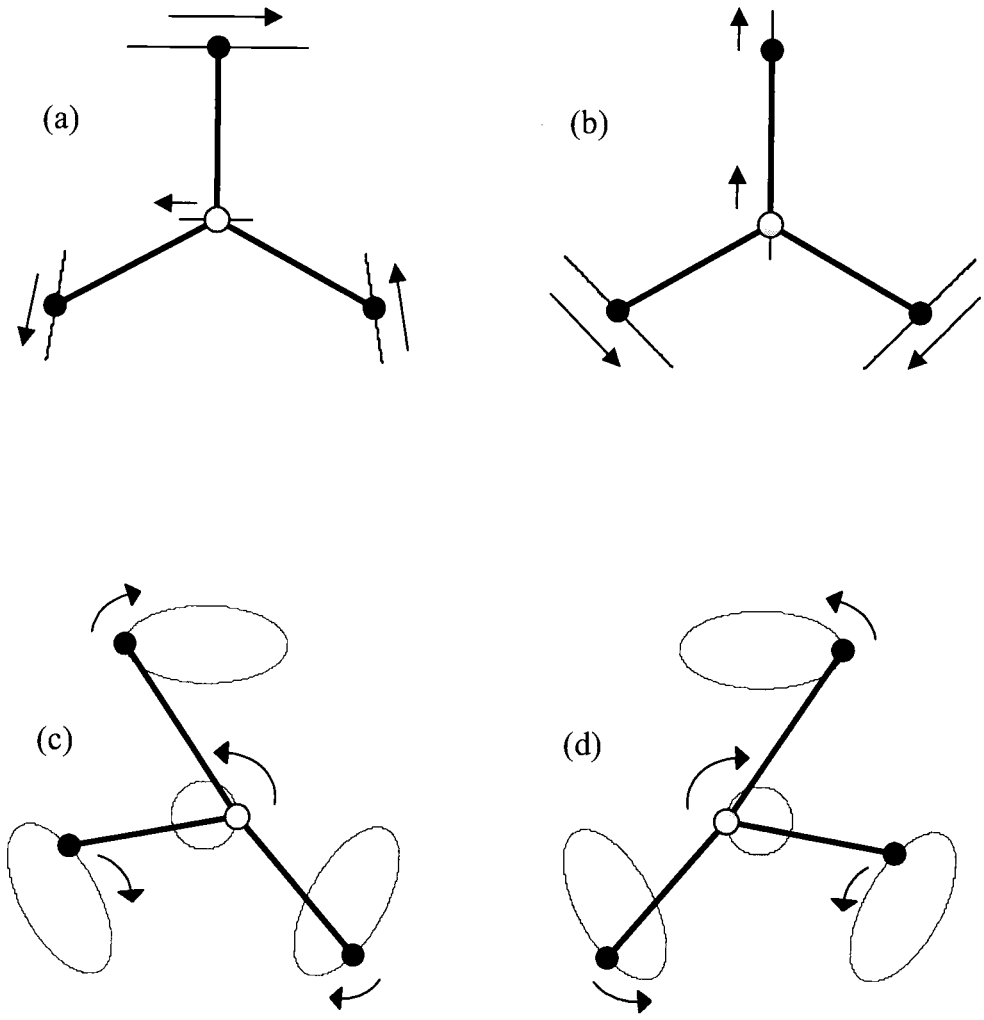

Fig. 1.1. Origin of vibrational angular momentum in v_4. Arrows indicate initial direction of travel of atoms along paths denoted by thin solid lines. The two independent normal modes of v_4 (a–b) are taken in linear combination to give circular motion by the sulfur atom (c–d). By convention, one linear combination is designated as $+l$, the other $-l$.

$$\mathbf{H}_{rot} = \mathbf{H}_{02} + \mathbf{H}_{04} + \mathbf{H}_{06} + \mathbf{H}_{split}, \text{ with} \quad [18]$$

$$\mathbf{H}_{02} = B\mathbf{J}^2 + (C - B)\mathbf{J}_z^2 \quad [19]$$

$$\mathbf{H}_{04} = -D_J\mathbf{J}^4 - D_{JK}\mathbf{J}^2\mathbf{J}_z^2 - D_K\mathbf{J}_z^4 \quad [20]$$

$$\mathbf{H}_{06} = H_J\mathbf{J}^6 + H_{JK}\mathbf{J}^4\mathbf{J}_z^2 + H_{KJ}\mathbf{J}^2\mathbf{J}_z^4 + H_K\mathbf{J}_z^6. \quad [21]$$

The form of $\mathbf{H}_{split}$ varies with the symmetry of the molecule. For the case of SO_3, D_{3h} in symmetry, two splitting terms are necessary. For nondegenerate states (A in symmetry), this term takes the form

$$\mathbf{H}_{split} = \Delta_v(\mathbf{J}_+^6 - \mathbf{J}_-^6) \quad [22]$$

where Δ_v is dependent on cubic potential constants, and $\mathbf{J}_\pm = \mathbf{J}_x \pm i\mathbf{J}_y$ are raising and lowering operators. Adding these terms in [13] yields the following equation for fitting the rotational constants of a nondegenerate vibrational state of a symmetric top

$$\begin{aligned} F(J,K) = {} & BJ(J+1) + (C-B)K^2 - D_J J^2(J+1)^2 - D_{JK}J(J+1)K^2 - D_K K^4 \\ & + H_J J^3(J+1)^3 + H_{JK}J^2(J+1)^2K^2 + H_{KJ}J(J+1)K^4 + H_K K^6 \\ & \pm \Delta_v J(J+1)[J(J+1)-2][J(J+1)-6]\delta_{K3} \end{aligned} \quad [23]$$

The coefficients in the Hamiltonian terms above differ from the rotational constants by a factor of $1/\hbar^2$. It should also be noted that $K = |k|$. The last term represents splitting of the $K = 3$ levels only, since these are the only K state that are appreciably perturbed by the $\mathbf{H}_{split}$ term in the Hamiltonian. For the $K = 3$ levels of SO_3, the + sign is used for even J values, the – sign for odd J values. For the case of a degenerate state (E in symmetry), the form of $\mathbf{H}_{split}$ becomes

$$\mathbf{H}_{split} = t_v(\mathbf{J}_+^4 - \mathbf{J}_-^4) \quad [24]$$

changing the last term in Eqn. [23] to $\pm t_v J(J+1)[J(J+1)-2]\delta_{K2}$

Likewise, the vibrational Hamiltonian can be expanded to higher order. The harmonic oscillator Hamiltonian would be termed $\mathbf{H}_{20}$ with the above convention. A simplification can be made to display the dimensionality of the harmonic oscillator terms in the Hamiltonian as

$$\mathbf{H}_{20} = \frac{1}{2}\sum_{k=1}^{3N-6}\omega_k\left(\mathbf{p}_k^2 + q_k^2\right) \quad [25]$$

where

$$\mathbf{p}_k = -i\frac{\partial}{\partial q_k} = \lambda_k^{-1/4}\hbar^{-1/2}\mathbf{P}_k, \qquad [26]$$

$$q_k = \left(\frac{\lambda_k}{\hbar^2}\right)^{1/4} Q_k, \qquad [27]$$

and $\omega_k = \nu_k/c$. The cubic anharmonic term $\mathbf{H}_{30}$ then takes the form

$$\mathbf{H}_{30} = \frac{1}{6}\sum_{l,m,n} k_{lmn} q_l q_m q_n \qquad [28]$$

where k_{lmn} is the cubic potential constant, the derivative of the vibrational potential energy with respect to the vibrational modes q_l, q_m, and q_n. For SO_3, the cubic terms k_{122} and k_{144} proved to be major comtributors that have a dramatic effect on the CARS spectra we obtained (Chapter 2).

Similarly, $\mathbf{H}_{40}$ gives rise to quartic potential contributions. Including both terms results in the following energy expression for the vibrational energy of a symmetric top:

$$\begin{aligned} G(v,l) = &\sum_s \omega_s\left(v_s + \frac{1}{2}\right) + \sum_t \omega_t(v_t + 1) + \sum_{s\geq s'} x_{ss'}\left(v_s + \frac{1}{2}\right)\left(v_{s'} + \frac{1}{2}\right) \\ &+ \sum_{s,t} x_{st}\left(v_s + \frac{1}{2}\right)(v_t + 1) + \sum_{t\geq t'} x_{tt'}(v_t + 1)(v_{t'} + 1) + \sum_{t\geq t'} x^{tt'} l_t l_{t'} \end{aligned} \qquad [29]$$

where x_{ij} and $x^{tt'}$ are made up of various combinations of cubic and quartic potential constants and corrections arising from vibrational angular momentum. $x^{tt'}$ is also written as $g_{tt'}$ in many texts.

1.2.5. Vibration-rotation interactions

Again, for high resolution work, one is not able to safely assume a simple model such as the rigid rotor/harmonic oscillator approach. There are terms in the complete Hamiltonian that couple vibrational motion with rotational motion. For example, the $\mathbf{H}_{21}$ term couples the total angular momentum $\mathbf{J}_\alpha$ and the vibrational angular momentum $\mathbf{p}_\alpha$ and takes the form

$$\mathbf{H}_{21} = -2\sum_\alpha B_\alpha \mathbf{J}_\alpha \sum_{k,l} \zeta_{kl}^\alpha (\omega_l/\omega_k)^{1/2} q_k \mathbf{p}_l. \qquad [30]$$

This term, called the Coriolis interaction, is seen when two vibrations are related through rotational motion. This becomes especially important when $\omega_t \approx \omega_k$. In the case of a degenerate vibration in a oblate symmetric top, the z-axis Coriolis coupling term gives rise to a $-2(C\zeta_v)kl$ term in the rotational energy expression. For this work, $\mathbf{H_{23}}$ has also been included to yield higher order J and K corrections to the energy expression.

To this point, most of the terms discussed are diagonal elements in the Hamiltonian matrix. From these diagonal elements, the unperturbed energies of the rovibrational levels are obtained, which are a first order approximation. However, additional interactions between states can occur to shift the energies of the levels from those predicted by the first order treatment. These interactions become especially appreciable when the energies of the states are close to one another. Through perturbation theory, one is able to successively add terms to the Hamiltonian to take account of these interactions. For example, Coriolis coupling of a nondegenerate vibration to a degenerate vibration via rotation around the x,y axes through $\mathbf{H_{21}}$ occurs as an off-diagonal element. This is similar to the Coriolis interaction between two degenerate modes, but is more complicated due to the need for linear combinations of $\mathbf{p}$ and $\mathbf{J}$ around the x,y axes. Due to the coupling of states that differ in k and l, these are no longer good quantum numbers. However, as shown by Papoušek (*5*), the quantity $(k-l)$ is constant and therefore a good quantum number.

Another off-diagonal interaction arises from the $\mathbf{H_{22}}$ term in the Hamiltonian. This is called l-type resonance, and is an interaction between the two states of a degenerate vibration that differ in l value by two. This gives rise to a correction term to the energy of the levels that is dependent on the quantum numbers v_t and l_t. In the case for SO_3, this couples states with $\Delta k = \pm 2$ and $\Delta l = \pm 2$ due to symmetry restrictions. This term becomes most important for the case where $k = l = \pm 1$. These levels are very close together (and sometimes degenerate), so in such a case, this interaction is termed l-type doubling due to its large effect.

An additional interaction arises from the cubic terms in the potential. This interaction, called Fermi resonance, is important when the sum of the frequencies $\omega_m + \omega_n$, or $2\omega_m$, is close to

that of ω_l. This coupling term k_{lmn} is nonzero when the symmetry of ω_l is the same as $\omega_m + \omega_n$. Since this is a purely vibrational term, the effect of such an interaction is seen as a shift in the vibrational energies that allows one to directly determine the cubic potential constant k_{lmn}. The most cited example of Fermi resonance is that seen in the vibrational spectrum of CO_2. The intensity of Fermi-coupled vibrations are also significantly affected, as is discussed in Chapter 2.

1.2.6. Nuclear spin statistics

In spectroscopy, it is necessary to know what levels can exist within the molecule. The quantum number J is a measure of the total angular momentum of the molecule. Its projection upon the symmetry axis, here the z-axis, is denoted as K. Normally for a symmetric top molecule such as BF_3, all integral values of J can exist such that $J = 0,1,2,3\ldots$ and $K = 0,1,2,3\ldots+J$. However, in some cases there are symmetry restrictions on the molecular wavefunction that exist that can simplify the energy level pattern that is seen.

The total wavefunction of a molecule is a product of the electronic, vibrational, rotational, and nuclear spin wavefunctions, ie

$$\psi_{total} = \psi_e\psi_v\psi_r\psi_s. \qquad [31]$$

Exchange of identical nuclei must operate on ψ_{total} to yield the result $+\psi_{total}$ for bosons (particles with integral nuclear spins) or $-\psi_{total}$ for fermions (particles with half-integral spins). Oxygen has a nuclear spin of zero, making it a boson. ψ_s is also symmetric as there is only one possible combination of the spins of the oxygens in SO_3 (all zeros). In this work, all spectroscopy has been performed on the ground electronic state which is also symmetric. Any restrictions on the energy levels must therefore arise from the product of $\psi_r\psi_v$.

The symmetries of the vibrational modes can be determined from group theory. For SO_3, there are four vibrations, two nondegenerate and two degenerate vibrations, as seen in Figure 1.2. The symmetric stretching mode, ν_1, is of A_1' symmetry. ν_2, the out-of-plane bend, is A_2'' in symmetry. Both ν_3, the antisymmetric stretch, and ν_4, the in-plane antisymmetric bend, have E' symmetry. Overtones and combinations of these vibrational modes are also examined in this work.

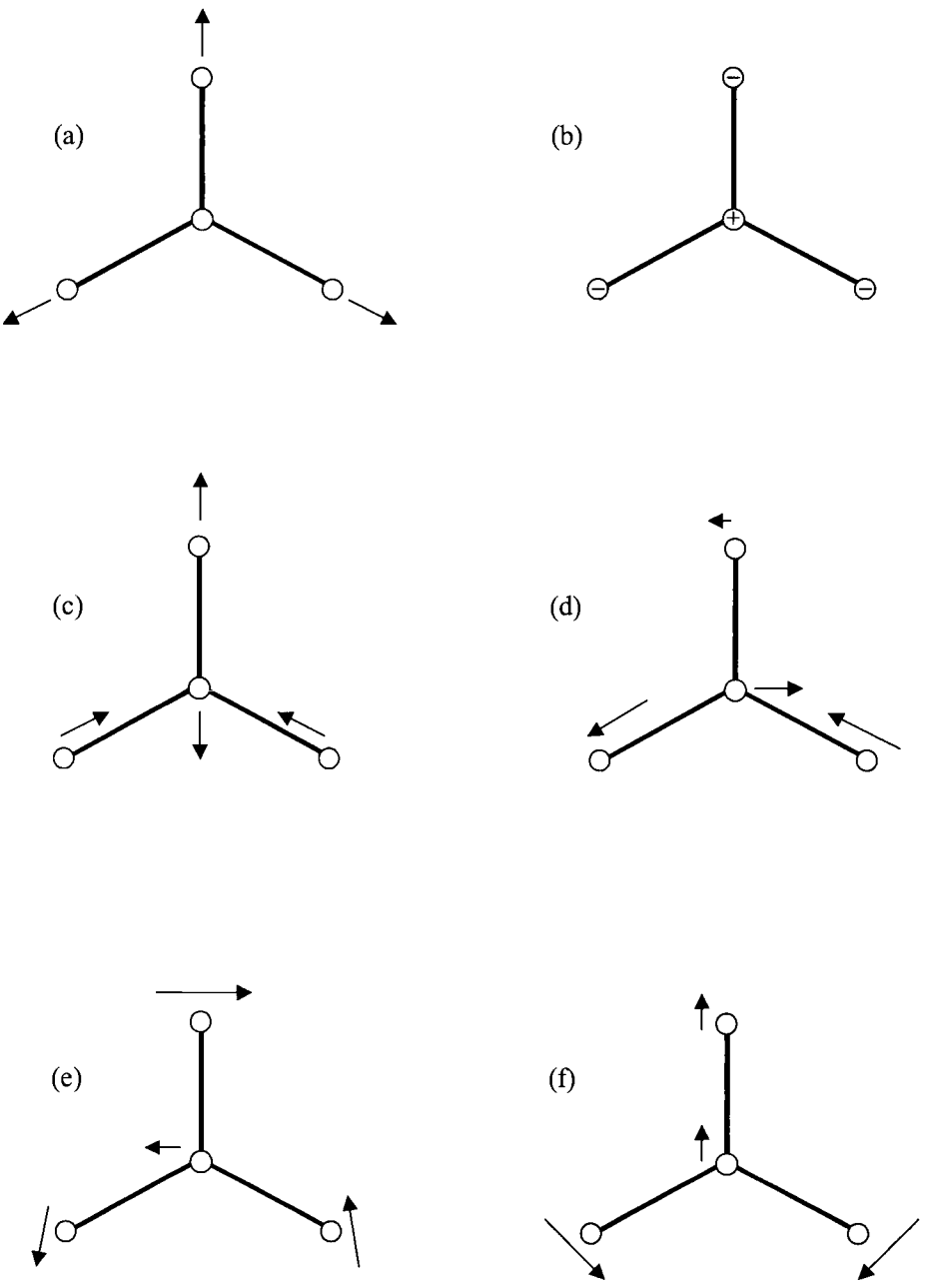

Fig. 1.2. The vibrational modes of SO_3. Arrows indicate direction of motion of atoms with length indicating relative displacement magnitude. Identification of modes are ν_1 (A_1') symmetric stretch (a), ν_2 (A_2'') out-of-plane bend (b), ν_3 (E') anti-symmetric stretch (c-d), and ν_4 (E') anti-symmetric bend (e-f).

The symmetry of these vibrational levels are determined from the products of the symmetries of the fundamental modes that make up these excited states.

SO_3 has D_{3h} symmetry. The rotational wavefunction will have the symmetry of the rotational subgroup, in this case D_3. This group is made up of three symmetry operations: E, the identity operation, C_3, a rotation of 120° around the symmetry axis, and C_2 a rotation of 180° around an axis perpendicular to the symmetry axis. The rotational wavefunction is defined as

$$\psi_r = \psi_{J,K,M}(\theta,\chi,\phi) = \Theta_{J,K,M}(\theta)\, e^{iK\chi}\, e^{\pm iM\phi} \qquad [32]$$

where $\Theta_{J,K,M}$ represents hypergeometric functions and M is projection of the total angular momentum on the laboratory-fixed z-axis. Acting upon the rotational wavefunction with the identity operator yields

$$\psi_{J,K,M}(\theta,\chi,\phi) \xrightarrow{E} \psi_{J,K,M}(\theta,\chi,\phi) \qquad [33]$$

or no change. The character of $\psi_{J,K,M}(\theta,\chi,\phi)$, $\chi_{E'}$, is one for $K = 0$, and two for all other values of K since these levels are doubly degenerate.

Acting upon the wavefunction with a C_3 operation, which changes χ by $2\pi/3$, gives

$$\psi_{J,K,M}(\theta,\chi,\phi) \xrightarrow{C_3} \psi_{J,K,M}\left(\theta,\chi+\frac{2\pi}{3},\phi\right) = e^{2\pi Ki/3}\psi_{J,K,M}(\theta,\chi,\phi) \qquad [34]$$

For $K = 0$, this leaves the wavefunction unchanged; its character $\chi_{C_3} = 1$. For $K \neq 0$, the levels are degenerate, so it is necessary to take a linear combination of wavefunctions such that

$$\chi_{C_3} = e^{+2\pi iK/3} + e^{-2\pi iK/3} = 2\cos\left(\frac{2\pi K}{3}\right) \text{for } K \neq 0. \qquad [35]$$

From this, it can been seen that for K values that are multiples of three, the wavefunction is unchanged upon rotation by 120°. This yields $\chi_{C_3} = 2$ for $K = 3p$ where p is an integer, and $\chi_{C_3} = -1$ for $K = 3p \pm 1$.

Operating on the wavefunction by a C_2 operation is a more complicated case with $\theta \rightarrow \pi - \theta$, $\phi \rightarrow \pi + \phi$, and $\chi \rightarrow \pi - \chi + 2\alpha$, where α is the angle between the molecular x-axis and

the axis of rotation. As shown by Allan and Cross (*4*), the results of a C_2 operation are for $K = 0$, $\chi_{C_2} = (-1)^J$, while for $K \neq 0$ states, $\chi_{C_2} = 0$.

Having the characters for the rotational levels, one can determine which rotational levels are present for the various vibrational states. In short, for SO_3, only those rotational levels that match the symmetry of the vibrational level exist for those states. For vibrational states that are totally symmetric (A_1) such as the ground vibrational state and ν_1, only $K = 3p$ levels exist with the additional restriction of only even J levels for $K = 0$, as only these states are A_1 in symmetry. For ν_2, A_2'' in symmetry, $K = 3p$ levels exist, but now only odd J levels for $K = 0$ are present. For those states that are E in symmetry, only $K = 3p \pm 1$ exist as these states are also E in symmetry.

1.2.7. Selection rules and rovibrational transition intensities

A transition between rovibrational states can occur when light interacts with a molecule. In infrared spectroscopy, absorption will occur when the molecule has an oscillating dipole whose frequency ν matches that of the incoming electromagnetic field. Quantum mechanically, the probability of a state change is governed by the transition moment, which can be written as

$$\langle \psi'' | \mu | \psi' \rangle = \int \psi'' \mu \psi' d\tau \qquad [36]$$

where ψ'' and ψ' are the lower and upper state wavefunctions respectively, and μ is dipole moment of the molecule, which can be written as a vibrational expansion around the equilibrium position

$$\mu^g = (\mu^g)_0 + \sum_k^{3N-6} \left(\frac{\partial \mu^g}{\partial Q_k} \right)_{Q_k=0} Q_k + \ldots \qquad [37]$$

where g is for the molecular x-, y-, and z-axes. SO_3 is a non-polar molecule, so the zeroth order term disappears for all coordinates.

Spectroscopy is performed in the laboratory-fixed axis system. To convert the components of the dipole moment from the molecule-fixed system to the laboratory-fixed system, it is necessary to use direction cosines between the two sets of coordinate axes. For example, the component of the dipole moment along the lab-fixed X-axis is

$$\mu_X = \mu^x \cos(xX) + \mu^y \cos(yX) + \mu^z \cos(zX) \qquad [38]$$

allowing one to write the general expression

$$\mu_F = \sum_g \Phi_{Fg} \mu^g \qquad F = X, Y, Z; \qquad g = x, y, z \qquad [39]$$

with Φ_{Fg} being the direction cosines, a function of the rotational coordinates. Equation [36] can now be rewritten as

$$\begin{aligned} \langle \psi'' | \mu_F | \psi' \rangle &= \langle V'', R'' | \mu_F | V', R' \rangle = \int \psi_V'' \psi_R'' \mu_F \psi_V' \psi_R' d\tau \\ &= \sum_g \langle V'' | \mu^g | V' \rangle \langle R'' | \Phi_{Fg} | R' \rangle \\ &= \sum_g \int \psi_V'' \sum_k \frac{\partial \mu^g}{\partial Q_k} Q_k \psi_V' \int \psi_R'' \Phi_{Fg} \psi_R' d\tau \end{aligned} \qquad [40]$$

separating the transition dipole moment into vibrational and rotational pieces.

The vibrational piece of the transition dipole moment is generally difficult to calculate since it requires knowledge of the exact wavefunctions involved (both electronic and vibrational). For the calculation of relative rovibrational intensities, it is only necessary to determine if the vibrational piece is non-zero. This can be done via group theory. If the product of the symmetries of the upper and lower state vibrations with the dipole moment operator is totally symmetric, the vibrational term will be non-zero, hence the transition will be infrared active. For D_{3h} symmetry, μ^x and μ^y have E′ symmetry whereas μ^z has A_2'' symmetry. ν_2 and ν_4 are both infrared active because their symmetry matches that of a dipole moment operator (the ground vibrational state is A_1'). It should be noted that the product of two identical symmetries will always yield a totally symmetric component.

The selection rules and individual rovibrational line strengths can now be determined from the matrix elements $\langle R'' | \Phi_{Fg} | R' \rangle$ that are non-zero. Allan and Cross (*4*) give an extensive derivation of these elements involving commutations of the direction cosines. For a parallel-type band such as

ν_2 where the dipole moment oscillates in the z-axis only, the selection rules depend on the elements of Φ_{Fz}, yielding

$$K = 0 \qquad \Delta J = \pm 1 \qquad \Delta K = 0,$$
$$K \neq 0 \qquad \Delta J = 0, \pm 1 \qquad \Delta K = 0. \qquad [41]$$

For a perpendicular-type band such as ν_4 where the dipole oscillates perpendicularly to the symmetry axis, the selection rules depend on Φ_{Fx} and Φ_{Fy}, and are

$$\Delta J = 0, \pm 1 \qquad \Delta K = \pm 1. \qquad [42]$$

The actual values of the matrix elements are important for the calculation of the line strengths, defined as $\sum_{Fg} \left| \left\langle R'' \middle| \Phi_{Fg} \middle| R' \right\rangle \right|^2$.

For the purposes of infrared spectral analysis, it is helpful to reproduce a calculated spectrum such that one can properly identify transitions. The intensity of a rovibrational transition $n'' \rightarrow n'$ is (*4*)

$$I_{n'',n'} = \frac{8\pi^3 \nu N g_{n''} \left(1 - e^{-hc\nu/kT}\right) \exp\left(-hcE_{n''}/kT\right)}{3hc \sum_n g_{n''} \exp\left(-hcE_n/kT\right)} \left| \left\langle n'' \middle| \mu \middle| n' \right\rangle \right|^2 \qquad [43]$$

where n stands for all quantum numbers of the state, $E_{n''}$ is the energy of the lower state, $g_{n''}$ is a weight factor, N is the number of molecules per cubic centimeter, and ν is the transition frequency. Since only relative intensities are necessary, many of the terms in Equation [43] can be combined together into a scaling factor, which includes the denominator, the constants in the numerator, and the vibrational piece of the transition moment. For SO_3, the infrared intensities of some bands are complicated by complex mixing of states. A more detailed analysis on the intensity perturbations seen in the ν_2, ν_4 spectrum has been performed and will be discussed in Chapter 3. Intensity perturbations also occur in the spectra discussed in Chapters 2 and 4, but those are largely ignored in those cases.

1.3. THIS WORK

The first manuscript, Chapter 2, relates to the parent isotopomer for SO_3, $^{32}S^{16}O_3$. Using our high resolution CARS apparatus, spectra of the ν_1 symmetric stretching mode were obtained at 0.001 cm^{-1} resolution. Its rich spectral pattern was found to be a complex mixture of states through Coriolis interactions, Fermi resonance, and *l*-resonance. The states that mixed with ν_1 are only accessible through infrared-active hot-band transitions from the ν_2 and ν_4 levels (010^00^0) and (000^01^1), where the label is $\left(v_1v_2v_3^{l_3}v_4^{l_4}\right)$. This manuscript presents the detailed analysis of these infrared bands and the reproduction of the ν_1 CARS spectrum. Remarkably, the CARS spectrum shows most directly the complex perturbations present in SO_3, but in the final analysis, the fitting parameters were determined solely by the more accurate infrared data. Rovibrational parameters for the ν_1 state, allowing the extrapolation down to the equilibrium structure, are presented for the first time.

Chapter 3 is the first of two manuscripts dealing with the sulfur-34 isotopomer of SO_3. Here, the infrared-active ν_2 and ν_4 fundamental modes are modeled extensively. The first known rovibrational parameters for this isotopomer are presented and compared with those available for $^{32}S^{16}O_3$. In addition, intensity perturbations arise from the mixing of the ν_2, ν_4 states have been modeled for both $^{32}S^{16}O_3$ and $^{34}S^{16}O_3$, yielding information about the dipole derivatives for these isotopomers. The third and final manuscript repeats for $^{34}S^{16}O_3$ the analysis performed in Chapter 2.

This thesis thus presents the results of our analysis of the two ^{16}O isotopomers of SO_3, $^{32}S^{16}O_3$ and $^{34}S^{16}O_3$. Over 18 000 individual transitions for these two isotopomers have been measured and assigned. The CARS spectra of both isotopomers have been analyzed in detail and reproduced using the complex mixing of the rovibrational levels of ν_1 with the nearby states $2\nu_2$, $\nu_2+\nu_4$, and $2\nu_4$. Rovibrational constants for numerous states are presented and discussed. An

analysis of intensity perturbations seen in the spectra of the ν_2, ν_4 fundamental is also included. Finally, a comparison of the parameters for the equilibrium structure of SO_3 is shown.

1.4. REFERENCES

1. S.-Y. Tang and C.W. Brown, *J. Mol. Spectrosc.* **3**, 387-390 (1975)
2. M.L. Orlov, J.F. Ogilvie, and J.W. Nibler, *J. Mol. Spectrosc.* **185**, 128-141 (1997).
3. D. Papoušek and M.R. Aliev, "Molecular Vibrational-Rotational Spectra", Elsevier Scientific Publishing Company, Amsterdam (1982)
4. H.C. Allen, Jr. and P.C. Cross, "Molecular Vib-Rotors", John Wiley and Sons, Inc., New York (1963)
5. E.B. Wilson, Jr., J.C. Decius, and P.C. Cross, "Molecular Vibrations", Dover Publications, Inc., New York (1980)
6. P.F. Bernath, "Spectra of Atoms and Molecules", Oxford University Press, New York (1995)
7. E.t.H. Chrysostom, "Applications of High Resolution Coherent Anti-Stokes Raman Scattering Spectroscopy", Ph.D. Thesis, Oregon State University (2001)

ANALYSIS OF ν_2, ν_4 INFRARED HOT BANDS OF $^{32}S^{16}O_3$: RESOLUTION OF THE PUZZLE OF THE ν_1 CARS SPECTRUM

Jeffrey Barber, Engelene t.H. Chrysostom, Tony Masiello, Joseph W. Nibler[1], Department of Chemistry, Oregon State University, Corvallis, OR 97331-4003; Arthur Maki, 15012 24th Ave. S.E., Mill Creek, WA 98012; Alfons Weber, National Science Foundation, Arlington, VA 22230, and National Institute of Standards and Technology, Gaithersburg, MD 20899; and Thomas A. Blake, Robert L. Sams, Pacific Northwest National Laboratory, P.O. Box 999, Mail Stop K8-88, Richland, WA 99352

Journal of Molecular Spectroscopy

Editorial Office

525 B Street, Suite 1900

San Diego, California 92101-4495

J. Mol. Spectrosc. **216**, 105-112 (2002)

---

[1] To whom correspondence should be sent.

2. ANALYSIS OF ν_2, ν_4 INFRARED HOT BANDS OF $^{32}S^{16}O_3$: RESOLUTION OF THE PUZZLE OF THE ν_1 CARS SPECTRUM

2.1. ABSTRACT

Further analysis of the high resolution (0.0015 cm^{-1}) infrared spectrum of $^{32}S^{16}O_3$ has led to the assignment of more than 3100 hot band transitions from ν_2 and ν_4 levels to the states $2\nu_2$ (l=0), $\nu_2+\nu_4$ (l=±1), and $2\nu_4$ (l=0, ±2). These levels are strongly coupled via Fermi resonance and indirect Coriolis interactions to the ν_1 levels which are IR-inaccessible from the ground state. The unraveling of these interactions has allowed for the solution of the unusual and complicated structure of the ν_1 CARS spectrum. This has been accomplished by locating over 400 hot-band transitions to levels that contain at least 10 % ν_1 character. The complex CARS spectrum results from a large number of avoided energy level crossings between these states. Accurate rovibrational constants are deduced for all the mixed states for the first time, leading to deperturbed values of 1064.924(11), 0.000 840 93(64), and 0.000 418 19(58) cm^{-1} for ν_1, α_1^B, and α_1^C respectively. The uncertainties in the last digits are shown in parentheses and represent two standard deviations. In addition, new values for some of the anharmonicity constants have been obtained. Highly accurate values for the equilibrium rotational constants B_e and C_e are deduced, yielding independent, nearly identical values for the SO r_e bond length of 141.734 03(13) and 141.732 54(18) pm, respectively.

2.2. INTRODUCTION

We have solved the riddle of the coherent anti-Stokes Raman (CARS) spectrum of ν_1 of $^{32}S^{16}O_3$! In the first paper of this series (*1*) we presented the CARS spectra of several isotopomers of SO_3. The spectra were clearly abnormal and at that time it was speculated that the peculiarities of

the spectra could probably be explained by interactions with the nearby levels of $2\nu_4$. We have now used an analysis of the hot bands accompanying the ν_2 and ν_4 bands to quantify the interactions with ν_1 and to obtain a calculated CARS spectrum for ν_1 that is in excellent agreement with the observed spectrum.

Earlier (*2*) we presented the results of a new analysis of the infrared spectrum of the three IR-active fundamentals, ν_2, ν_3, and ν_4 and the overtone $2\nu_3$. Using the same spectra for which we had identified 4106 transitions due to ν_2 and ν_4, we have now been able to assign a large number of transitions due to the hot bands 020^00^0–010^00^0, 010^01^1–010^00^0, 010^01^1–000^01^1, 000^02^0–000^01^1, and 000^02^2–000^01^1. The upper states of these transitions are interconnected through the same Coriolis interaction that couples ν_2 to ν_4 and that has been treated in several earlier papers (*2-4*). In addition there is a coupling between the $l = 0$ and $l = \pm 2$ components of $2\nu_4$, similar to what was found for $2\nu_3$ (*2*). We have also identified more than 400 100^00^0–000^01^1 transitions to upper state levels that are mixed but are at least 10 % ν_1 in character. In all, 3123 hot-band transitions were fit with an overall RMS deviation of 0.000 12 cm^{-1}.

Fermi-resonant interactions serve to couple the $2\nu_4$ ($l = 0$) and $2\nu_2$ levels to those of ν_1. Martin (*5*) has performed an *ab initio* calculation of the force field for SO_3 and calculates the cubic potential constants k_{144} and k_{122} that govern, respectively, these interactions. Both interactions prove to be important perturbations to the ν_1 spectrum. Even though the vibrational resonance between $2\nu_4$ and ν_1 is small, the vastly different rotational energy level structure of $2\nu_4$ vis-à-vis ν_1 accounts for a large number of level crossings (actually avoided crossings) where the energy levels of $2\nu_4$ are strongly mixed with those of ν_1. The vibrational symmetry forbids a direct vibrational interaction between ν_1 (A_1') and the $l = \pm 2$ levels of $2\nu_4$ (E′). However, the rotational coupling between the $l = 0$ (A_1') and $l = \pm 2$ (E′) levels of $2\nu_4$ results in a significant interaction between certain rotational levels of ν_1 and $2\nu_4$ ($l = -2$) when those levels are close together. Many such avoided crossings occur as a result of the different rotational structure for the two nearby vibrational states and it is the

resultant pattern of rotational levels in ν_1 that is the cause of the unusual CARS spectrum. Figure 2.1 summarizes the relevant levels, transitions, and primary interactions examined in this work.

2.3. EXPERIMENTAL DETAILS

This analysis is based on the same infrared spectra used in Ref. (*2*). The data were recorded with a Bruker IFS 120 HR Fourier transform spectrometer[2] at the PNNL facilities. The room temperature spectra were recorded from 405 to 708 cm^{-1} with a resolution of 0.0015 cm^{-1}. More details on the absorption cell and various parameters related to the spectra are given in Ref. (*2*).

The top of Figure 2.2 gives an overview of the experimental spectrum, which is dominated by the strong ν_2 and ν_4 bands, whose analyses are given in (*2*). Buried in these complex bands are various hot bands; the lower traces in the figure are the calculated spectra for the bands analyzed in this work, at approximately the correct relative intensities. Figure 2.3 shows a small segment of the spectrum. The excellent signal-to-noise and reproducibility of the spectra were essential to the confident assignment of many of the weak features. Minor features due to the natural abundance (4.2 %) of $^{34}S^{16}O_3$ were also identified from spectra of isotopically-enriched samples, work that will be described in a separate publication.

The hot-band assignments were not trivial, due to the strong perturbations among the states. For example, we identify in Fig. 2.3 lines in the series ${}^{P}P_{K}(41)$ from K''=29 to K''=38 for the $2\nu_4$ ($l = -2$) – ν_4 band. The dashed vertical lines indicate the position of the lines calculated when the Fermi resonance constants k_{122} and k_{144} are set to zero. For other hot-band regions the shifts are

---

[2] Certain commercial equipment, instruments, and materials are identified in the paper to adequately specify the experimental procedure. Such identification does not imply recommendations or endorsements by the National Institute of Standards and Technology, the National Science Foundation, or the Pacific Northwest National Laboratory (PNNL), nor does it imply that the materials or equipment identified are necessarily the best available for the purpose.

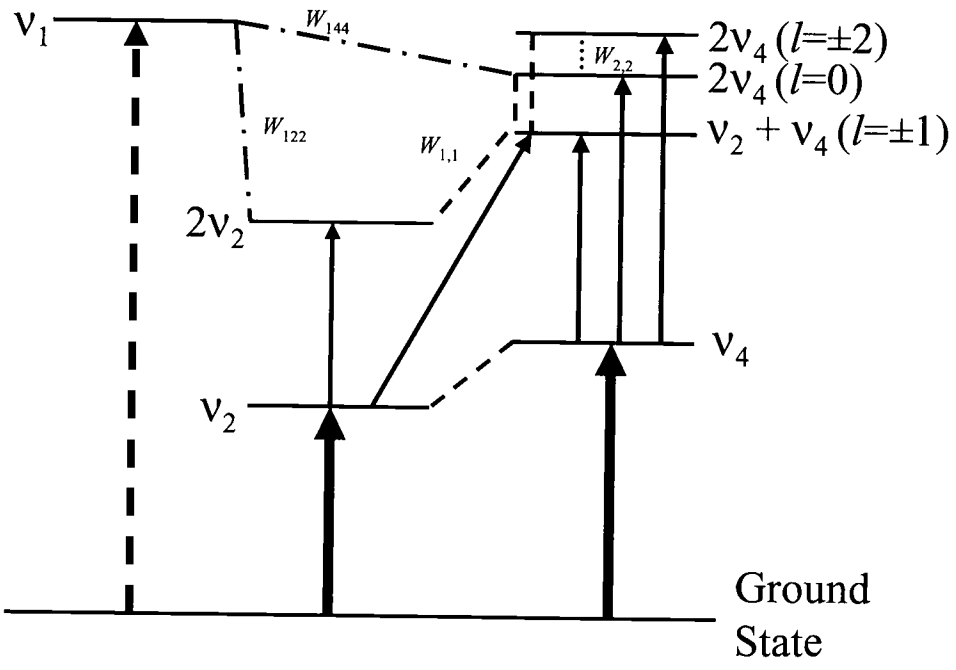

Fig. 2.1. Vibrational energy level diagram for SO_3. Arrows indicate Raman (dashed) and infrared (solid) transitions. Lines between levels indicate the couplings between states, including Fermi resonances (– ▪ –), Coriolis interactions (– – –), and *l*-resonances (• • •). Not shown are the *l*-resonance interactions within the $\nu_2+\nu_4$ (l=±1) and $2\nu_4$ (l=±2) states.

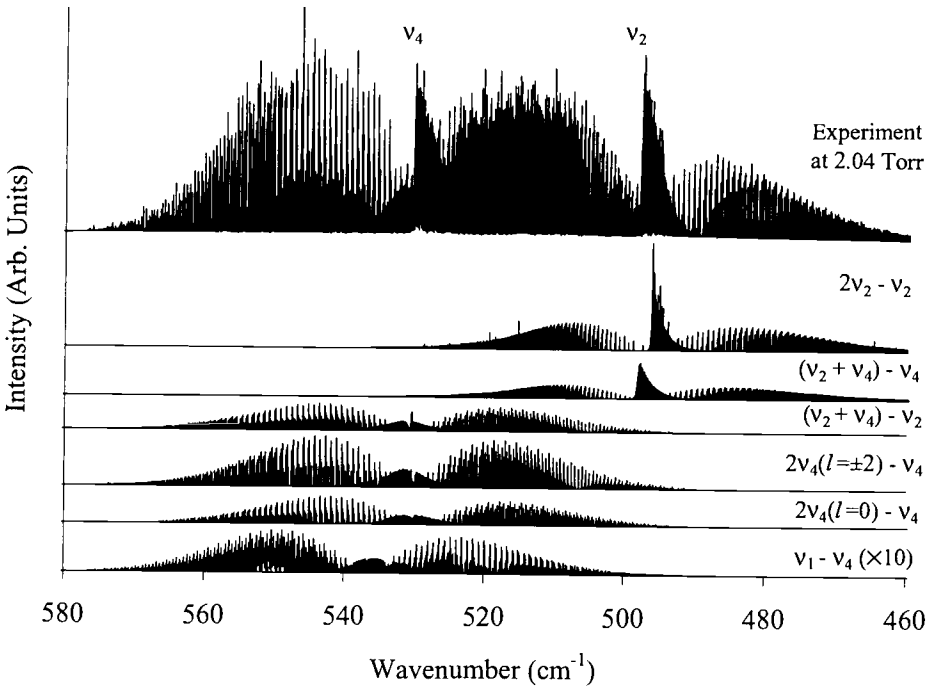

Figure 2.2. Infrared spectrum of the ν_2, ν_4 region of $^{32}S^{16}O_3$ (top) and calculated spectra of hot bands involving ν_1 and its perturbing states. Calculated spectra are at their approximate intensities relative to the experiment, with $\nu_1 - \nu_4$ magnified to show its structure.

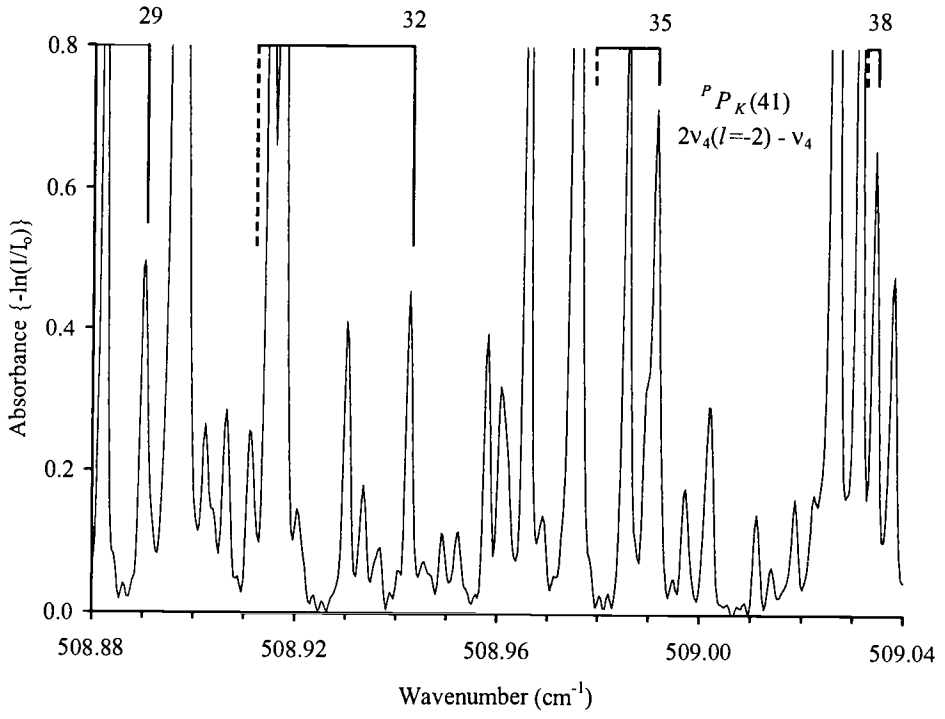

Fig. 2.3. A small portion of the ν_2, ν_4 region showing the series $^{P}P_K(41)$ from $K = 29$ to $K = 38$ for the $2\nu_4$ (l=– 2) – ν_4 band. The dashed vertical lines indicate the position of the lines when the Fermi resonance constants k_{122} and k_{144} are set to zero. (The shift for $K = 29$ is large, –0.059 cm^{-1}, so the dashed line is off scale.)

even larger, as much as 2 cm^{-1}, so that knowing the approximate location of the ν_1 levels from the CARS spectrum was essential to the bootstrap operation used in making hot-band assignments. This process involved identifying low-J and -K transitions to the least perturbed states, $2\nu_2$ and $\nu_2+\nu_4$, followed by extension to higher J and K values and to the $2\nu_4$ levels. Periodically, CARS spectra were simulated as a test of the overall correctness of the assignments.

The CARS spectrum was measured on the CARS apparatus at Oregon State University, which was described in Ref. (*6*). Details related to the recording of the CARS spectrum are given in Ref. (*1*). The CARS spectrum of the ν_1 region for $^{32}S^{16}O_3$ is given in Fig. 2.4, which also gives the spectrum that was calculated as a result of the present work. It should be noted that the spectrum consists only of Q-branch transitions and that, despite an instrumental resolution of about 0.001 cm^{-1}, the resolved structure is not that of individual lines but is of K subbands containing many low J transitions. The puzzle in this spectrum was the irregular nature of these subbands and, in particular, the gap in the middle of the spectrum, which resisted all fitting efforts in terms of simple conventional models.

2.4. HOW THE DATA WERE FIT

First, we note that, although the CARS spectrum served as an essential guide and as a final test of the validity of the analysis of the infrared spectrum, only well-resolved infrared hot-band transitions were used in the least-squares fitting that gave the constants for ν_1. Since the lower states of the hot-band transitions were either ν_2 or ν_4, the least-squares analysis included all the transitions that were reported in our earlier paper (*2*). The final least-squares analysis contained nearly 11 000 transitions and resulted in only minor modifications of the ground state constants and of the constants for the other vibrational states. Table 2.1 includes the revised constants for ν_2 and ν_4. The revised constants for the ground, ν_3, and $2\nu_3$ states are included in supplementary tables that

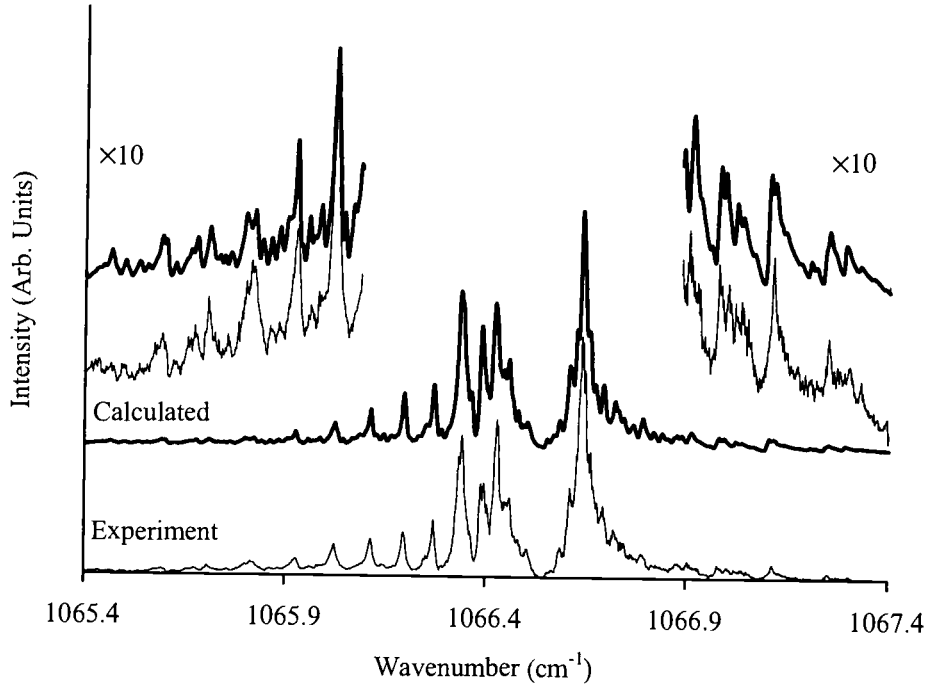

Fig. 2.4. The CARS spectrum of ν_1 of $^{32}S^{16}O_3$. The fit of the CARS spectrum using parameters derived only from infrared hot-band transitions is displayed above the experimental curve.

Table 2.1. The Rovibrational Constants in cm^{-1} for the ν_2, ν_4 States Involved in This Work on the Fundamentals and Hot Bands of $^{32}S^{16}O_3$

constant	ν_2	$2\nu_2$	$\nu_2+\nu_4$	ν_4	$2\nu_4(l=0)$	$2\nu_4(l=2)$
ν_0	497.567 736(16)[a]	995.018(12)	1027.902 357(21)	530.086 424(14)	1059.814 0(11)	1060.452 702(28)
$\Delta C^b \times 10^3$	0.127 783(42)	0.252 70(41)	−0.030 69(21)	−0.157 285(28)	−0.315 936(86)	[−0.315 936]
$\Delta B \times 10^3$	0.804 0(49)	1.616(31)	0.712 9(78)	−0.075 2(25)	−0.147(15)	[−0.147]
$\Delta D_J \times 10^{10}$	18.35(38)	44.5(18)	20.8(16)	10.73(32)	21.2(12)	[21.2]
$\Delta D_{JK} \times 10^{10}$	−23.34(88)	−63.2(52)	−41.7(38)	−38.24(66)	−75.3(32)	[−75.3]
$\Delta D_K \times 10^{10}$	6.28(59)	21.4(37)	22.6(24)	28.10(39)	55.2(18)	[55.2]
$\Delta H_J \times 10^{13}$	−0.673(72)	[−1.345]	[−0.157]	0.516(70)	[1.032]	[1.032]
$\Delta H_{JK} \times 10^{13}$	2.86(23)	[5.71]	[0.63]	−2.23(21)	[−4.45]	[−4.45]
$\Delta H_{KJ} \times 10^{13}$	−4.11(27)	[−8.22]	[−0.96]	3.15(24)	[6.29]	[6.29]
$\Delta H_K \times 10^{13}$	1.93(11)	[3.86]	[0.51]	−1.421(91)	[−2.842]	[−2.842]
$(C\zeta_4)$			−0.084 798(11)	−0.085 195 2(11)		−0.085 025 2(37)
$\eta_J \times 10^7$			−8.93(40)	−9.06(14)		−9.02(44)
$\eta_K \times 10^7$			8.56(40)	8.69(14)		8.64(44)
$q \times 10^4$			4.72(16)	4.616(49)	4.53(15)	
$(B\zeta_{24})$		0.200 94(31)[c]		0.200 57(10)	0.200 93(31)[d]	
$z^J_{24} \times 10^7$		−5.35(11)[c]		−5.013(31)	−4.771(96)[d]	
$z^K_{24} \times 10^7$		3.59(56)[c]		3.354(11)	3.187(52)[d]	
$t_4 \times 10^{11}$				9.5(11)		
$Q_4 \times 10^6$						−3.72(30)
Number of transitions	2921	704	1173	4383	456	790
RMS deviation	0.00012 cm^{-1}	0.00013 cm^{-1}	0.00012 cm^{-1}	0.00011 cm^{-1}	0.00013 cm^{-1}	0.00010 cm^{-1}

[a] The uncertainties are two standard deviations. They refer to the last digits and are shown in parentheses. Values in brackets are assumed.
[b] $\Delta C = C' - C_0$, $\Delta B = B' - B_0$, *etc.*
[c] Contained in the $W_{1,1}$ term for $\nu_2+\nu_4$ interacting with $2\nu_2$.
[d] Contained in the $W_{1,1}$ term for $\nu_2+\nu_4$ interacting with $2\nu_4(l=0)$ and $2\nu_4(l=2)$.

have been deposited with the journal and are also available from the authors. All the unpublished revisions are well within the uncertainties given in the published tables (*2*). The remaining part of this section is concerned with the fit of the upper states of the hot-band transitions, the fit of the lower states having been described in Ref. (*2*).

The data were fit to a Hamiltonian matrix that included the following vibrational energy levels: 100^00^0, 000^02^0, 020^00^0, 000^02^2, and 010^01^1. With the exception of a few low J levels, the matrix contained a minimum of seven rows and seven columns for each value of J:

$E(\nu_1,k,0)$	W_{144}	W_{122}	0	0	0	0
W_{144}	$E(2\nu_4,k,0)$	0	$W_{2,2}$	$W_{2,2}$	$W_{1,1}$	$W_{1,1}$
W_{122}	0	$E(2\nu_2,k,0)$	0	0	$W_{1,1}$	$W_{1,1}$
0	$W_{2,2}$	0	$E(2\nu_4,k+2,2)$	$W_{4,4}$	$W_{1,1}$	0
0	$W_{2,2}$	0	$W_{4,4}$	$E(2\nu_4,k-2,-2)$	0	$W_{1,1}$
0	$W_{1,1}$	$W_{1,1}$	$W_{1,1}$	0	$E(\nu_2+\nu_4, k+1,1)$	$W_{2,2}$
0	$W_{1,1}$	$W_{1,1}$	0	$W_{1,1}$	$W_{2,2}$	$E(\nu_2+\nu_4, k-1,-1)$

Because of various off-diagonal matrix elements coupling different l and k levels, the matrix in the largest case had dimensions of 37×37.

The diagonal elements of the Hamiltonian matrix had the standard form

$$\begin{aligned} E(\mathrm{v}, J, k, l) = {} & G(\mathrm{v}, l) + B_\mathrm{v} J(J+1) + (C_\mathrm{v} - B_\mathrm{v})\, k^2 - 2(C\zeta_\mathrm{v})kl + \eta^K_\mathrm{v} J(J+1)kl \\ & + \eta^K_\mathrm{v} k^3 l - D^J_\mathrm{v} J^2(J+1)^2 - D^{JK}_\mathrm{v} J(J+1)k^2 - D^K_\mathrm{v} k^4 \\ & + H^J_\mathrm{v} J^3(J+1)^3 + H^{JK}_\mathrm{v} J^2(J+1)^2 k^2 + H^{KJ}_\mathrm{v} J(J+1)k^4 \\ & + H^K_\mathrm{v} k^6 + \text{splitting terms.} \end{aligned} \qquad [1]$$

Here we use the convention that lower case k and l are signed quantities and we use l and l_4 interchangeably. Much of the discussion in this paper gives the sign of l on the assumption that k is positive. Using Eq. [1] the band centers are given by

$$\nu_0 = G(v, l)' - G(v, l)''. \quad [2]$$

In Table 2.1 we give the $2\nu_2$, $\nu_2+\nu_4$, and $2\nu_4$ vibrational energy levels in wavenumbers with respect to a zero ground state so that $G(0, 0) = 0$. The splitting terms were the same as described in Ref. (*2*). The only new one that might be significant was a splitting of the $K = 3$ levels of $2\nu_2$ given by

$$\pm\delta_{3K}\Delta_{22}[J(J+1)][J(J+1)-2][J(J+1)-6]. \quad [3]$$

The off-diagonal matrix elements could be divided into three categories, vibrational (Fermi-resonances), Coriolis between vibrational states, and Coriolis within a vibrational state (*l*-resonances). The vibrational off-diagonal matrix elements were:

$$W_{144} = \langle v_1, v_4, J, k, l \,|H|\, v_1+1, v_4-2, J, k, l\rangle$$
$$= k_{144} + k^J_{144}J(J+1) + k^K_{144}k^2 \quad [4]$$

and

$$W_{122} = \langle v_1, v_2, J, k, l \,|H|\, v_1+1, v_2-2, J, k, l\rangle$$
$$= [k_{122} + k^J_{122}J(J+1)]. \quad [5]$$

The Coriolis terms that coupled states with different vibrational quantum numbers were the same terms that coupled ν_2 with ν_4, namely:

$$W_{1,1} = \langle v_2, v_4, J, k \pm 1, l_4 \pm 1 \,|H|\, v_2+1, v_4-1, J, k, l_4\rangle$$
$$= \pm[(B\zeta_{24}) + z^J_{24}J(J+1) + z^K_{24}k(k\pm1)][(v_2+1)(v_4 \pm l_4 + 1)]^{1/2}$$
$$\times[J(J+1) - k(k\pm1)]^{1/2} \quad [6]$$

It should be noted that this definition of z^J_{24} and z^K_{24} differs from that in Ref. (2), where the vibrational factor containing ν_2 and ν_4 was not separated out.

The Coriolis terms that coupled different k and l levels within a vibrational state were of three types, $W_{2,2}$, $W_{2,-4}$, and $W_{4,4}$, where

$$W_{2,2} = \langle v_4 \neq 0, J, k, l_4 \,|H|\, v_4, J, k\pm2, l_4\pm2\rangle$$
$$= \tfrac{1}{4}q_4\{[(v_4+1)^2 - (l_4\pm1)^2][J(J+1) - k(k\pm1)]$$
$$\times[J(J+1) - (k\pm1)(k\pm2)]\}^{1/2}, \quad [7]$$

$$W_{2,-4} = \langle v_4 = 2, J, k, l_4 \mid H \mid v_4 = 2, J, k \pm 2, l_4 \mp 4 \rangle$$

$$= \tfrac{1}{2} Q_4 \{[J(J+1) - k(k \pm 1)][J(J+1) - (k \pm 1)(k \pm 2)]\}^{1/2}, \quad [8]$$

and

$$W_{4,4} = \langle v_4 = 2, J, k, l_4 \mid H \mid v_4 = 2, J, k \pm 4, l_4 \pm 4 \rangle$$

$$= \rho_{44} \{[J(J+1) - k(k \pm 1)][J(J+1) - (k \pm 1)(k \pm 2)][J(J+1) - (k \pm 2)(k \pm 3)]$$

$$\times [J(J+1) - (k \pm 3)(k \pm 4)]\}^{1/2}. \quad [9]$$

As in our earlier paper the off-diagonal Coriolis matrix elements are labeled so that the first subscript indicates the Δk and the second subscript indicates the Δl of the coupling. In preliminary fits we determined values for Δ_2, Δ_{22}, and ρ_{44} but the uncertainties were so large that we decided to leave them out of the final fit. Without these constants the overall RMS deviation of the fit was degraded by less than one percent.

The observed transition wavenumbers were fit with a non-linear least-squares program that combined all of the present measurements with those used in our earlier paper (*2*) and with the microwave results (*7*). Since the ΔH terms were not well determined for the hot bands, they were fixed at the appropriate combinations of the ΔH terms found for ν_2 and ν_4. For ν_1 all the ΔH terms were set to zero because the fit was insensitive to the ΔH terms. Table 2.1 gives the constants determined from the analysis of the hot-band transitions, except that the parameters for ν_1 are listed in Table 2.2. In both tables we give the changes in the constants from the ground state values so that, for instance, $\Delta D^J_v = D^J_v - D^J_0$.

Table 2.2. The Rovibrational Constants in cm^{-1} for ν_1 of $^{32}S^{16}O_3$

ν_0	1064.924(11)[a]
ΔC[b] $\times 10^3$	−0.418 19(58)
$\Delta B \times 10^3$	−0.840 93(64)
$\Delta D_J \times 10^{10}$	28.5(37)
$\Delta D_{JK} \times 10^{10}$	−54.1(74)
$\Delta D_K \times 10^{10}$	25.1(41)

[a] The uncertainties are two standard deviations. They refer to the last digits and are shown in parentheses.
[b] $\Delta C = C' - C_0$, $\Delta B = B' - B_0$, *etc.*

2.5. DETERMINING THE ROVIBRATIONAL CONSTANTS

Enough vibrational states have now been measured to determine the equilibrium internuclear distance for SO_3 and a number of rovibrational constants. The equilibrium rotational constants are usually written as

$$B_e = B_v + \sum_i \alpha_i^B (v_i + \tfrac{1}{2}d_i) - \sum_{ij} \gamma_{ij}^B (v_i + \tfrac{1}{2}d_i)(v_j + \tfrac{1}{2}d_j) \qquad [10]$$

and similarly for C_e. One also expects γ^{II} type terms in Eq. [10] but they could not be determined in this work. Table 2.3 gives the rotational constants obtained from the analysis, both with and without the $\gamma_{ij}^{B,C}$ terms. The α^C and γ^C constants are well determined with reasonable values and uncertainties and the α^C results compare favorably with the values obtained by Martin from *ab initio* calculations (*5*). Such is not the case for the α_2^B and α_4^B results, where the uncertainties are large and the signs are opposite to those deduced by Martin. However, as noted in Ref. (1), these two constants are strongly correlated and the combination $\frac{1}{2}\alpha_2^B + \alpha_4^B$ is well determined and is in good accord with Martin's predictions. For example, if the variance-covariance among these α's is included, the uncertainty calculated for the linear combination is reduced by a factor of 74. Similarly, it is found that the linear combination $\frac{1}{4}\gamma_{22} + \gamma_{44} + \frac{1}{2}\gamma_{24}$ for B is well determined even though the individual γ's are not. This is a fortunate outcome since both these α and γ combinations occur explicitly in correcting the B_0 constant to B_e. We are also fortunate that microwave data for the centrifugally-distorted molecule has given an accurate value for C_0 (*7*), a parameter not normally available from conventional rotational or vibrational spectroscopy of symmetric tops. This allows two independent determinations of the SO bond length r_e which, if extrapolation of B_0 and C_0 to the planar equilibrium values is adequate, should be identical.

For a planar XY_3 molecule the moments of inertia are $I_C = 3M_Y r_e^2 = 2I_B$. The difference in r_e values obtained from B_e and C_e when the γ corrections are included is 0.0015 pm, slightly smaller than when they are omitted (0.0025 pm). Even so, in the former case, the difference is still about 10

Table 2.3. Rotational Constants[a] for $^{32}S^{16}O_3$

constant[b]	*B* constants	*B* constants[c]	Ref. (*5*)	*C* constants	*C* constants[c]	Ref. (*5*)
B_0, C_0	0.348 543 33(5)[d]		0.348 44	0.173 988 13(3)		0.173 93
$\alpha_1\times10^3$	0.840 93(64)	0.840 93(64)	0.81	0.418 19(58)	0.418 19(58)	0.41
$\alpha_2^*\times10^3$	–0.811 44(3854)	–0.803 96(493)	0.31	–0.131 84(42)	–0.127 78(4)	–0.13
$\alpha_3\times10^3$	1.127 11(36)	1.130 48(9)	1.11	0.597 48(22)	0.599 25(7)	0.58
$\alpha_4^*\times10^3$	0.072 52(1902)	0.075 24(245)	–0.50	0.154 64(21)	0.157 29(3)	0.15
$(\frac{1}{2}\alpha_2^* + \alpha_4^*)\times10^3$	–0.333 20(34)	–0.326 74(5)	–0.35	0.088 72(33)	0.093 39(4)	0.09
$\gamma_{22}\times10^5$	0.417(1513)			–0.143(21)		
$\gamma_{33}\times10^5$	–0.112(10)			–0.059(6)		
$\gamma_{44}\times10^5$	0.173(747)			–0.068(4)		
$\gamma_{24}\times10^5$	–1.583(762)			–0.119(20)		
$(\frac{1}{4}\gamma_{22} + \gamma_{44} + \frac{1}{2}\gamma_{24})\times10^5$	–0.514(27)			–0.164(13)		
B_e, C_e	0.349 763 96(64)	0.349 767 53(34)	0.349 62	0.174 885 65(44)	0.174 889 87(31)	0.174 81
r_e (pm)[e]	141.734 027(130)	141.733 303(71)	141.764	141.732 538(179)	141.730 830(126)	
r_0 (pm)[e]	141.981 993(19)		142.004	142.097 633(19)		
Δ_e (amu pm^2)[e]	–20.3(30)	–33.6(20)				
Δ_0 (amu pm^2)[e]	1576.4(4)					

[a] In cm^{-1} except for *r* and inertial defect Δ values.

[b] The constants followed by an asterisk, *, are the constant with the ν_2/ν_4 Coriolis perturbation removed, the so-called deperturbed constants.

[c] Value calculated without inclusion of γ terms.

[d] The uncertainties are two standard deviations. They refer to the last digits and are shown in parentheses.

[e] Inertial defects and *r* values calculated using NIST Physical Reference Data values of h = 6.62606876(52) ×10^{-34} J s, N_A = 6.02214199(47) ×10^{23} mol^{-1}, and m(^{16}O) = 15.9949146221(15) amu.

times that implied by the uncertainties, suggesting that γ_{11} and other neglected γ_{ij} corrections are still significant. Including the available γ's in obtaining B_e and C_e leads to an average value of r_e of 141.7333(15) pm, in remarkably good agreement with the *ab initio* value of 141.76 pm calculated by Martin (*5*). We also compute an inertial defect $\Delta = I_C - 2I_B$ of –20(3) amu pm^2, about 60 % smaller than the value –34(2) amu pm^2 obtained when the γ's are omitted. As expected, in both cases the small negative defect value is much closer to zero than is the value of Δ_0 = +1576.35(37) amu pm^2 deduced using the rotational constants for the ground state.

The extrapolation of the D and H centrifugal distortion coefficients to the equilibrium values can be done with expressions similar to that in Eq. [10]. The uncertainties in the H's were too large to warrant such corrections but this was not the case for the D's. Including only corrections linear in $(v_i + \frac{1}{2}d_i)$, we obtain equilibrium values for D_J, D_{JK} and D_K ($\times 10^7$ cm^{-1}) of 3.0700(20), –5.4067(39), and 2.5206(22) respectively. For comparison, the corresponding values from Martin's *ab initio* calculations are 3.092, –5.452 and 2.543. The planarity condition for the D's is $2D_J + 3D_{JK} + 4D_K = 0$. The equilibrium constants yield a value of 0.002 34 $\times 10^{-7}$ cm^{-1} for this sum, about 7 times smaller than the result obtained using ground state values.

Our results provide a test of the not-uncommon assumption of the planarity condition for D_v's of higher vibrational levels to reduce the number of fitting parameters, e.g. setting $D^K_v = -(2D^J_v + 3D^{JK}_v)/4$. While this is not really correct, it is interesting that the D^K_v values calculated in this way for the eight higher levels characterized in this work are quite close to the determined values (average difference is 14 %, maximum difference is 33 %). Similarly, differences of 4, 19, and 2 % are found for ν_2, ν_3, and ν_4 H^K_v values calculated from the analogous H planarity condition $3H^J_v + 4H^{JK}_v + 5H^{KJ}_v + 6H^K_v = 0$. Thus our results for SO_3 indicate that these simplifying conditions are not unreasonable in other cases where the data do not permit determination of all D and H constants.

A few more vibrational constants can also be determined from the present results. For this we use the usual expression

$$G(v, l) = \sum_i \omega_i (v_i + \tfrac{1}{2}d_i) + \sum_{i \le j} x_{ij} (v_i + \tfrac{1}{2}d_i)(v_j + \tfrac{1}{2}d_j) + \sum_{t \le t'} x^{tt'} l_t l_{t'}. \quad [11]$$

The constants found in this work, as well as those given in the earlier paper (*2*), are given in Table 2.4 which also gives the values taken from the *ab initio* work of Martin (*5*) and the force field calculation of Dorney *et al.* (*8*). As one might expect, the most recent calculation gives values much closer to our observed values. In fact, the agreement is much better than we had anticipated. Table 2.4 also gives the vibrational potential constants responsible for the resonance between ν_1 and both $2\nu_2$ and $2\nu_4$. Martin (*5*) also calculated those constants and it is a pleasure to see the good agreement, including the difference in signs between k_{122} and k_{144}.

2.6. DISCUSSION OF THE RESULTS

2.6.1. ν_1 levels and the CARS spectrum

The present analysis involves infrared transitions to 91 levels that are predominantly (>50 %) ν_1, to 183 levels that are at least 25 % ν_1 and to 407 levels that are at least 10 % ν_1. Thus there are enough transitions to levels that strongly interact with ν_1 that ν_1 is now well characterized. The proof of that is given by the comparison of the observed and calculated CARS spectrum of ν_1 as shown in Fig. 2.4. The procedures and programs for the simulation of CARS spectra from calculated line positions, strengths, and assumed widths have been described previously (*6*). In the simulation, it was assumed that the Raman intensity derives solely from the isotropic scattering component for ν_1, reduced by the square of the appropriate upper state-mixing coefficient. The intrinsic intensity of Raman transitions to the $2\nu_2$, $\nu_2+\nu_4$, and $2\nu_4$ levels is expected to be very small and was not included. The importance of including all the coupling terms is evident in Figure 2.5, which displays CARS spectra calculated with k_{144}, k_{122}, or both constants set equal to zero. It is seen that the k_{122} constant produces a larger Fermi shift of the Q-branch but that both constants are

Table 2.4. Vibrational Constants in cm^{-1} for $^{32}S^{16}O_3$

constant	This work	Ref. (*5*)	Ref. (*8*)
x_{22}	−0.058 7(62)[a]	0.078[b]	−3.21
x_{33}	−5.451 2(42)	−5.434	−4.63
x_{44}	−0.019 75(28)	−0.011	−2.63
x_{24}	0.248 197(20)	0.284	−2.18
x^{33}	2.866 7(42)	2.828	2.47
x^{44}	0.159 67(28)	0.150	2.08
k_{122}	9.943(44)	11.12	
$k^{J}_{122}\times10^{5}$	−2.51(19)		
k_{144}	−1.519 0(23)	−1.56	
$k^{J}_{144}\times10^{5}$	−2.695(91)		
$k^{K}_{144}\times10^{5}$	2.617(89)		

[a] The uncertainties are two standard deviations. They refer to the last digits and are shown in parentheses.
[b] Deperturbed value (Private communication, Ref. 5)

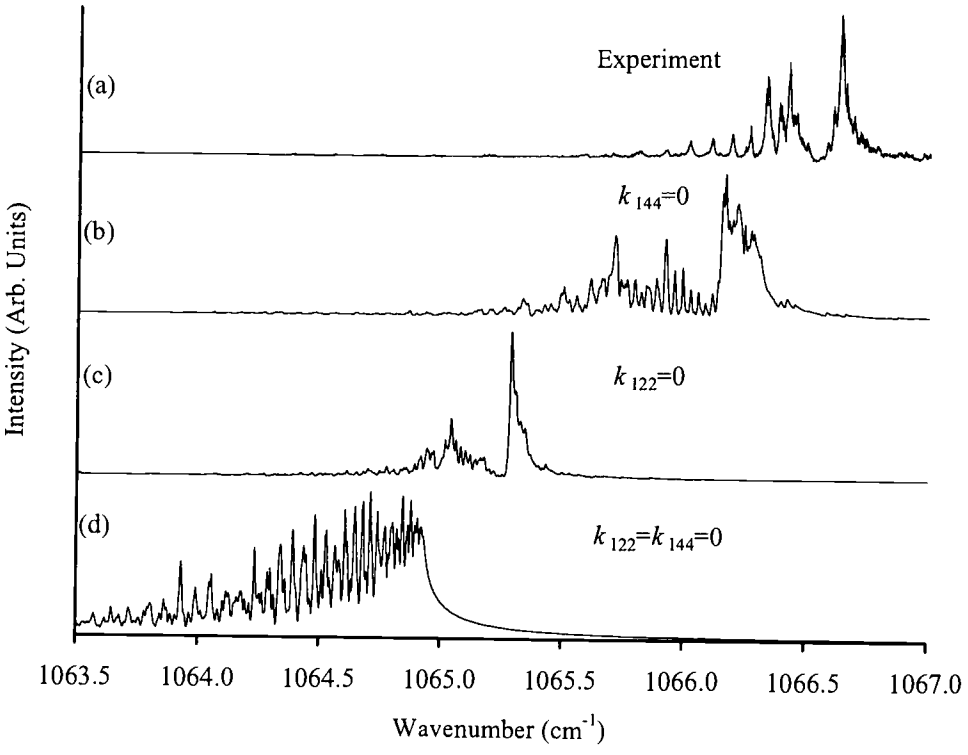

Fig. 2.5. Effect on the v_1 CARS spectrum (a, experimental spectrum) of setting the Fermi resonance constants k_{122} and k_{144} to zero (b-d, calculated spectra).

needed to reproduce the pattern of K subband structure, as shown in Figure 2.4. It is very pleasing that, aside from noise spikes, virtually every little wiggle in the CARS spectrum is duplicated in the calculated spectrum. The constants for ν_1 are given in Table 2.2 and agree with our expectation that the centrifugal distortion terms should be within a few percent of the values for the ground state.

In order to better display the effect of interactions among the various levels of SO_3 near the ν_1 fundamental, we show in Fig. 2.6 a reduced energy level diagram. This was calculated by subtracting the ground state energies from the upper state levels that are coupled for common J and k–l quantum numbers. To make a realistic comparison, the same ground state wavenumbers were subtracted from the $2\nu_4$ levels for each J value. With this definition, the reduced energy levels for ν_1 are the same wavenumbers as the Q-branch transitions expected for the CARS spectrum. The identification of states which are at least 50 % ν_1 or $2\nu_4(l=-2,0,+2)$ are indicated by unique symbols; those with no mixing component greater than 50 % are denoted as mixed states (+). From the calculated mixing of the levels it is clear that the major perturbers of ν_1 are the $l=-2$ and $l=0$ levels of $2\nu_4$, even though the $l=-2$ levels are not directly coupled to ν_1. The $l=\pm2$ levels are indirectly coupled to ν_1 through the l-type resonance with $l=0$ of $2\nu_4$, which in turn is coupled to ν_1 through the vibrational resonance term k_{144}. Mixing with $2\nu_2$ and $\nu_2+\nu_4$ levels was included in the calculation but these states are less perturbed and fall below the lower limit of the figure.

The level pattern is complex and clear regions of avoided crossings are apparent. For example for k–l=±15 levels, which are highlighted as bold dots, state switching occurs between $\nu_1(k=15,\ l=0)$ and $2\nu_4(k=13,\ l=-2)$ at J=18 and then between $\nu_1(k=15,\ l=0)$ and $2\nu_4(k=15,\ l=0)$ at J=36. An expanded view of the region corresponding to the ν_1 CARS spectrum is shown at the bottom of Fig. 2.7 and the first state switch for k–l=±15 is emphasized. It is clear from the level patterns that this and other avoided crossings produce the unusual gap in the CARS spectrum and that the horizontal clusterings of levels near K=J produce the distinct K subband structure. Marked

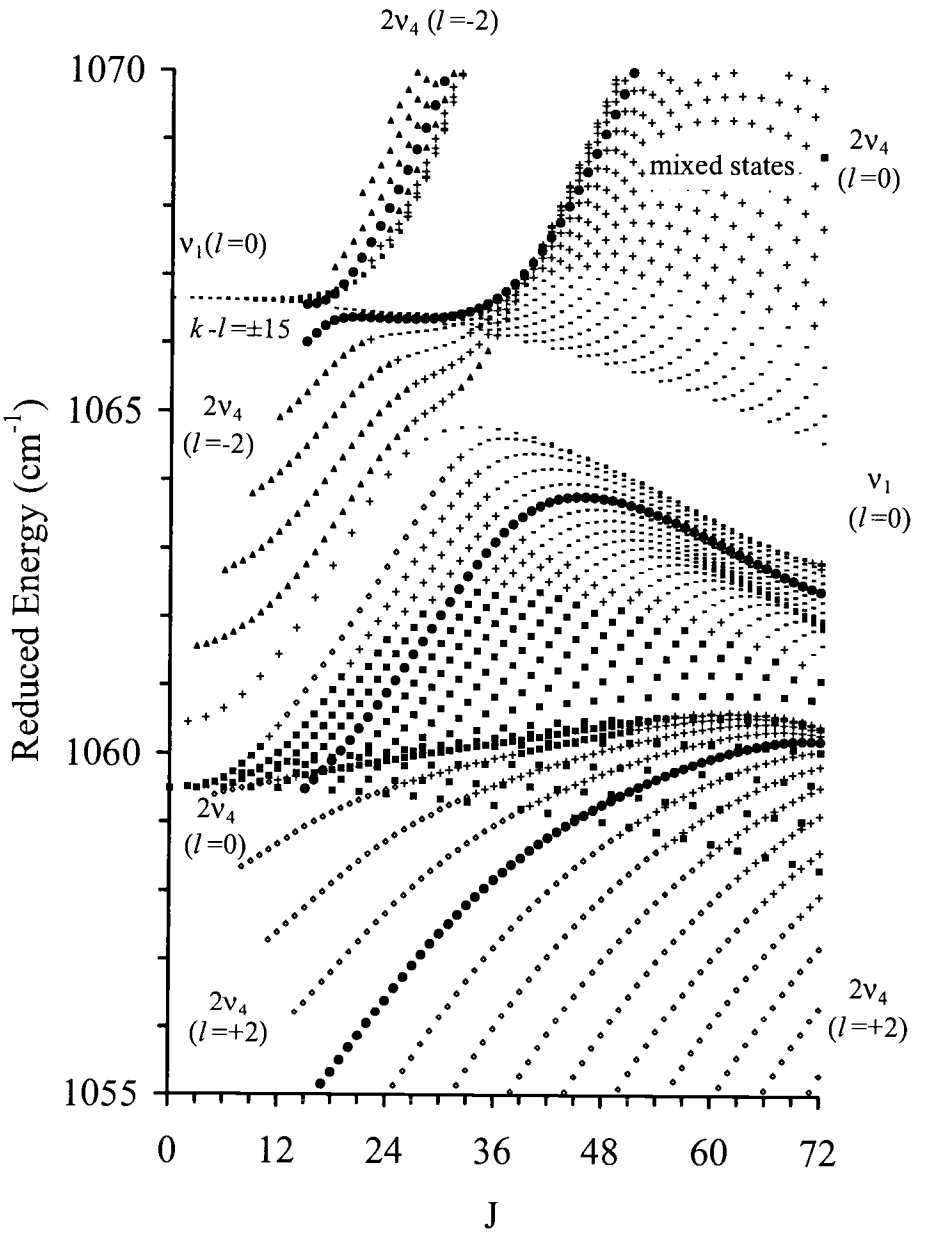

Fig. 2.6. Reduced energy diagram of Q-branch transitions from the ground state of $^{32}S^{16}O_3$ to ν_1 and its perturbing states. States identified as ν_1 (–), $2\nu_4$ (l=–2) (▲), $2\nu_4$ (l=0) (■), and $2\nu_4$ (l=+2) (◊) are at least 50% of the identified states. States that do not have any component greater than 50% are denoted as mixed states (+). K–l=15 (●) is emphasized to show the K structure.

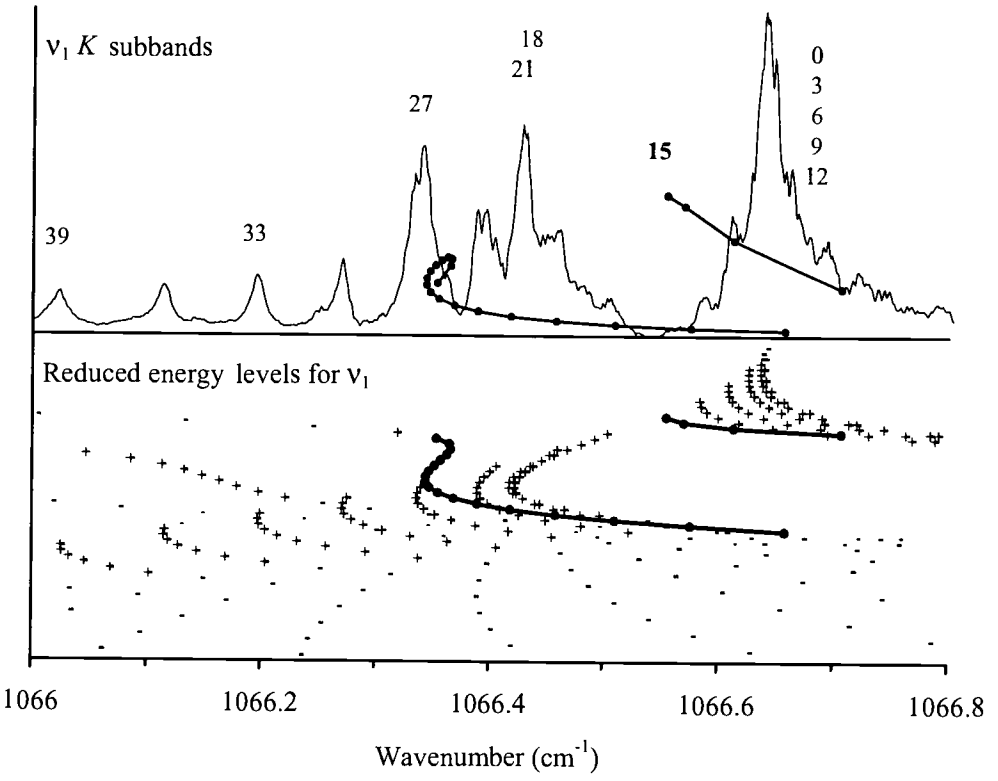

Fig. 2.7. Expanded view of Fig. 2.6 oriented to show how the levels (bottom) produce the pattern seen in the ν_1 CARS spectrum (top). Marked with a plus symbol are levels responsible for most of the CARS intensity (contribution greater than 10% of the line of maximum contribution). The production of the K subbands results from overlap of the strongest transitions (those with $J = K$, $K + 1$, $K + 2$,...). The $K = 15$ levels for ν_1 are highlighted to emphasize the avoided crossings that give rise to the unusual structure of the spectrum.

in this figure with a + symbol are levels which are most important in determining the CARS intensity.

2.6.2. Comparison of equivalent terms for different states

The ΔB and ΔC terms shown in Table 2.1 for $2\nu_2$, $\nu_2+\nu_4$, and $2\nu_4$ are in good agreement with the values found for ν_2 and ν_4. The ΔD terms for $2\nu_4$ are very close to what one would expect, *i.e.* twice the values of the ΔD terms for ν_4. The ΔD terms for $2\nu_2$ and $\nu_2+\nu_4$ are not so close to the expected values. However, we have found that if ΔD_{JK} is fixed at the values expected from ν_2 and ν_4, then the agreement for the ΔD_J and ΔD_K terms is much better and the RMS deviation is actually improved but by less than 2 %. In Table 2.1 we have preferred to leave all the ΔD terms floating even though it could be argued that fixing the ΔD_{JK} terms decreases the interdependence of the ΔD terms. The more constants that are fixed, the greater the burden that is placed on the remaining constants to fit the inevitable measurement errors.

As seen in Table 2.1, the values of q_4 are nearly the same for ν_4, $2\nu_4$, and $\nu_2+\nu_4$. The ζ_4 or $(C\zeta_4)$ terms as well as the η_J and η_K terms are also nearly the same for all three vibrational levels. As expected, the combination $(\eta_J + \eta_K)$ is even closer to being the same for all three levels, ranging from -0.370×10^{-7} to -0.380×10^{-7} cm^{-1}. Similarly, the Coriolis terms coupling ν_2 and ν_4, $\nu_2+\nu_4$ and $2\nu_2$, and $\nu_2+\nu_4$ and $2\nu_4$ are nearly the same.

In preliminary fits it was found that Q_4 is smaller than Q_3 by a factor of ten and ρ_{44} is on the order of 5×10^{-10} cm^{-1}. As indicated earlier, we have dropped ρ_{44} from the final fit. The criterion used was that we omitted those minor constants that were less than eight times their estimated uncertainty, thus eliminating Δ_2, Δ_{22}, and ρ_{44}. This was done in part to obtain the smallest set of significant constants for eventual comparison of parameters for different isotopomers.

From the fit alone, the signs of the q_4 terms could not be determined. It also was impossible to determine the absolute signs of the Fermi resonance constants although it was determined that the sign of k_{122} must be opposite to the sign of k_{144}. It also was not possible to

determine the sign of the ($B\zeta_{24}$) term. Thus that term can be multiplied by -1 as long as the z_{24J} and z_{24K} terms also are multiplied by -1.

Comparing the present results with the *ab initio* calculations of Martin (*5*), as shown in Table 2.4, indicates that our value of k_{144} is nearly identical to the *ab initio* value calculated by Martin. However our value of k_{122} is smaller by 12 percent and the sign of the x_{22} constant is opposite to that of Martin. This is a consequence of a strong correlation between k_{122} and the 020^00^0 ν_0 value that also produces the anomalously large uncertainty seen for the latter in Table 2.1. Since our deperturbation calculation of the 020^00^0 vibrational level is dependent on the value for k_{122}, we have also fit the data with the value of k_{122} fixed at the value given by Martin. That fit has a standard deviation that is only three percent worse than the fit with k_{122} floating but the vibrational levels are in better accord with the constants given by Martin. In particular, the value of x_{22} becomes +0.119 cm^{-1}. The other constants are only marginally different. In an attempt to better define k_{122}, CARS spectra were simulated for both choices but the resulting spectra were judged equally acceptable. It may be that analyses and calculations underway for the other isotopomers of SO_3 will clarify this matter.

2.7. ACKNOWLEDGEMENTS

We acknowledge support by the National Science Foundation and Oregon State University for the CARS work and analysis performed at OSU. The research described in this paper was performed, in part, in the Environmental Molecular Sciences Laboratory, a national scientific user facility sponsored by the Department of Energy's Office of Biological and Environmental Research and located at Pacific Northwest National Laboratory.

2.8. REFERENCES

1. E.t.H. Chrysostom, N. Vulpanovici, T. Masiello, J. Barber, J. W. Nibler, A. Weber, A. Maki, and T.A. Blake, *J. Mol. Spectrosc.* **210**, 233-239 (2001).

2. A. Maki, T.A. Blake, R.L. Sams, N. Vulpanovici, J. Barber, E.t.H. Chrysostom, T. Masiello, J.W. Nibler, and A. Weber, *J. Mol. Spectrosc.* **210**, 240-249 (2001).

3. A. Kaldor, A.G. Maki, A.J. Dorney, and I.M. Mills, *J. Mol. Spectrosc.* **45**, 247-252 (1973); N.F. Henfrey and B.A. Thrush, *Chem. Phys. Lett.* **102**, 135-138 (1983).

4. J. Ortigoso, R. Escribano, and A.G. Maki, *J. Mol. Spectrosc.* **138**, 602-613 (1989).

5. J.M.L. Martin, *Spectrochim. Acta Part A* **55**, 709-718 (2000), and private communication.

6. M.L. Orlov, J.F. Ogilvie, and J.W. Nibler, *J. Mol. Spectrosc.* **185**, 128-141 (1997).

7. V. Meyer, D.H. Sutter, and H. Dreizler, *Z. Naturforsch. A* **46**, 710-714 (1991).

8. A.J. Dorney, A.R. Hoy, and I.M. Mills, *J. Mol. Spectrosc.* **45**, 253-260 (1973)

HIGH RESOLUTION INFRARED STUDIES OF THE ν_2, ν_4 BANDS OF $^{34}S^{16}O_3$, INCLUDING BOTH INTENSITY AND WAVENUMBER PERTURBATIONS

Jeffrey Barber, Tony Masiello, Engelene t.H. Chrysostom, Joseph W. Nibler[1], Department of Chemistry, Oregon State University, Corvallis, OR 97331-4003; Arthur Maki, 15012 24th Ave. S.E., Mill Creek, WA 98012; Alfons Weber, National Science Foundation, Arlington, VA 22230, and National Institute of Standards and Technology, Gaithersburg, MD 20899; and Thomas A. Blake, Robert L. Sams, Pacific Northwest National Laboratory, P.O. Box 999, Mail Stop K8-88, Richland, WA 99352

Journal of Molecular Spectroscopy

Editorial Office

525 B Street, Suite 1900

San Diego, California 92101-4495

J. Mol. Spectrosc. **218**, 197-203 (2003)

[1] To whom correspondence should be sent.

3. HIGH RESOLUTION INFRARED STUDIES OF THE ν_2, ν_4 BANDS OF $^{34}S^{16}O_3$, INCLUDING BOTH INTENSITY AND WAVENUMBER PERTURBATIONS

3.1. ABSTRACT

The infrared spectrum of the ν_2, ν_4 bending mode region of ^{34}S-substituted sulfur trioxide, $^{34}S^{16}O_3$, has been recorded at a resolution of 0.0025 cm^{-1}. The ν_2 and ν_4 levels are coupled by a Coriolis interaction, yielding significant spectral shifts that have been successfully analyzed to obtain rovibrational constants for the ground state and both fundamentals. Comparisons are made with $^{32}S^{16}O_3$ parameters and the B_0 rotational constant is found to be 0.348 556 03(28) cm^{-1}, only very slightly larger than the corresponding value of 0.348 543 33(5) cm^{-1} for $^{32}S^{16}O_3$. Coriolis and *l*-type resonance interactions between the ν_2 and ν_4 levels produce frequency shifts and strong intensity perturbations in the spectra that are considered for both $^{34}S^{16}O_3$ and $^{32}S^{16}O_3$. The resulting analysis yields an average value of ±0.62(8) for the dipole derivative ratio $(\partial\mu^x/\partial Q_{4x})/(\partial\mu^z/\partial Q_2)$ and a positive sign for the product of this ratio with the ζ^y_{24} Coriolis constant, for which experiment gives ±0.5940(15). *Ab initio* calculations indicate that the signs of $\partial\mu^x/\partial Q_{4x}$ and $\partial\mu^z/\partial Q_2$ are both positive and hence ζ^y_{24} is also positive, in agreement with earlier calculations. These signs indicate that the effective charge movement in the *xz* plane has the same sense of rotation as Q_2, Q_{4x} atom motion in this plane that produces a p_y vibrational angular momentum component, correlated motion that is confirmed by *ab initio* calculations.

3.2. INTRODUCTION

Sulfur trioxide, SO_3, is a molecule of importance both industrially and environmentally and has been the subject of infrared and Coherent Raman studies by us and by others (*1-7*). Very recently, we reported the analysis of the high resolution spectra of $^{32}S^{16}O_3$, a case that proved challenging because of extensive mixing of some of the vibrational levels due to Fermi resonance and Coriolis interactions (*8*). From detailed analysis of 11 states and over 11 000 transitions, all observed perturbations were accounted for and accurate rovibrational constants were obtained for all four fundamental modes and for a number of combination/overtone levels. The constants determined for $^{32}S^{16}O_3$ are believed to be one of the most accurate and complete sets available for any nonlinear polyatomic molecule.

All previous high resolution studies have been on the $^{32}S^{16}O_3$ isotopomer since it is the most abundant form of SO_3. To fully characterize the spectral and physical properties of this "prototypical" symmetric top molecule, we are engaged in a comprehensive study of ^{34}S- and ^{18}O-substituted isotopomers; the $^{34}S^{16}O_3$ isotopic form is considered here. No prior experimental work has been performed on this isotopomer but estimates have been made of the fundamental frequencies in three previous force field calculations (*9-11*). Isotopic replacement by ^{34}S is especially advantageous since substitution takes place at the center of mass, leaving the ground state rotational constants and the ν_1 totally symmetric stretching frequency almost unchanged. Compared to substitution by ^{18}O, the spectra are not complicated by contributions from mixed isotopic species such as $S^{16}O^{18}O_2$ or $S^{16}O_2{}^{18}O$, hence they are more readily analyzed.

This paper presents the results of a detailed analysis of the infrared active bending mode fundamentals, ν_2 and ν_4, of $^{34}S^{16}O_3$. From a fitting of more than 7000 transitions, accurate rovibrational constants are obtained for the ν_2 and ν_4 levels and also for the ground state. Intensity perturbations arising from Coriolis coupling and *l*-type resonance have been examined, and a comparison between experiment and *ab initio* calculations is included.

3.3. EXPERIMENTAL DETAILS

The equipment and procedures used in these experiments are described in Ref. (7). The $^{34}S^{16}O_3$ sample was prepared by oxidation of elemental ^{34}S (99.8 %, Cambridge Isotope Laboratories[2]). Typically, 0.1 g ^{34}S and a small sheet of platinum foil were placed in a glass cylinder with a Teflon stopcock and heated at 50°C for an hour while pumping to remove any residual water. Excess gaseous $^{16}O_2$ was then added and the cylinder was sealed and heated at 450°C for 24 hours, the platinum serving to catalyze oxidation of the initial SO_2 product further to the desired SO_3 form (Contact process).

After cooling, a liquid nitrogen bath was used to freeze the sample and the remaining oxygen was pumped off. The sample was warmed to about −60°C and any residual SO_2 was removed, leaving sulfur trioxide remaining as a white solid form. Initial infrared spectra suggested a purity of about 70 % for the sulfur-34 isotopomer. The sulfur-32 contaminant is believed to be due to exchange with traces of $^{32}S^{16}O_3$ adsorbed on the walls and windows within the sample cell in previous experiments; the isotopic purity improved to about 90 % with flushing of the cell.

The final spectra were recorded at 25.00 ± 0.02°C at a pressure of 0.47 kPa (3.5 torr) using a gold-plated cell of 19.95 cm length that was fitted with AgCl windows. The wavenumber calibration was performed in the same way for $^{34}S^{16}O_3$ as described in our earlier paper (7) and it is estimated that the absolute accuracy of the wavenumber shifts for the different isotopomers is on the order of ±0.00015 cm^{-1}. The two measurements were made within a few days of each other.

---

[2] Certain commercial equipment, instruments, and materials are identified in the paper to adequately specify the experimental procedure. Such identification does not imply recommendations or endorsements by the National Institute of Standards and Technology, the National Science Foundation, or the Pacific Northwest National Laboratory (PNNL), nor does it imply that the materials or equipment identified are necessarily the best available for the purpose.

3.4. ANALYSIS OF THE SPECTRUM

3.4.1. The Ground State Constants

All of the measurements reported in this work were combined in a single least-squares fit. Of the 7156 assigned transitions, 5618 of these originated specifically from the ground state. This includes those for the infrared-active bands ν_3 and $2\nu_3$, which will be discussed in a future publication. The remaining transitions are for hot bands originating from ν_2 and ν_4 levels and these too will be discussed in a subsequent publication. The wavenumber values of all transitions will be provided here in a supplementary data file.

The expression used to fit the rotational constants of a nondegenerate vibrational state of quantum number v is

$$\begin{aligned} F_v(J,K) = {} & B_v J(J+1) + (C_v - B_v)K^2 - D^J_v J^2(J+1)^2 - D^{JK}_v J(J+1)K^2 \\ & - D^K_v K^4 + H^J_v J^3(J+1)^3 + H^{JK}_v J^2(J+1)^2 K^2 + H^{KJ}_v J(J+1)K^4 \\ & + H^K_v K^6 \pm \delta_{3K}\,\Delta_v[J(J+1)][J(J+1)-2][J(J+1)-6]. \end{aligned} \qquad [1]$$

The rotational constants are given by the power series

$$B_v = B_e - \sum_i \alpha_i^B (v_i + \tfrac{1}{2}d_i) + \ldots , \qquad [2]$$

with a similar equation for C_v. The rotational parameters are the standard ones, the only added constant being a small Δ_v splitting term which proved determinable for the K=3 levels of the ground state.

In the case of $^{32}S^{16}O_3$, microwave measurements (*12*) of rotational transitions in centrifugally-distorted molecules allowed the determination of C_0, D_K and H_K. These three parameters are not normally accessible from ordinary vibration-rotation spectroscopy and they could not be determined for the sulfur-34 isotopomer. For this reason, the value of C_0 was calculated assuming the same inertial defect as determined for the ground state of $^{32}S^{16}O_3$ (*8*), an approximation believed to be an improvement over the simple planarity assumption that $B_0 = 2C_0$. The constants D_K and H_K were determined using the planarity relations,

$$D_K = -(2D_J + 3D_{JK})/4 \quad [3]$$

$$H_K = -(3H_J + 4H_{JK} + 5H_{KJ})/6 \quad [4]$$

These planarity conditions are considered reasonable choices because they were found to be quite good in the case of $^{32}S^{16}O_3$. The resultant ground state constants are given in Table 3.1.

3.4.2. Analysis of the ν_2 and ν_4 bands

Infrared spectra for $^{34}S^{16}O_3$ in the bending mode region are shown in Figures 3.1 and 3.2. The experimental trace (b) of Fig. 3.1 shows the well-developed *P-Q-R* structure of both the ν_2 and ν_4 bands while Fig. 3.2 shows an expanded portion of the ν_4 band. Although the experimental spectrum is "rich", one is still able to make out the regular structure arising from different subbands originating from K=3 to 9 levels of the ground state. Calculated stick spectra are shown in Fig. 3.2 for ^pQ, ^rR, and ^pR transitions for these K values. The regularity of the ^pQ branches made these assignments straightforward and the absence of Q branches for K not equal to a multiple of three is apparent, as expected from nuclear spin considerations. The change in intensities in the ^rR branch as K increases is quite noticeable, aiding in identification, while the weaker ^pR branch for K=3 can be seen growing in intensity as J increases.

The rovibrational analysis of $^{34}S^{16}O_3$ was performed in the same fashion as done in our previous study (*7*) of the parent isotopomer $^{32}S^{16}O_3$. A 3 × 3 energy matrix is necessary to properly account for the strong Coriolis interaction between ν_2 and ν_4. The matrix used here is of the form

$$\begin{array}{c|ccc|} & |\psi_{4+}\rangle & |\psi_2\rangle & |\psi_{4-}\rangle \\ & E_1 & W_{1,1} & W_{2,2} \\ & W_{1,1} & E_2 & W_{1,1} \\ & W_{2,2} & W_{1,1} & E_3 \end{array}$$

Table 3.1. Ground-State Rotational Constants in cm^{-1}

	$^{32}S^{16}O_3$ [a]	$^{34}S^{16}O_3$
C_0	0.173 988 132(27)[b]	[0.173 994 475][c]
B_0	0.348 543 328(54)	0.348 556 028(275)
$D_J \times 10^7$	3.108 56(47)	3.106 22(205)
$D_{JK} \times 10^7$	−5.492 15(57)	−5.488 90(414)
$D_K \times 10^7$	2.568 79(29)	[2.564][d]
$H_J \times 10^{12}$	0.676(11)	0.645(49)
$H_{JK} \times 10^{12}$	−2.630(23)	−2.442(127)
$H_{KJ} \times 10^{12}$	3.233(31)	2.884(93)
$H_K \times 10^{12}$	−1.273(21)	[−1.1][e]
$\Delta_0 \times 10^{14}$	−0.67(12)	−0.30(23)

[a] From Ref. (*8*).
[b] The uncertainties in the last digits (twice the standard deviation) are given in parentheses.
[c] The value of C_0 for $^{34}S^{16}O_3$ was calculated assuming the inertial defect is the same as that in $^{32}S^{16}O_3$.
[d] The value of D_K was calculated using the planarity condition.
[e] The value of H_K was calculated using the planarity condition.

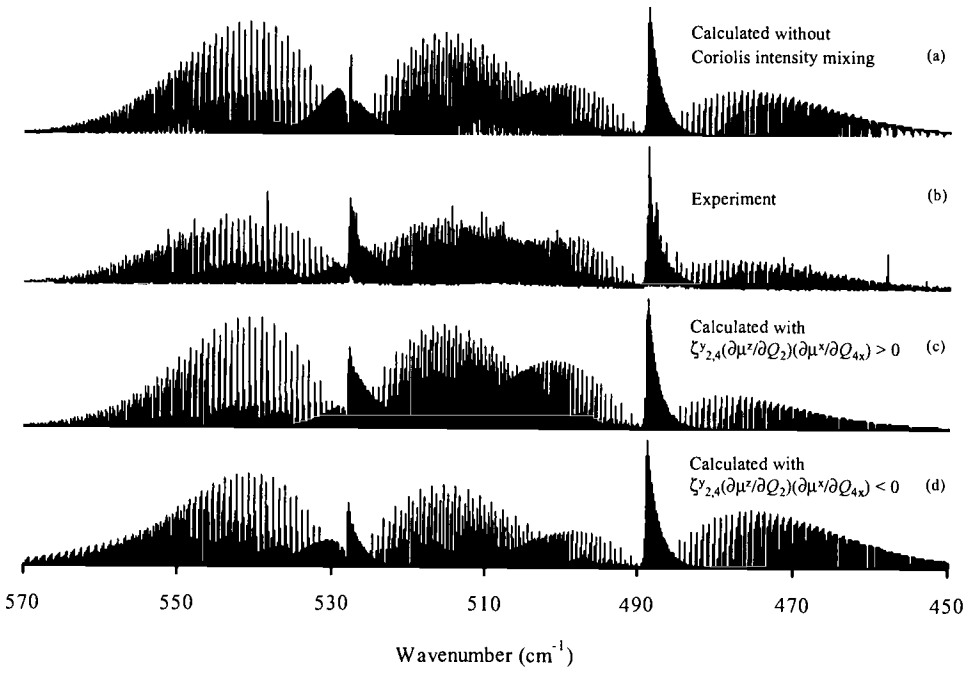

Figure 3.1. Experimental spectra of ν_2 and ν_4 for $^{34}S^{16}O_3$ and calculated spectra showing the intensity effect of Coriolis coupling between these vibrational modes. Trace (b) is the experimental spectrum while (a) shows a calculated stick spectrum in which intensity mixing is neglected. Traces (c) and (d) include the mixing with positive and negative signs, respectively, for the intensity perturbation parameter defined in the text.

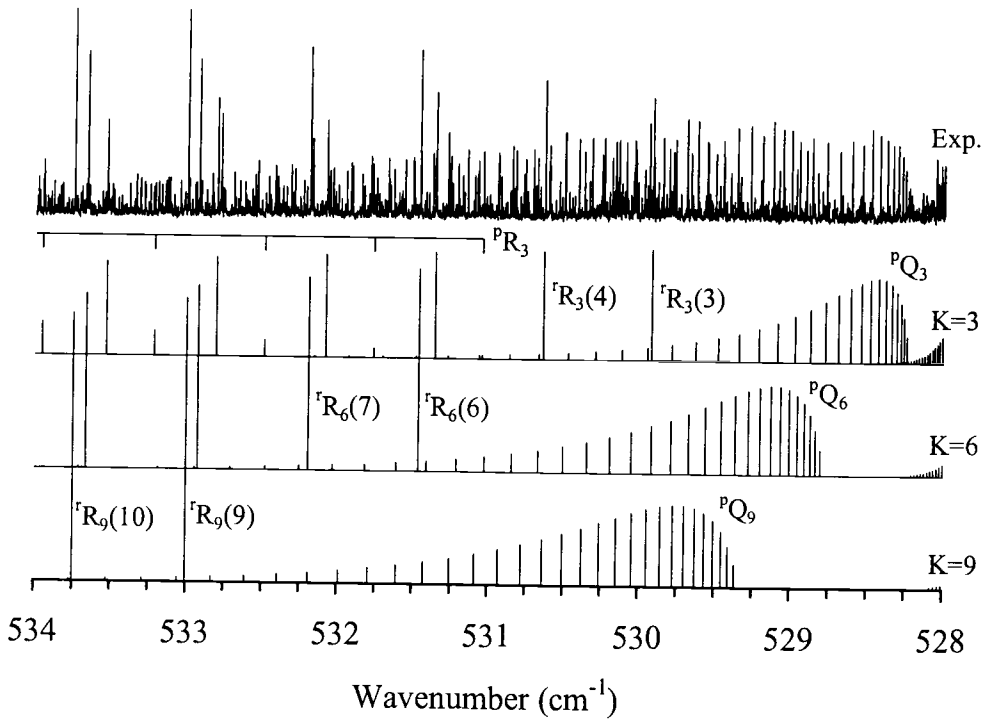

Figure 3.2. View of the ν_4 $^{P}Q/R/^{P}R$ region of the spectrum from 528 cm^{-1} to 534 cm^{-1}, along with calculated stick spectra for ν_4 subbands K=3 through 9. The first two J lines for each ^{r}R sequence have been labeled.

with $E_1 = E(\nu_4, J, k \pm 1, l_4 \pm 1)$, $E_2 = E(\nu_2, J, k, l_4 = 0)$, $E_3 = E(\nu_4, J, k \mp 1, l_4 \mp 1)$,

$$E(\nu, J, k, l) = G(\nu, l) + F(J, K) + F_{\perp}(J, k, l). \quad [5]$$

Here, k is a signed quantum number, $G(\nu, l)$ is the usual vibrational term value, and the band centers are defined as

$$\nu_0 = G(\nu, l)' - G(0, 0)''. \quad [6]$$

$F(J, K)$ is given by Eq. [1] and, for the degenerate ν_4 levels, the following term is added

$$F_{\perp}(J, k, l) = -2(C\zeta_{\nu})kl + \eta^{J}_{\nu}J(J+1)kl + \eta^{K}_{\nu}k^3 l \pm \delta_{2K}\, t_{\nu}[J(J+1)][J(J+1) - 2]. \quad [7]$$

In this equation, the t_ν term describes a small splitting for the K=2 levels of ν_4, with the upper sign used for even J-levels and the lower sign for odd J-levels.

The off-diagonal matrix element, $W_{2,2}$, is a l-type resonance term that couples the $l_4 = \pm 1$ levels of ν_4 and is defined as

$$\begin{aligned} W_{2,2} &= \langle \nu_4, J, k, l_4 \,|\, \mathrm{H} \,|\, \nu_4, J, k \pm 2, l_4 \pm 2 \rangle \\ &= \tfrac{1}{4}[q_4 + q^{J}_{4}J(J+1) + q^{JJ}_{4}J^2(J+1)^2][(\nu_4+1)^2 - (l_4 \pm 1)^2]^{1/2}[J(J+1) - k(k \pm 1)]^{1/2} \\ &\quad \times [J(J+1) - (k \pm 1)(k \pm 2)]^{1/2}. \end{aligned} \quad [8]$$

As discussed in References (*2*), (*5*), and (*7*), the ν_2 and ν_4 levels are coupled by a strong Coriolis interaction that can be described by the off-diagonal term

$$\begin{aligned} W_{1,1} &= \langle \nu_2, \nu_4, J, k \pm 1, l_4 \pm 1 \,|\, H \,|\, \nu_2 + 1, \nu_4 - 1, J, k, l_4 \rangle \\ &= \pm[(B\zeta^{y}_{24}) + z_{24J}J(J+1) + z_{24K}k(k \pm 1)]\,[(\nu_2+1)(\nu_4 \pm l_4 + 1)]^{1/2} \\ &\quad \times [J(J+1) - k(k \pm 1)]^{1/2}. \end{aligned} \quad [9]$$

This interaction produces appreciable frequency shifts in the spectra; in Figure 3.2, for example, its neglect produces a shift of –0.05 cm^{-1} in the line labeled $^{r}R_9(9)$. The $^{P}Q_K$ Q-branch structure of ν_4 is even more dependent on $W_{1,1}$. $^{P}Q_9(9)$ and $^{P}Q_9(40)$, experimentally found to be separated by 4.40 cm^{-1}, would be only 0.07 cm^{-1} apart and in reversed order if the Coriolis interaction were absent. Clearly, it is necessary to properly take the $W_{1,1}$ and $W_{2,2}$ interactions into account to avoid incorrect assignments of the transitions.

The $W_{1,1}$ term also causes significant perturbations to the intensities. DiLauro and Mills (*13*) have discussed such effects and we follow their approach in our intensity analysis of the ν_2, ν_4 spectra. Basically, the coupling serves to mix the three excited-state basis functions to yield three combined states, each of the form

$$\psi' = a\psi_{4+}' + b\psi_2' + c\psi_{4-}'. \qquad [10]$$

For a transition from the ground state to one of these, the intensity is proportional to the square of the transition moment

$$\langle\psi''|\mu|\psi'\rangle^2 = [a\langle\psi''|\mu|\psi_{4+}'\rangle + b\langle\psi''|\mu|\psi_2'\rangle + c\langle\psi''|\mu|\psi_{4-}'\rangle]^2. \qquad [11]$$

By expanding the dipole operator in terms of Q_2 and Q_4 normal coordinates, it can be shown (*13*) that the cross-terms give rise to interference effects that can be modeled to determine the sign and value of the product $(\zeta^y_{24})(\partial\mu^z/\partial Q_2)(\partial\mu^x/\partial Q_{4x})$. We present below such an analysis for both $^{32}S^{16}O_3$ and $^{34}S^{16}O_3$ isotopomers.

3.5. DISCUSSION

3.5.1. The Ground State Constants

Not surprisingly, the ground state rotational parameters of the sulfur-32 and 34 isotopomers are very similar in value. The $^{34}S^{16}O_3$ B_0 value is 0.348 556 03(28) cm^{-1}, 0.000 013 cm^{-1} larger than the corresponding value for $^{32}S^{16}O_3$. The uncertainties (2σ) are much less than this difference, indicating that the vibrational α_i^B corrections are significantly different for the two isotopomers. The r_0 value 141.979 406(58) pm calculated from B_0 is accordingly smaller than the corresponding $^{32}S^{16}O_3$ value of 141.981 993(11) pm. Within the uncertainties, the D_J centrifugal distortion constants are identical for both isotopomers, as are the D_{JK} parameters. Similarly, the higher order centrifugal distortion corrections H_J, H_{JK} and H_{KJ}, and Δ_0, the K=3 splitting term, are almost unchanged and are of reasonable magnitude. For all parameters, the uncertainties are about five

times larger for the 34-isotopomer, a consequence of the smaller number of lines fit and also the absence of microwave data. Due to the latter absence, no determination of C_0, D_K, or H_K was possible and these were fixed using the assumptions described earlier.

3.5.2. Constants for ν_2 and ν_4

The parameters determined for the 010^00^0 and 000^01^1 states are given in Table 3.2. The fit of ν_2 and ν_4 also included transitions for the hot bands 020^00^0–010^00^0, 010^01^1–010^00^0, 010^01^1–000^01^1, 000^02^0–000^01^1, and 000^02^2–000^01^1. This was done to obtain the most accurate constants possible and to facilitate comparison with $^{32}S^{16}O_3$ parameters, for which the fitting also included hot bands (*8*). As mentioned earlier, the details of the analysis for $^{34}S^{16}O_3$ of these hot bands and their coupling to the ν_1 mode will be presented in a separate publication.

The most noticeable change upon isotopic substitution of sulfur is the vibrational shift in the band centers, as expected. For the a_2'' out-of-plane bend the ν_2 values are 497.57 and 488.80 cm^{-1} for 32 and 34 isotopomers respectively, each about 1 cm^{-1} lower than corresponding *ab initio* values of 498.6 and 489.8 cm^{-1} calculated by Martin (*11*). The experimental ν_2 ratio is 0.9824, slightly larger than the 0.9822 ratio calculated from the *G*-matrix relation $G_{22} = 9(1/M_O + 3/M_S)/(4r^2)$ that applies for purely harmonic motion. For the e' in-plane bend the ν_4 values are 530.09 and 527.68 cm^{-1} and the near unity value of the frequency ratio, 0.9977, indicates significantly less sulfur motion for this vibrational mode. The ν_4 values are again in good accord with the *ab initio* values of Martin, which are 528.2 and 525.7 cm^{-1} for the respective isotopomers (*11*).

Like the ground state, the rotational constants for the ν_2 and ν_4 levels are little changed by isotopic substitution for the sulfur. For the out-of-plane bend, the vibration-rotation coupling constants $\alpha_2^B = -\Delta B_2$ and $\alpha_2^C = -\Delta C_2$ are both negative, as expected since movement of the sulfur atom above or below the plane will tend to drag the O atoms towards the c axis, thus reducing the inertial moment about the c (and apparently b) axes. For the in-plane bend, an opposite positive sign is seen for α_4^B and α_4^C, suggesting that there is an extension of the SO bond length as bending occurs. It is noteworthy that the uncertainties for α_2^B and α_4^B are two orders of magnitude larger

Table 3.2. The Rovibrational Constants in cm^{-1} for ν_2 and ν_4

	$^{32}S^{16}O_3$ [a]	$^{34}S^{16}O_3$
ν_2		
ν_0	497.567 736(16)[b]	488.799 189(17)
ΔC[c] $\times 10^3$	0.127 783(42)	0.125 693(114)
$\Delta B \times 10^3$	0.804 0(49)	0.769 1(221)
$\Delta D_J \times 10^{10}$	18.35(38)	19.10(34)
$\Delta D_{JK} \times 10^{10}$	−23.34(88)	−25.05(123)
$\Delta D_K \times 10^{10}$	6.28(59)	7.28(111)
$\Delta H_J \times 10^{13}$	−0.673(72)	[−0.67][d]
$\Delta H_{JK} \times 10^{13}$	2.86(23)	2.52(34)
$\Delta H_{KJ} \times 10^{13}$	−4.11(27)	−3.12(59)
$\Delta H_K \times 10^{13}$	1.93(11)	1.27(28)
Number of transitions	2921	1743
RMS Deviation	0.00012 cm^{-1}	0.00013 cm^{-1}
ν_4		
ν_0	530.086 424(14)	527.681 547(13)
$\Delta C \times 10^3$	−0.157 285(28)	−0.161 791(59)
$\Delta B \times 10^3$	−0.075 2(25)	−0.063 1(110)
$\Delta D_J \times 10^{10}$	10.73(32)	10.33(25)
$\Delta D_{JK} \times 10^{10}$	−38.24(66)	−37.29(70)
$\Delta D_K \times 10^{10}$	28.10(39)	27.47(57)
$\Delta H_J \times 10^{13}$	0.516(70)	[0.52]
$\Delta H_{JK} \times 10^{13}$	−2.23(21)	−2.07(18)
$\Delta H_{KJ} \times 10^{13}$	3.15(24)	2.73(32)
$\Delta H_K \times 10^{13}$	−1.421(91)	−1.168(151)
$(C\zeta_4)$	−0.085 195 2(11)	−0.082 001 1(53)
$\eta_J \times 10^7$	−9.06(14)	−8.33(54)
$\eta_K \times 10^7$	8.69(14)	7.95(54)
$q \times 10^4$	4.616(49)	4.307(221)
$(B\zeta^y_{24})$	0.200 57(10)	0.207 06(52)
$z_{24J} \times 10^7$	−5.013(31)	−4.848(127)
$z_{24K} \times 10^7$	3.354(11)	3.437(29)
$t_4 \times 10^{11}$	9.5(11)	11.8(17)
Number of transitions	4383	2437
RMS Deviation	0.00011 cm^{-1}	0.00011 cm^{-1}

[a] From Ref. (*8*).
[b] The uncertainties in the last digits (twice the standard deviation) are given in parentheses.
[c] The value of C_0 for $^{34}S^{16}O_3$ was calculated assuming the inertial defect is the same as that in $^{32}S^{16}O_3$.
[d] The value of D_K was calculated using the planarity condition.
[e] The value of H_K was calculated using the planarity condition.

than for α_2^C and α_4^C. This is a consequence of the strong correlation between these constants and has been discussed previously for $^{32}S^{16}O_3$ (*7*, *13*). Taking the covariance between these parameters into account, one finds a greatly reduced uncertainty for the linear combination $\frac{1}{2}\alpha_2^B + \alpha_4^B$ = –0.000 321 428(65) cm^{-1}, a fortunate result since this combination is needed in correcting B_0 to the equilibrium B_e value.

In general, since fewer lines were fitted than for $^{32}S^{16}O_3$, the constants for $^{34}S^{16}O_3$ are not determined to the same accuracy, although they are still of high quality. The $C\zeta_4$, q, ΔD and ΔH constants were essentially the same for both isotopomers but, in the case of ΔH_J for $^{34}S^{16}O_3$, the value was poorly determined so it was set equal to that of the value for $^{32}S^{16}O_3$ times the ratio of ground state H_J values. The $B\zeta^y_{24}$ term responsible for coupling of the ν_2 and ν_4 levels was about 0.20 cm^{-1} for both isotopomers and, as mentioned earlier, its inclusion in the fit was essential to an accurate modeling of both transition frequencies and intensities of the spectra.

3.5.3. Intensity Perturbations

The effect of the $B\zeta^y_{24}$ term on intensities can be seen in Fig. 3.1 by comparing the experimental trace (b) with (a), the stick spectrum calculated by ignoring the cross terms in Eq. [11] (mixing of the $\pm l$ states of ν_4 by the q l-type resonance term is included however). Clearly, the Q branch structure of ν_4 near 530 cm^{-1} does not match that of the experiment nor are the relative P and R branch intensities of ν_2 reproduced. DiLauro and Mills (*13*) have discussed the need to account for the Coriolis perturbations to rovibrational line intensities of molecules, and Kaldor *et al.* (*3*) previously fit the band contours of the ν_2 and ν_4 modes of $^{32}S^{16}O_3$. For SO_3, the perturbations depend most heavily (*13*) on the quantity $(\zeta^y_{24})(\partial\mu^z/\partial Q_2)(\partial\mu^x/\partial Q_{4x})$, referred to as the "intensity perturbation product" in the remainder of this paper.

We have gone beyond the rough contour-fitting procedure of Kaldor *et al.* by performing a least-squares fit of individual line intensities for 2743 and 2024 transitions of $^{32}S^{16}O_3$ and $^{34}S^{16}O_3$ respectively. Peak line intensities were used and only transitions employed in the fitting of the rovibrational constants were included. Only well-defined lines that fell within a range of 0.1 to 1.5

absorbance units were utilized and any lines thought to be overlapped (width greater than 0.002 cm^{-1}) were excluded. The intensities were calculated by including all mixing terms in Eq. [11], along with the usual Boltzmann and line strength factors. Because the absorption cell was carefully temperature controlled, the uncertainty in the temperature of the gas is only a minor contributor to the uncertainty in the intensity measurement. The most important source of error is expected to be our estimate of the line intensities from measurements of the peak intensities of each line. Since the intensity measurements for each isotopomer were taken from a single FTS spectrum, the uncertainty in the pressure of the gas did not contribute to the error in the estimate of the ratio of the dipole derivatives.

The program used to calculate the line intensities (SymCalc) is a greatly modified version of the program used by Kaldor *et al.* (3) which in turn was developed by Mills and coworkers. The fitting gives the sign of the intensity perturbation product, as well as the absolute ratio of the dipole derivatives.

Figure 3.3 shows for both isotopomers plots of reduced χ^2 as the ratio $|(\partial\mu^x/\partial Q_{4x})/(\partial\mu^z/\partial Q_2)|$ was varied in our intensity analysis. In this figure χ^2 is the sum of $(I_{calc}-I_{exp})^2$ values, normalized such that the minimum value of reduced χ^2 for each isotopomer is equal to unity. As seen in this figure, double minima are produced which correspond to ratios of ±0.64(8) for $^{32}S^{16}O_3$ and ±0.61(8) for $^{34}S^{16}O_3$. For the sulfur-32 isotopomer, our value is in good agreement with a ratio of ±0.7 determined by Kaldor *et al.* in fitting the overall band contours. We have also calculated this ratio in *ab initio* computations using Gaussian 98 (*14*) and obtain a similar, but somewhat larger, value of ±0.84 for a 6-311G** basis set at the B3LYP level. In no case is the sign of the dipole derivative ratio determined from experiment, nor is it in the present work. The lower reduced χ^2 minimum shown in Fig. 3.2 for a positive dipole derivative ratio is misleading since a positive value has been assumed for ζ^y_{24} in the calculations. In fact, the intensity modeling simply determines that the sign of the product $(\zeta^y_{24})(\partial\mu^z/\partial Q_2)(\partial\mu^x/\partial Q_{4x})$ is positive. A direct visual confirmation is seen in Fig. 3.1, where the overall fit for positive sign (trace c) is clearly better than

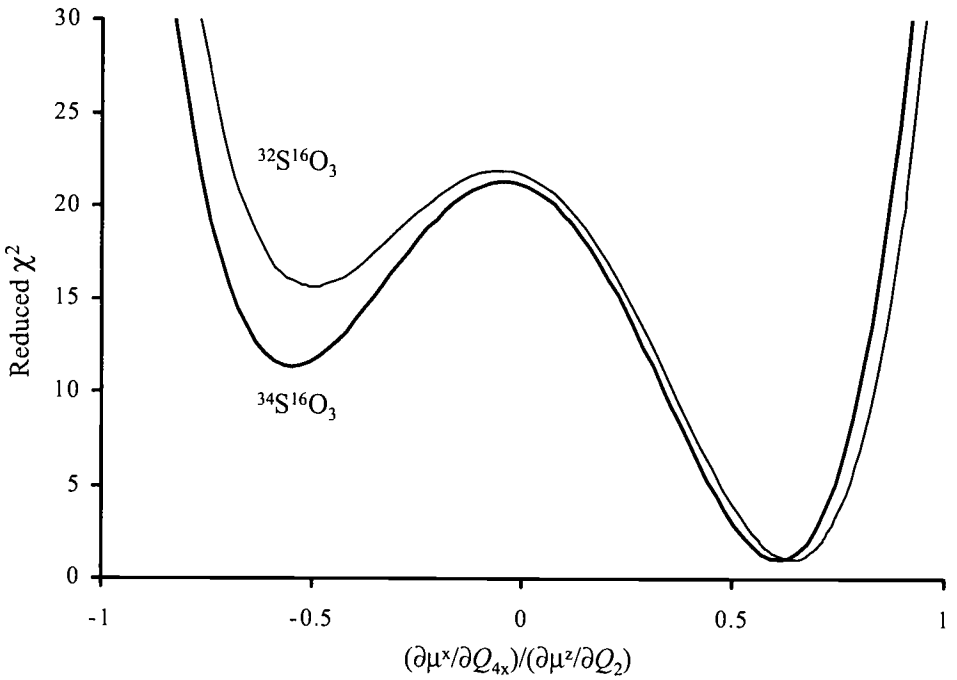

Figure 3.3. Plot of Reduced χ^2 versus $(\partial\mu^x/\partial Q_{4x})/(\partial\mu^z/\partial Q_2)$ for the least-squares fitting of experimental intensities for $^{32}S^{16}O_3$ and $^{34}S^{16}O_3$. For the latter, the two minima occur at +0.61 and –0.61 and yield the calculated traces c and d respectively in Fig. 3.1.

that for negative sign (trace d). In particular, the relative intensities of the ν_2 ^qP and ^qR branches gives the best indication as to which sign is correct. We note that the intensities of the different ν_2, ν_4 branches are in good accord with the relative intensity predictions in Table III of DiLauro and Mills. (*13*)

Although the signs of the dipole derivatives are not directly accessible from experiment, they can be deduced from *ab initio* calculations of the dipole moment as the molecule is distorted from the equilibrium geometry along the Q_2 and Q_{4x} coordinates. Fig. 3.4 shows the coordinates Q_2, taken to be positive for displacement of the sulfur along the positive z-axis and Q_{4x}, taken to be positive for an increase of the angle α_1. The dipole moment is taken as positive when the dipole points to the positive end of the charge asymmetry. With these definitions, a B3LYP Gaussian calculation with a 6-311G** basis set indicates that $(\partial\mu^z/\partial Q_2)$ and $(\partial\mu^x/\partial Q_{4x})$ are both positive (the same signs are also obtained for other level and basis set choices). The sense of the transition dipoles are indicated in the figure and it is seen that these are consistent with the simple conceptual picture of movement of a positively-charged sulfur atom relative to negatively-charged oxygen atoms. Since the overall perturbation term $(\zeta^y_{24})(\partial\mu^z/\partial Q_2)(\partial\mu^x/\partial Q_{4x})$ is positive, these results indicate that the ζ^y_{24} term is of positive sign. It is gratifying that this sign agrees with that deduced, not from intensity considerations, but from force field calculations by Dorney, Hoy and Mills (*15*) and by Martin (*11*).

Finally, we note that, by analogy with the arguments of DiLauro and Mills (*13*), the overall positive sign of the intensity perturbation product implies that the direction of rotation of effective charge in the xz plane is the same as that for the atom motion in the Q_2 and Q_{4x} modes that produces the p_y vibrational angular momentum component, i.e. both clockwise or both counterclockwise. This has been confirmed by our *ab initio* calculations, in which the direction of rotation of the dipole moment was found to follow that of atom displacements that produces a clockwise rotational motion such as that depicted in Fig. 3.4.

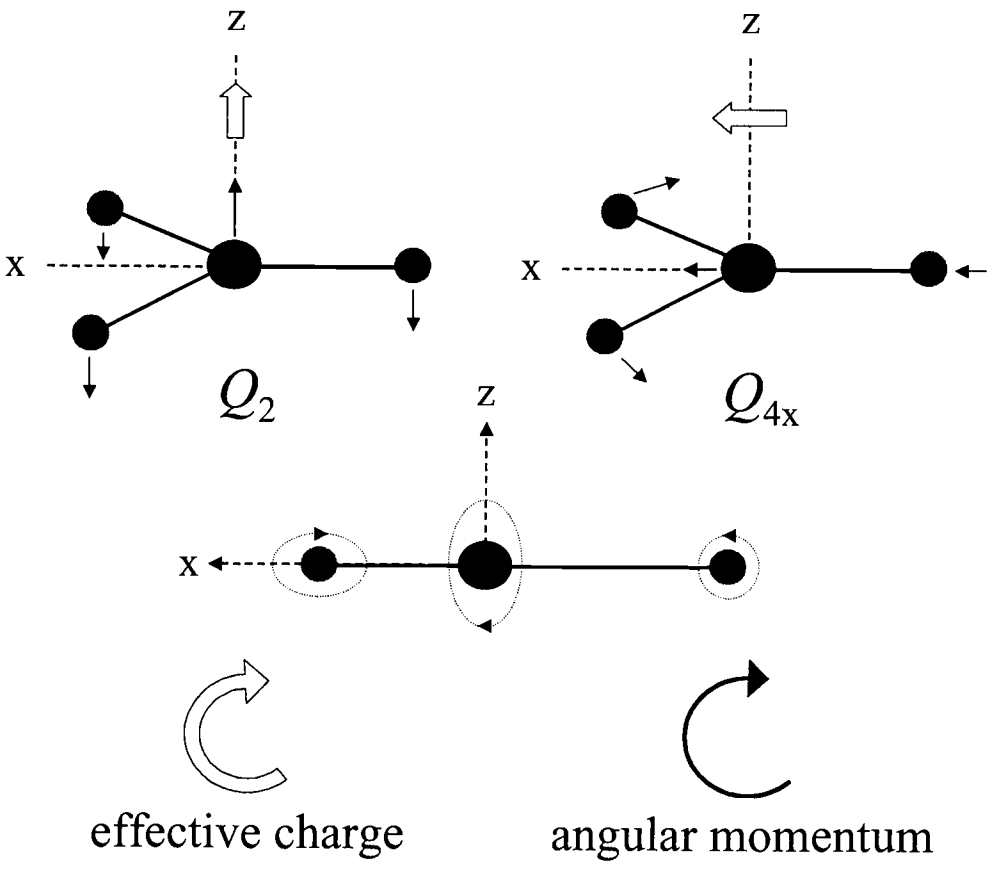

Figure 3.4. Cartesian displacements and effective charge displacements in Q_2 and Q_{4x} of SO_3, showing the sign relation between the dipole moment derivatives. Positive values of Q_2 and Q_{4x} are indicated by the arrows on the atoms and *ab initio* calculations give the transition dipole directions shown in the figure, with the dipole taken as positive when the arrow points to the positive charge. The coupling of Q_{2z} and Q_{4x} by the $B\zeta^{y}_{24}$ term produces a p_y component of vibrational angular momentum. The bottom figure shows that for p_y corresponding to a net clockwise motion of the atoms in the *xz* plane, a similar clockwise rotation of the effective charge (dipole moment) is predicted from both experimental and *ab initio* results.

3.6. ACKNOWLEDGEMENTS

We acknowledge support by the National Science Foundation and Oregon State University for the CARS work and analysis performed at OSU. The research described in this paper was performed, in part, in the Environmental Molecular Sciences Laboratory, a national scientific user facility sponsored by the Department of Energy's Office of Biological and Environmental Research and located at Pacific Northwest National Laboratory.

3.7. REFERENCES

1. J.B. Milne and A. Ruoff, *J. Mol. Spectrosc.* **23**, 408-415 (1967).
2. A. Kaldor and A.G. Maki, *J. Mol. Struct.* **15**, 123-130 (1973).
3. A. Kaldor, A.G. Maki, A.J. Dorney, and I.M. Mills, *J. Mol. Spectrosc.* **45**, 247-252 (1973).
4. N.F. Henfrey and B.A. Thrush, *Chem. Phys. Lett.* **102**, 135-138 (1983).
5. J. Ortigoso, R. Escribano, and A.G. Maki, *J. Mol. Spectrosc.* **138**, 602-613 (1989).
6. E.t.H. Chrysostom, N. Vulpanovici, T. Masiello, J. Barber, J.W. Nibler, A. Weber, A.G. Maki, and T.A. Blake, *J. Mol. Spectrosc.* **210**, 233-239 (2001)
7. A. Maki, T.A. Blake, R.L.Sams, N. Vulpanovici, J. Barber, E.t.H. Chrysostom, T. Masiello, J.W. Nibler, and A. Weber, *J. Mol. Spectrosc.* **210**, 240-249 (2001)
8. J. Barber, E.t.H. Chrysostom, T. Masiello, J.W. Nibler, A. Maki, A Weber, T.A. Blake and R.L. Sams, *J. Mol. Spectrosc.* **216**, 105-112 (2002)
9. L.H. Jones, *Acta. Chem. Scand.* **23**, 335 (1969).
10. S.X. Weng, O.S. Binbrek, and A. Anderson, *Spectrosc. Lett.* **24**, 959-973 (1991).
11. J.M.L. Martin, *Spectrochim. Acta. Part A* **55**, 709-718 (2000), and private communication.
12. V. Meyer, D.H. Sutter, and H. Dreizler, *Z. Naturforsch. A* **46**, 710-714 (1991).
13. C. DiLauro and I.M. Mills, *J. Mol. Spectrosc.* **21**, 386-413 (1966).

14. Gaussian 98, Revision A.9, M. J. Frisch, G. W. Trucks, H. B. Schlegel, G. E. Scuseria, M. A. Robb, J. R. Cheeseman, V. G. Zakrzewski, J. A. Montgomery, Jr., R. E. Stratmann, J. C. Burant, S. Dapprich, J. M. Millam, A. D. Daniels, K. N. Kudin, M. C. Strain, O. Farkas, J. Tomasi, V. Barone, M. Cossi, R. Cammi, B. Mennucci, C. Pomelli, C. Adamo, S. Clifford, J. Ochterski, G. A. Petersson, P. Y. Ayala, Q. Cui, K. Morokuma, D. K. Malick, A. D. Rabuck, K. Raghavachari, J. B. Foresman, J. Cioslowski, J. V. Ortiz, A. G. Baboul, B. B. Stefanov, G. Liu, A. Liashenko, P. Piskorz, I. Komaromi, R. Gomperts, R. L. Martin, D. J. Fox, T. Keith, M. A. Al-Laham, C. Y. Peng, A. Nanayakkara, M. Challacombe, P. M. W. Gill, B. Johnson, W. Chen, M. W. Wong, J. L. Andres, C. Gonzalez, M. Head-Gordon, E. S. Replogle, and J. A. Pople, Gaussian, Inc., Pittsburgh PA, 1998.

15. A.J. Dorney, A.R. Hoy, and I.M. Mills, *J. Mol. Spectrosc.* **45**, 253-260 (1973).

ANALYSIS OF THE ν_2, ν_4 INFRARED HOT BANDS AND ν_1 CARS SPECTRUM OF $^{34}S^{16}O_3$

Jeffrey Barber, Engelene t.H. Chrysostom, Tony Masiello, Joseph W. Nibler[1], Department of Chemistry, Oregon State University, Corvallis, OR 97331-4003; Arthur Maki, 15012 24th Ave. S.E., Mill Creek, WA 98012; Alfons Weber, National Science Foundation, Arlington, VA 22230, and National Institute of Standards and Technology, Gaithersburg, MD 20899; and Thomas A. Blake, Robert L. Sams, Pacific Northwest National Laboratory, P.O. Box 999, Mail Stop K8-88, Richland, WA 99352

Journal of Molecular Spectroscopy

Editorial Office

525 B Street, Suite 1900

San Diego, California 92101-4495

J. Mol. Spectrosc. **218**, 204-212 (2003)

[1] To whom correspondence should be sent.

4. ANALYSIS OF THE ν_2, ν_4 INFRARED HOT BANDS AND ν_1 CARS SPECTRUM OF $^{34}S^{16}O_3$

4.1. ABSTRACT

High resolution (0.0015 cm^{-1}) infrared spectroscopy has been used to study the $^{34}S^{16}O_3$ IR-active hot bands originating from the ν_2 and ν_4 bending mode levels and terminating in the states $2\nu_2$ (l=0), $\nu_2+\nu_4$ (l=±1), and $2\nu_4$ (l=0, ±2). The upper states are strongly coupled via Fermi resonance and indirect Coriolis interactions to the ν_1 symmetric stretching mode levels that are only directly accessible from the ground state via a Raman-active transition. A Coherent anti-Stokes Raman (CARS) spectrum of ν_1 for $^{34}S^{16}O_3$ is presented which is dramatically different from the corresponding one for $^{32}S^{16}O_3$. From the infrared transitions, accurate rovibrational constants are deduced for all the mixed states, leading to deperturbed values for ν_1, α_1^B, and α_1^C of 1064.920(84), 0.000 834 5(54), and 0.000 410(11) cm^{-1} respectively. The uncertainties in the last digits are shown in parentheses and represent two standard deviations. These parameters reproduce the unresolved Q-branch contour of the CARS spectrum very well. Various other rotational and vibrational parameters have been determined, leading to values of B_e = 0.349 760 6(33) cm^{-1} and r_e = 141.734 70(68) pm, values that are identical (within experimental error) to those found for $^{32}S^{16}O_3$.

4.2. INTRODUCTION

Sulfur trioxide has been the subject of a number of infrared and coherent Raman studies by us and by others (*1-8*). Recently, we reported the analysis of the high resolution spectra of $^{32}S^{16}O_3$, a case that proved challenging because of extensive mixing of some of the vibrational levels due to

Fermi resonance and Coriolis interactions (*8*). From this analysis, accurate rovibrational constants were obtained for all four fundamental modes, including ν_1, the Raman active symmetric stretch, and for a number of combination/overtone levels. Using only information available from infrared active transitions, we were able to simulate the complex and irregular ν_1 coherent anti-Stokes Raman (CARS) spectrum with remarkable accuracy (*8*).

No high resolution IR or Raman data have been reported previously for any ^{34}S- or ^{18}O-substituted form of SO_3, a situation we are correcting. Our interest in $^{34}S^{16}O_3$ was spurred in part by the ν_1 complexity seen in the case of $^{32}S^{16}O_3$. Fig. 4.1 compares ν_1 CARS spectra for the $^{32}S^{16}O_3$ and $^{34}S^{16}O_3$ isotopomers. Substitution at the center of mass for this symmetric stretching mode should leave the band center and rotational constants virtually unchanged but, clearly, the spectra of these two isotopomers are very different. Upon ^{34}S substitution, the *Q*-branch is lowered by approximately 0.7 cm^{-1} and the distinct rotational *K*-band structure seen in the case of $^{32}S^{16}O_3$ has coalesced into a "lumpy' *Q*-branch of about 0.3 cm^{-1} width. These differences seemed likely to be a consequence of subtle mass effects on the ν_1 level interactions and, in light of the successful analysis made on these interactions in $^{32}S^{16}O_3$ (*8*), we undertook a similar treatment for $^{34}S^{16}O_3$.

We have now completed the analysis of all four fundamental modes of the ^{34}S-substituted isotopomer of sulfur trioxide. A paper on the ν_3 and $2\nu_3$ transitions is in preparation, and very recently we reported the rovibrational constants for the ground state and the ν_2 and ν_4 levels of $^{34}S^{16}O_3$ (*9*). Buried in the ν_2 and ν_4 spectral region, we have identified transitions corresponding to the hot bands 02^00^0–01^00^0, 01^01^1–01^00^0, 01^01^1–00^01^1, 00^02^0–00^01^1, and 00^02^2–00^01^1. Here, we present accurate rovibrational constants for these upper states and, indirectly from the subtle interactions that exist between these upper levels and the ν_1 levels, the parameters responsible for the ν_1 CARS band of Fig. 4.1. These parameters are compared with those obtained for the parent isotopomer and also with those from an *ab initio* calculation (*10*).

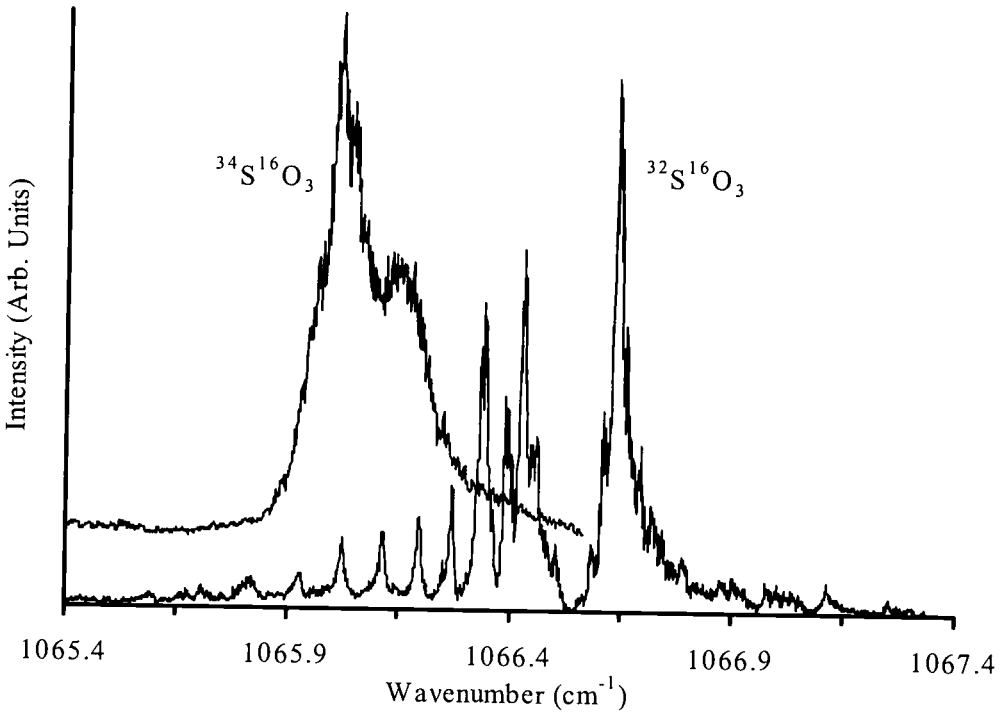

Figure 4.1. The CARS spectra of ν_1 for $^{32}S^{16}O_3$ and $^{34}S^{16}O_3$

4.3. EXPERIMENTAL DETAILS

The equipment and procedures used in these experiments are described in Ref. (*9*). The $^{34}S^{16}O_3$ sample was prepared by oxidation of elemental ^{34}S (99.8 %, Cambridge Isotope Laboratories[2]) in excess gaseous $^{16}O_2$ in the presence of Pt foil at 450°C (Contact process). The remaining O_2 and some SO_2 were removed via vacuum distillation. Our spectra showed a ^{32}S isotopic content of about 10 %, presumably as a result exchange on the walls of the manifold and absorption cell that had previously held a sample of $^{32}S^{16}O_3$. The final spectra were recorded at 25.0 °C at a pressure of 0.47 kPa (3.5 torr) using a gold-plated cell of 19.95 cm length that was fitted with AgCl windows. The wavenumber calibration was performed in the same way for $^{34}S^{16}O_3$ as described in our earlier paper (*7*) and it is estimated that the absolute accuracy of the wavenumber shifts for the different isotopomers is on the order of $\pm 0.000\ 15\ cm^{-1}$.

The CARS spectrum was measured on the coherent Raman apparatus at Oregon State University, which was described in Ref. (*11*). Details related to the recording of the CARS spectrum are given in Ref. (*6*) and the CARS spectrum of the ν_1 region for $^{34}S^{16}O_3$ is given in Figure 4.1. It should be noted that the spectrum consists only of *Q*-branch transitions and that, despite an instrumental resolution of about 0.001 cm^{-1}, no rotational structure is resolved. Nonetheless, as in the case of $^{32}S^{16}O_3$ (*8*), the CARS spectrum served as a important guide in locating the region of interacting levels and in making assignments. We emphasize however that only well-resolved infrared hot-band transitions were used in the least-squares fitting that gave the constants for ν_1.

---

[2] Certain commercial equipment, instruments, and materials are identified in the paper to adequately specify the experimental procedure. Such identification does not imply recommendations or endorsements by the National Institute of Standards and Technology, the National Science Foundation, or the Pacific Northwest National Laboratory (PNNL), nor does it imply that the materials or equipment identified are necessarily the best available for the purpose.

4.4. RESULTS

Figure 4.2 shows the experimental spectrum (top) for the ν_2 and ν_4 region of $^{34}S^{16}O_3$ and about 5700 features resolved in this trace have been assigned to ν_2 or ν_4 transitions (*9*). After also accounting for those features due to $^{32}S^{16}O_3$, it was possible to identify and assign an additional 1743 lines to the hot bands $2\nu_2-\nu_2$, $(\nu_2+\nu_4)-\nu_2$, $(\nu_2+\nu_4)-\nu_4$, $2\nu_4(l=0)-\nu_4$, $2\nu_4(l=2)-\nu_4$. The bands calculated for these are shown in the lower traces of the figure, with the intensities based on appropriate Boltzmann and line strength factors but not adjusted for intensity perturbations caused by state mixing. In the analogous case of $^{32}S^{16}O_3$ it was also possible to identify a number of $\nu_1-\nu_4$ hot band transitions but for $^{34}S^{16}O_3$ these were less intense and hence deduction of the ν_1 levels was achieved indirectly through small perturbations seen in the other hot band lines of Fig. 4.2. A listing of all observed and calculated transitions assigned in the ν_2 and ν_4 region, along with intensities and deduced molecular parameters is provided in a supplementary file provided in Ref. (*9*).

4.5. ANALYSIS OF SPECTRA

Since the lower states of the hot-band transitions were either ν_2 or ν_4, the least-squares analysis included all the transitions reported in our earlier paper (*9*) as well as those involving the states ν_3 and $2\nu_3$ (parameters for the latter states will be reported in a future publication). The remaining part of this section is concerned with the fit of the upper states of the hot-band transitions, the fit of the lower states having been described in Ref. (*9*).

The data were fit to a Hamiltonian matrix that included the following vibrational energy levels: 100^00^0, 000^02^0, 020^00^0, 000^02^2, and 010^01^1. The form of this is given in Ref. (*7*); generally,

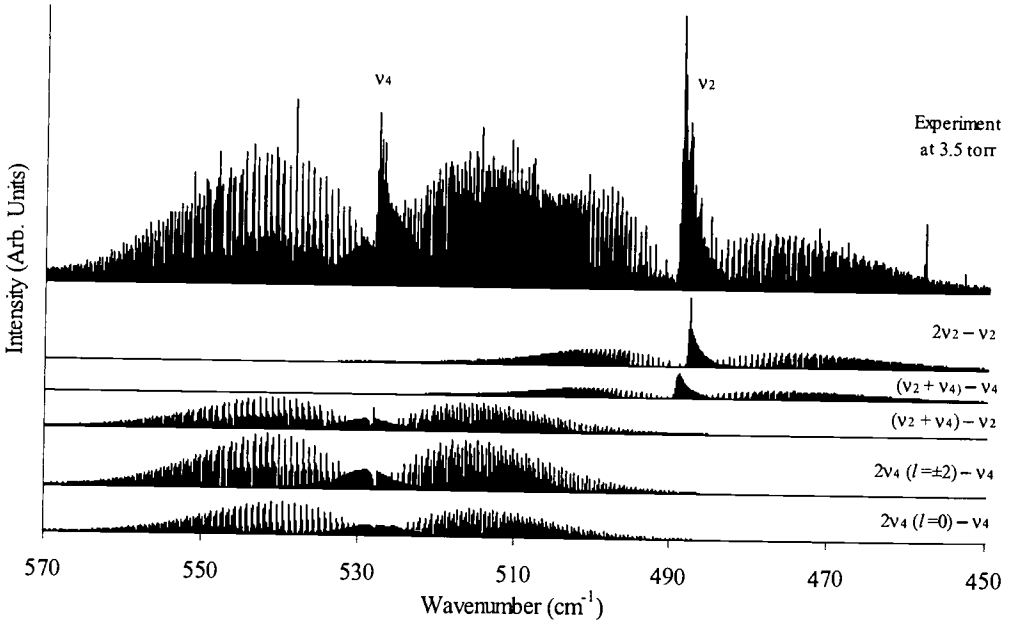

Figure 4.2. Infrared spectrum of the ν_2, ν_4 region of $^{34}S^{16}O_3$ (top) and calculated spectra of hot bands involving the ν_1-perturbing states. Calculated spectra are approximately at the correct relative intensities.

with the exception of a few low J levels, the matrix contained a minimum of seven rows and seven columns for each value of J.

The diagonal elements of the Hamiltonian matrix take the standard form

$$\begin{aligned} E(v, J, k, l) = G(v, l) + B_v J(J+1) + (C_v - B_v)\, k^2 - 2(C\zeta_v)kl + \eta_v^J J(J+1)kl \\ + \eta_v^K k^3 l - D^J_v J^2(J+1)^2 - D^{JK}_v J(J+1)k^2 - D^K_v k^4 \\ + H^J_v J^3(J+1)^3 + H^{JK}_v J^2(J+1)^2 k^2 + H^{KJ}_v J(J+1)k^4 \\ + H^K_v k^6 + \text{splitting terms.} \end{aligned} \quad [1]$$

Here we use the convention that lower case k and $l = l_4$ are signed quantities and much of the discussion in this paper gives the sign of l on the assumption that k is positive. Using Eq. [1] the band origins are given by

$$\nu_0 = G(v, l)' - G(v, l)''. \quad [2]$$

In Table 4.1 we give the $2\nu_2$, $\nu_2+\nu_4$, and $2\nu_4$ vibrational energy levels in wavenumbers with respect to a zero ground state so that $G(0,0) = 0$. The splitting terms were the same as described in Ref. (*7*); as an example, the splitting of the $K = 2$ levels of ν_4 is given by

$$\pm\delta_{2K}\, t_4\, [J(J+1)][J(J+1)-2] \quad [3]$$

The off-diagonal matrix elements (*8*) represent interactions of three types: vibrational (Fermi-resonances), Coriolis between vibrational states, and Coriolis within a vibrational state (l-resonances). The vibrational off-diagonal matrix elements were:

$$W_{144} = \langle \nu_1, \nu_4, J, k, l \,|H|\, \nu_1 + 1, \nu_4 - 2, J, k, l \rangle = k_{144} + k^J_{144}\, J(J+1) + k^K_{144}\, k^2 \quad [4]$$

and

$$W_{122} = \langle \nu_1, \nu_2, J, k, l \,|H|\, \nu_1 + 1, \nu_2 - 2, J, k, l \rangle = k_{122} + k^J_{122}\, J(J+1). \quad [5]$$

The Coriolis terms that coupled states with different vibrational quantum numbers were the same terms that coupled ν_2 with ν_4, namely:

$$\begin{aligned} W_{l,l} &= \langle \nu_2, \nu_4, J, k \pm 1, l_4 \pm 1 \,|H|\, \nu_2 + 1, \nu_4 - 1, J, k, l_4 \rangle \\ &= \pm[(B\zeta_{24}) + z_{24J}\, J(J+1) + z_{24K}\, k(k\pm1)]\, [(\nu_2+1)(\nu_4 \pm l_4 + 1)]^{1/2}\, [J(J+1) - k(k\pm1)]^{1/2} \end{aligned} \quad [6]$$

Two types of Coriolis terms were included to couple different k and l levels within a vibrational state;

$$W_{2,2} = \langle v_4 \neq 0, J, k, l_4 \,|H|\, v_4, J, k \pm 2, l_4 \pm 2\rangle$$

$$= \tfrac{1}{4} q_4 \{[(v_4 + 1)^2 - (l_4 \pm 1)^2][J(J+1) - k(k \pm 1)][J(J+1) - (k \pm 1)(k \pm 2)]\}^{1/2}, \quad [7]$$

$$W_{2,-4} = \langle v_4 = 2, J, k, l_4 \,|H|\, v_4 = 2, J, k \pm 2, l_4 \mp 4\rangle$$

$$= \tfrac{1}{2} Q_4 \{[J(J+1) - k(k \pm 1)][J(J+1) - (k \pm 1)(k \pm 2)]\}^{1/2}, \quad [8]$$

As in our earlier papers (*7-9*), the off-diagonal Coriolis matrix elements are labeled so that the first subscript indicates the Δk and the second subscript indicates the Δl of the coupling.

The observed transition wavenumbers were fit with a non-linear least-squares program that combined all of the present measurements on $^{34}S^{16}O_3$. Since the data set was not as extensive as that of the parent isotopomer, an exactly equivalent set of parameters could not be determined and some assumptions were made. The ΔD terms for ν_1 all had large uncertainties in our initial fit, so these differences were fixed to those determined for $^{32}S^{16}O_3$. The same assumption was made for the ΔD and ΔH_J terms for $2\nu_2$, $2\nu_4$, and $\nu_2 + \nu_4$ states. The other ΔH terms for these hot band levels were fixed at appropriate combinations of the ΔH terms found for ν_2 and ν_4, e.g. $\Delta H_{JK}(2\nu_2) = 2\,\Delta H_{JK}(\nu_2)$, etc.. For ν_1 all the ΔH terms were set to zero because the fit was insensitive to them. Table 4.1 gives the constants determined from the analysis of all the hot-band transitions, except that the parameters for ν_1 are listed in Table 4.2. In both tables we give the changes in the constants from the ground state values so that, for instance, $\Delta D_v^J = D_v^J - D_0^J$.

Table 4.1. The Rovibrational Constants in cm^{-1} for the ν_2, ν_4 States Involved in This Work on the Fundamentals and Hot Bands of $^{34}S^{16}O_3$

constant	ν_2	$2\nu_2$	$\nu_2+\nu_4$	ν_4	$2\nu_4(l=0)$	$2\nu_4(l=2)$
ν_0	488.799 189(17)[a]	977.584(86)	1016.732 783(65)	527.681 547(13)	1055.001 1(71)	1055.636 902(65)
$\Delta C^b \times 10^3$	0.125 693(114)	0.249 42(150)	–0.036 99(144)	–0.161 791(59)	–0.324 881(576)	[–0.324 881]
$\Delta B \times 10^3$	0.769 1(221)	1.525(239)	0.685 0(626)	–0.063 1(110)	–0.112(120)	[–0.112]
$\Delta D_J \times 10^{10}$	19.10(34)	{44.5}[c]	{20.8}	10.33(25)	{21.2}	[21.2]
$\Delta D_{JK} \times 10^{10}$	–25.05(123)	{–63.2}	{–41.7}	–37.29(70)	{–75.3}	[–75.3]
$\Delta D_K \times 10^{10}$	7.28(111)	{21.4}	{22.6}	27.47(57)	{55.2}	[55.2]
$\Delta H_J \times 10^{13}$	{–0.67}	[–1.34][d]	[–0.150]	{0.52}	[1.04]	[1.04]
$\Delta H_{JK} \times 10^{13}$	2.52(34)	[5.04]	[0.45]	–2.07(18)	[–4.15]	[–4.15]
$\Delta H_{KJ} \times 10^{13}$	–3.12(59)	[–6.24]	[–0.39]	2.73(32)	[5.47]	[5.47]
$\Delta H_K \times 10^{13}$	1.27(28)	[2.55]	[0.11]	–1.168(151)	[–2.34]	[–2.34]
$(C\zeta_4)$			–0.081 623(90)	–0.082 001 1(53)		–0.081 828 7(295)
$\eta_J \times 10^7$			–7.99(278)	–8.33(54)		–8.04(294)
$\eta_K \times 10^7$			7.61(277)	7.95(54)		7.65(294)
$q \times 10^4$			4.30(121)	4.307(221)	4.11(121)	
$(B\zeta_{24})$		0.207 15(283)[e]		0.207 06(52)	0.207 14(285)[f]	
$z_{24J} \times 10^7$		–5.08(73)[e]		–4.848(127)	–4.611(695)[f]	
$z_{24K} \times 10^7$		3.66(24)[e]		3.437(29)	3.333(224)[f]	
$t_4 \times 10^{11}$				11.8(17)		
$Q_4 \times 10^6$						{–3.72}
Number of transitions	1743	449	443	2437	243	401
RMS deviation	0.00013 cm^{-1}	0.00017 cm^{-1}	0.00017 cm^{-1}	0.00011 cm^{-1}	0.00021 cm^{-1}	0.00016 cm^{-1}

[a] The uncertainties are two standard deviations. They refer to the last digits and are shown in parentheses. Values in brackets are assumed.
[b] $\Delta C = C' - C_0$, $\Delta B = B' - B_0$, *etc.*
[c] Constants enclosed in {brackets} were fixed to the same value as for $^{32}S^{16}O_3$.
[d] Constants enclosed in [brackets] were fixed to the appropriate combination of values from the ν_2/ν_4 fundamentals.
[e] Contained in the $W_{1,1}$ term for $\nu_2+\nu_4$ interacting with $2\nu_2$.
[f] Contained in the $W_{1,1}$ term for $\nu_2+\nu_4$ interacting with $2\nu_4(l=0)$ and $2\nu_4(l=2)$.

Table 4.2. The Rovibrational Constants in cm^{-1} for ν_1

constant	$^{32}S^{16}O_3$[a]	$^{34}S^{16}O_3$
ν_0	1064.924(11)[b]	1064.920(84)
ΔC[c] $\times 10^3$	−0.418 19(58)	−0.410 40(1123)
$\Delta B \times 10^3$	−0.840 93(64)	−0.834 47(539)
$\Delta D_J \times 10^{10}$	28.5(37)	{28.5}[d]
$\Delta D_{JK} \times 10^{10}$	−54.1(74)	{−54.1}
$\Delta D_K \times 10^{10}$	25.1(41)	{25.1}

[a] From Ref. (*8*)

[b] The uncertainties are two standard deviations. They refer to the last digits and are shown in parentheses.

[c] $\Delta C = C' - C_0$, $\Delta B = B' - B_0$, *etc*

[d] Constants enclosed in {brackets} were fixed to the same value as for $^{32}S^{16}O_3$.

4.6. DISCUSSION

4.6.1. The Rovibrational Constants for the ν_2/ν_4 Hot Bands

Table 4.1 lists the ν_2/ν_4 rovibrational parameters deduced from a global fit of all transitions observed for $^{34}S^{16}O_3$, including hot band transitions mentioned above. An analogous list of values for $^{32}S^{16}O_3$ can be found in Table 4.1 of Ref. (*8*). Not surprisingly, the ν_2/ν_4 parameters are very similar for the two isotopomers, although the standard errors are generally several times larger in the present case due to the reduced number (79 %) of fitted transitions. As expected, the values for ν_0, ΔB, and ΔC for the various hot bands are decreased slightly due to the increased mass upon substitution of ^{32}S with ^{34}S. The ν_0 values permit evaluation of some of the anharmonicity constants, as discussed below.

It is noteworthy that the values of ΔB and ΔC for the $2\nu_2$, $2\nu_4$ overtone levels are very nearly twice the corresponding values for the ν_2, ν_4 levels; in most cases, within the uncertainties, the ratio may be taken to be exactly two. Similarly, the ΔB and ΔC values determined for the $\nu_2+\nu_4$ state are within 3 % of the sum of ν_2, ν_4 values. Similar results were obtained for $^{32}S^{16}O_3$ and it is seen from these and other overtone results that, when the data do not permit determination of all parameters, it is quite a good approximation to simply fix the ΔB and ΔC values of overtone/combinational levels at appropriate combinations of the values determined for fundamental transitions.

The $(C\zeta_4)$ and $(B\zeta_{24})$ Coriolis terms for the two molecules are interesting. Here the effect of vibrational quantum number has been removed and, for the 0001 state, we are using the usual convention that for the ΔK=+1 transitions the product kl used in Eq. (1) is positive and for ΔK=−1 the product is negative. However, for the 0002 state the reverse is the case. The constants should be nearly identical for different levels and indeed it is seen that $(C\zeta_4)$ is nearly constant at an average value of −0.818 cm^{-1} for the degenerate levels ν_4, $2\nu_4$, and $\nu_2+\nu_4$. This value is slightly

smaller in magnitude than the corresponding average of –0.850 cm^{-1} observed for $^{32}S^{16}O_3$. Assuming the same $^{32}S^{16}O_3$ value of $C = C_e$ for both isotopomers we obtain ζ_4 values of –0.468 and –0.486 respectively. These results compare well with ζ_4 values of –0.452 and –0.471 calculated using the observed vibrational frequencies for $^{34}S^{16}O_3$ and $^{32}S^{16}O_3$ in the harmonic force field program ASYM 40 (*12*).

For the ν_2/ν_4 interaction constant ($B\zeta_{24}$), it is seen in Table 4.1 that this value is also virtually identical for all the interacting states. It is interesting that the average ($B\zeta_{24}$) for the 34-16 isotopomer, 0.2071 cm^{-1}, is actually larger than the corresponding average, 0.2008 cm^{-1}, for $^{32}S^{16}O_3$. This indicates that the ζ_{24} term increases somewhat on ^{34}S substitution. In fact, this behavior is predicted by the force field calculations, the values of ζ_{24} being +0.5234 and +0.5143 for $^{34}S^{16}O_3$ and $^{32}S^{16}O_3$, respectively. We note that the signs of both ζ_4 and ζ_{24} depend upon the symmetry coordinate definition, for which we adopt the convention of Dorney, Hoy and Mills *(13)*. As discussed in Ref. (*9*), intensity considerations confirm a positive sign for ζ_{24}.

Finally, we note that the values of the small J and K corrections to the various parameters show a pleasing consistency and similarity, as does the value of the off-diagonal coupling constant q. In the case of $2\nu_4(l=2)$, the value of the term Q_4 in the $W_{2,-4}$ matrix element could not be determined for $^{34}S^{16}O_3$, so it was set equal to the value of $^{32}S^{16}O_3$.

4.6.2. The ν_1 Constants and the Calculated CARS Spectrum

Upon isotopic substitution at the center of mass, the frequency of ν_1 is expected to remain constant since the symmetric stretch does not involve movement of the center of mass. However, since the levels of ν_1 interact with those of the hot bands of ν_2 and ν_4, both of which do have a component of sulfur motion, these latter levels are expected to be further away from the ν_1 levels for $^{34}S^{16}O_3$ than for $^{32}S^{16}O_3$. For example, the $2\nu_2$ and $2\nu_4$ ($l=0$) levels that have a direct Fermi-resonance interaction with ν_1 drop in frequency by 17.4 cm^{-1} and 4.8 cm^{-1} respectively. This

change in energy for the perturbing bands is the major cause of the rotational structure changes that are seen in the CARS spectrum of $^{34}S^{16}O_3$.

Because of state mixing, the infrared hot band studies of the $2\nu_2$, $2\nu_4$ and $\nu_2+\nu_4$ levels give information about the "hidden" ν_1 levels that determine the CARS spectrum. Figure 4.3 shows a reduced energy diagram for the case of $^{34}S^{16}O_3$ and an analogous display for $^{32}S^{16}O_3$ is given in Fig. 6 in Ref. (*8*). The reduced energy is the difference $E'(J,K) - E''(J,K)$ and hence can be compared directly with the Q-branch feature seen in the CARS spectrum. The display shows the energy variation as a function of J for the various $K-l$ bands of the interacting states. Although included in the fitting, the levels for $2\nu_2$ and $\nu_2+\nu_4$ are not displayed since they are at lower reduced energy and do not show the interesting avoided crossings that are apparent in the region near 1064 cm^{-1} in Figure 4.3.

For the case of $^{32}S^{16}O_3$ (*8*), the most important avoided crossings were found to occur in the $K-l=15$ series. Due to population factors, this value of $K-l$ contributes appreciably to the more intense portion of the ν_1 spectrum and the strong perturbations were very evident in the K subband structure. For $^{34}S^{16}O_3$, the corresponding avoided crossings are found to occur at a much higher $K-l$ value of 27. This is a consequence of the fact that the perturbing state, $2\nu_4$ ($l=-2$), is lower than for the parent isotopomer by 4.8 cm^{-1}. Since ν_1 for $^{34}S^{16}O_3$ is relatively unperturbed for the lower values of J and K, we see a concentration of these levels in a much smaller energy range, leading to the CARS spectrum about a quarter of the width seen for $^{32}S^{16}O_3$.

A detailed view of the level structure in the 1066 cm^{-1} region is displayed (horizontally) at the bottom of Fig. 4.4 to show how the level pattern leads to the Q-branch pattern seen in the CARS spectrum (top). An analogous display for $^{32}S^{16}O_3$ is given in Fig. 7 in Ref. (*8*) and in both cases, levels denoted by a + symbol are ones that contribute a CARS intensity equal to at least 10 % of that of the transition of maximum intensity. Also included for illustrative purposes are the calculated stick spectra for the ν_1 mode for K = 0, 24, and 27 subband sequences with $J=K$, $K+1$, $K+2$, ... In each case, the Q-branch transition for $J=K$ is indicated with an arrow. The $K=0$ series (Fig. 4.4e)

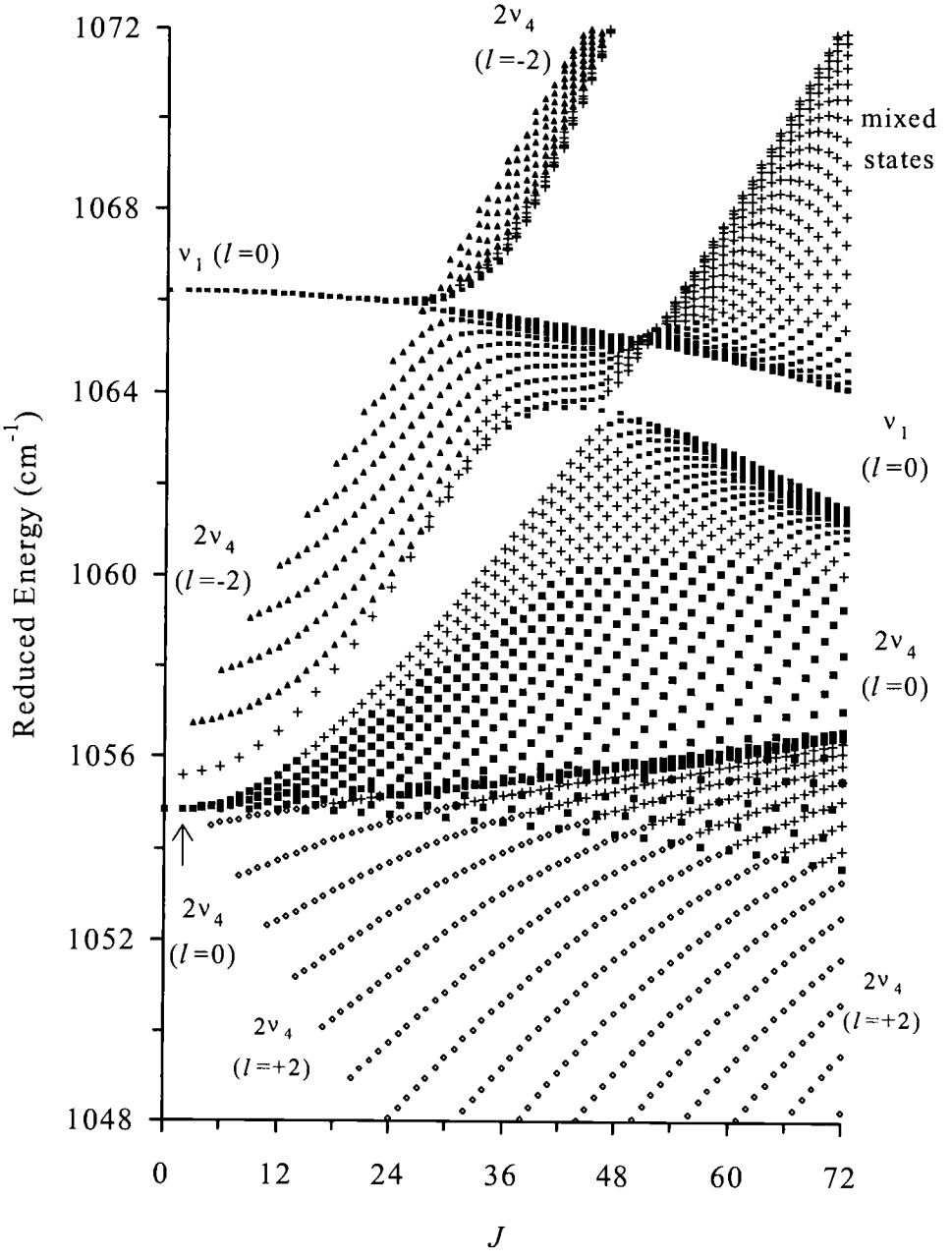

Figure 4.3. Reduced energy diagram of Q-branch transitions from the ground state of $^{34}S^{16}O_3$ to ν_1 and its perturbing states. States identified as ν_1 (—), $2\nu_4$ (l=-2) (▲), $2\nu_4$ (l=0) (■), and $2\nu_4$ (l=+2) (◊) are at least 50 % of the identified state. States that do not have any component greater than 50 % are denoted as mixed states (+).

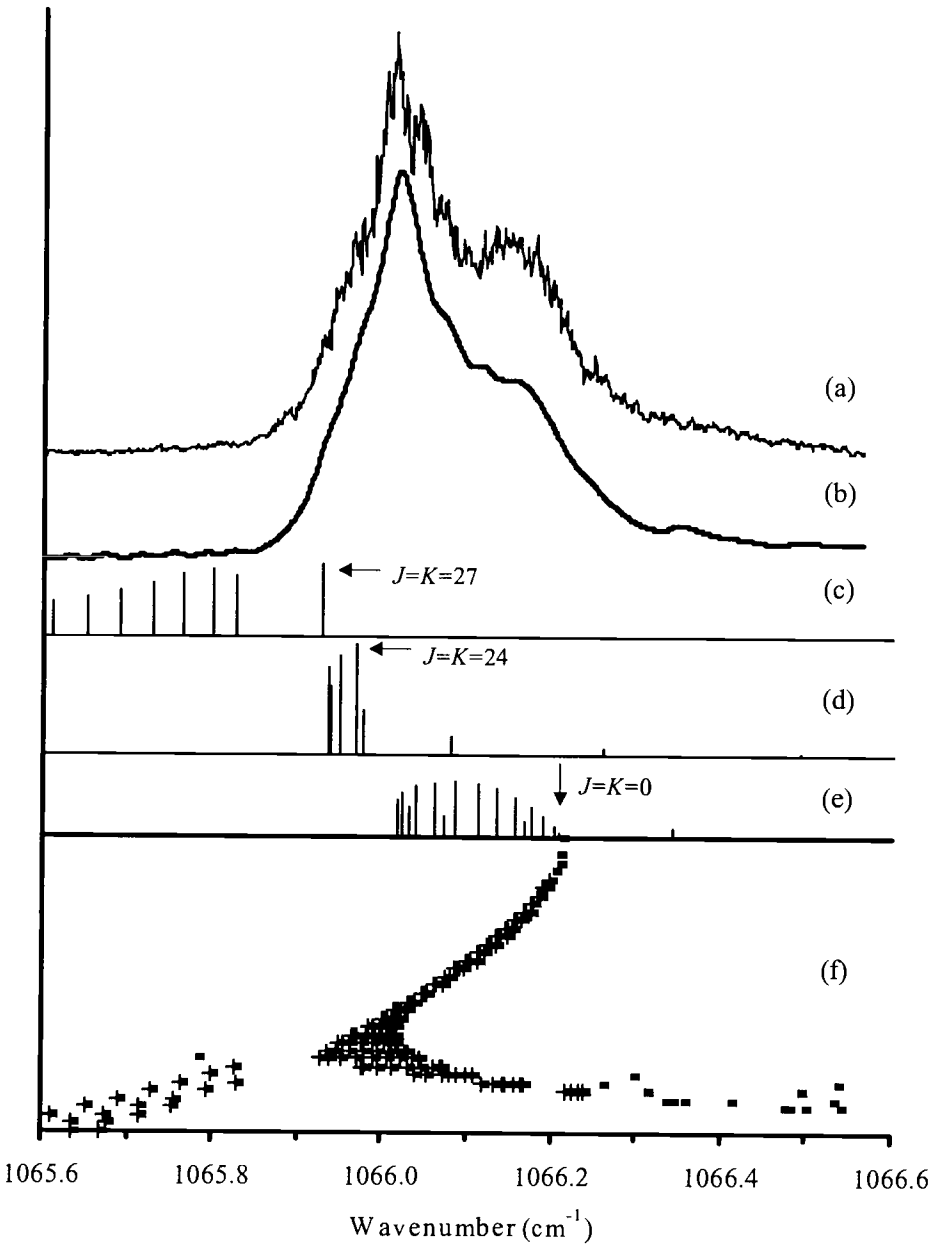

Figure 4.4. Experimental and calculated CARS spectra for $^{34}S^{16}O_3$ (a-b), along with an expanded view of Figure 4.3 showing the level pattern (f) to illustrate how this pattern contributes to the appearance of the spectrum. Those levels with 10% or greater of the maximum intensity are designated with a +. Stick spectra for K=27, 24, and 0 are included showing the level pattern for these K subbands to illustrate the role of perturbations on the spectrum (c-e). The start of each sequence (J=K) is indicated with an arrow.

begins at 1066.21 cm^{-1}, reaches a band head at J=24 and then reverses to higher energy, with J=32 at 1066.34 cm^{-1} being the last transition displayed. Similar band heads are seen for other K series; that for K=24 is shown as the middle stick spectrum (d). However at K=27 (Fig. 4.4c), the avoided crossing occurs, and instead of a band head, there is a dramatic negative jump of 0.1 cm^{-1} in going from the first line (J=27) to the J=28 feature at lower cm^{-1}. The spacing of the higher J lines then increases, spreading the intensity so that the distinct K subband structure seen for $^{32}S^{16}O_3$ at high K values is not apparent for the 34 isotopomer.

It is thus seen that the band heads of the low K series overlap to produce the narrow, lumpy Q-branch contour seen in the CARS spectrum. This pattern is well reproduced by the calculated CARS spectrum shown below the experimental trace at the top of Fig. 4.4. The corresponding parameters deduced for ν_1 (using only infrared transitions) are given in Table 4.2. We note that only 26 of the infrared transitions were to upper states that contained at least 10 % ν_1 character; in contrast over 400 such transitions were identified for $^{32}S^{16}O_3$. The consequence is that, even after fixing the ΔD terms at those for $^{32}S^{16}O_3$, the uncertainties in ν_1, ΔB and ΔC are almost an order of magnitude larger than those for $^{32}S^{16}O_3$. Nonetheless, it is pleasing that the ν_1 values for the symmetric stretching mode are found to be identical when all perturbations are accounted for. Within their uncertainties, the ΔB_1 and ΔC_1 values are also identical for both isotopomers and in each case ΔB_1 is very close to twice ΔC_1. Both constants are negative, corresponding to a decrease in the rotational constant and an increase in the average SO bond length when the symmetric stretch is excited.

4.6.3. The Anharmonic Constants for $^{34}S^{16}O_3$

The Fermi resonance coupling terms k_{122} and k_{144} that couple the ν_1 levels to the other states are given in Table 4.3, along with some of the other anharmonicity parameters deduced from overtone and combination levels. The consequence of neglecting the Fermi resonance terms is quite evident in the calculated CARS spectra shown in Figure 4.5. Clearly, all coupling terms must be included for a proper simulation of the observed spectra and an accurate determination of the

Table 4.3. Vibrational Constants in cm^{-1} for $^{32}S^{16}O_3$ and $^{34}S^{16}O_3$

	$^{32}S^{16}O_3$		$^{34}S^{16}O_3$	
constant	Ref. (*8*)	Ref. (*10*)	This work	Ref. (*10*)
x_{22}	−0.058 7(62)[a]	0.078[b]	−0.007 2(431)	0.075
x_{33}	−5.451 2(42)	−5.428	−5.279 9(4)	−5.263
x_{44}	−0.019 75(28)	−0.011	−0.022 04(177)	−0.007
x_{24}	0.248 197(20)	0.282	0.252 047(66)	0.284
x^{33}	2.866 7(42)	2.815	2.751 2(4)	2.699
x^{44}	0.159 67(28)	0.151	0.158 95(178)	0.143
k_{122}	9.943(44)	11.12	10.023(376)	10.93
$k^J_{122}\times10^5$	−2.51(19)		{−2.51}[c]	
k_{144}	−1.519 0(23)	−1.56	−1.338 3(292)	−1.45
$k^J_{144}\times10^5$	−2.695(91)		−2.990(792)	
$k^K_{144}\times10^5$	2.617(89)		2.890(744)	

[a] The uncertainties are two standard deviations. They refer to the last digits and are shown in parentheses.

[b] Deperturbed value (Private communication, Ref. 10).

[c] Constants enclosed in {brackets} were fixed to the same value as for $^{32}S^{16}O_3$.

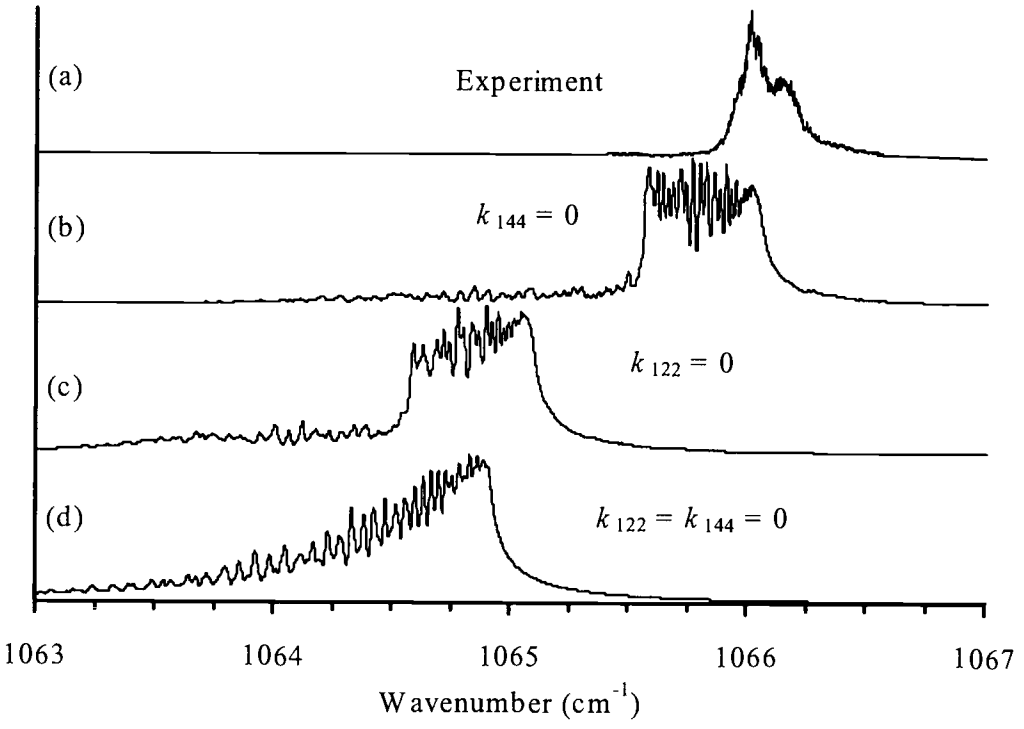

Figure 4.5. Effect on the ν_1 CARS spectrum (a, experimental spectrum) of setting the Fermi resonance constants k_{122} and k_{144} to zero (b-d, calculated spectra).

rovibrational constants. The anharmonic constant k_{122} is found to be nearly constant at 10.0 cm^{-1} for both isotopomers and is about 10 % smaller than *ab initio* values of 10.93 and 11.12 cm^{-1} calculated by Martin (*10*) for 34 and 32 forms respectively. The k_{144} constant is considerably smaller than k_{122} and the values for both isotopomers are closer to the corresponding *ab initio* values. It should be noted that the mass dependence of these "potential constants" comes from the fact that the corresponding cubic terms are written in terms of mass-weighted normal coordinates; if written in terms of internal coordinates, the potential is expected to be isotopically invariant.

Table 4.3 lists the x_{ii} anharmonicity parameters determined in our $^{34}S^{16}O_3$ studies and most are quite similar to those obtained for $^{32}S^{16}O_3$. Unfortunately we were not able to determine a reliable value for x_{22} for $^{34}S^{16}O_3$, but it might be noted that x_{33} and x^{33} are better determined than in the case of $^{32}S^{16}O_3$. Most of Martin's calculated *ab initio* parameters are in good accord with our experimental values, with x_{44} being a possible exception.

4.6.4. The Rotational Constants and Equilibrium Bond Length for $^{34}S^{16}O_3$

Table 4.4 gives values for the rotational parameters that have been determined for $^{34}S^{16}O_3$, along with those found previously for $^{32}S^{16}O_3$ (*8*). Since parameters for all four fundamentals have been obtained, it is possible to determine the α and γ corrections of the B_0 rotational constant to the equilibrium value in the usual equation

$$B_e = B_v + \sum_i \alpha_i^B (v_i + \tfrac{1}{2}d_i) - \sum_{ij} \gamma_{ij}^B (v_i + \tfrac{1}{2}d_i)(v_j + \tfrac{1}{2}d_j) \qquad [9]$$

A similar relation applies for the C constant but, unlike the case of $^{32}S^{16}O_3$, a microwave determination of C_0 is not available for $^{34}S^{16}O_3$ so C_e cannot be calculated.

The table gives constants obtained from the analysis both with and without the $\gamma_{ij}^{B,C}$ terms. The α and γ constants are quite similar for both 32 and 34 isotopomers but the uncertainties are larger for the latter, particularly for the $\alpha_1^{B,C}$ constants. As noted previously (*8*) the α_2^B and α_4^B constants are strongly correlated, resulting in large apparent uncertainties, but the combination $\frac{1}{2}\alpha_2^B + \alpha_4^B$ is well determined, as is the combination $\frac{1}{4}\gamma_{22} + \gamma_{44} + \frac{1}{2}\gamma_{24}$ for B. This is a fortunate outcome

Table 4.4. Rotational Constants[a] for $^{32}S^{16}O_3$ and $^{34}S^{16}O_3$

	$^{32}S^{16}O_3$[b]		$^{34}S^{16}O_3$	
constant[c]	*C* constants	*C* constants[d]	*C* constants	*C* constants[d]
C_0	0.173 988 13(3)[e]			
$\alpha_1\times10^3$	0.418 19(58)	0.418 19(58)	0.410 40(1123)	0.410 40(1123)
$\alpha_2^*\times10^3$	−0.131 84(42)	−0.127 78(4)	−0.128 55(293)	−0.125 69(11)
$\alpha_3\times10^3$	0.597 48(22)	0.599 25(7)	0.584 15(26)	0.585 61(7)
$\alpha_4^*\times10^3$	0.154 64(21)	0.157 29(3)	0.159 40(157)	0.161 79(6)
$(\frac{1}{2}\alpha_2^*+\alpha_4^*)\times10^3$	0.088 72(33)	0.093 39(4)	0.095 12(303)	0.098 94(11)
$\gamma_{22}\times10^5$	−0.143(21)		−0.098(75)	
$\gamma_{33}\times10^5$	−0.059(6)		−0.049(7)	
$\gamma_{44}\times10^5$	−0.068(4)		−0.065(29)	
$\gamma_{24}\times10^5$	−0.119(20)		−0.090(143)	
$(\frac{1}{4}\gamma_{22}+\gamma_{44}+\frac{1}{2}\gamma_{24})\times10^5$	−0.164(13)		−0.134(119)	
constant[c]	*B* constants	*B* constants[d]	*B* constants	*B* constants[d]
B_0	0.348 543 33(5)[e]		0.348 556 03(28)	
$\alpha_1\times10^3$	0.840 93(64)	0.840 93(64)	0.834 47(539)	0.834 47(539)
$\alpha_2^*\times10^3$	−0.811 44(3854)	−0.803 96(493)	−0.803 66(30382)	−0.769 10(2213)
$\alpha_3\times10^3$	1.127 11(36)	1.130 48(9)	1.109 02(33)	1.112 59(6)
$\alpha_4^*\times10^3$	0.072 52(1902)	0.075 24(245)	0.073 87(15113)	0.063 11(1101)
$(\frac{1}{2}\alpha_2^*+\alpha_4^*)\times10^3$	−0.333 20(34)	−0.326 74(5)	−0.327 96(88)	−0.321 44(7)
$\gamma_{22}\times10^5$	0.417(1513)		−0.678(11963)	
$\gamma_{33}\times10^5$	−0.112(10)		−0.119(10)	
$\gamma_{44}\times10^5$	0.173(747)		0.709(6023)	
$\gamma_{24}\times10^5$	−1.583(762)		−2.100(6256)	
$(\frac{1}{4}\gamma_{22}+\gamma_{44}+\frac{1}{2}\gamma_{24})\times10^5$	−0.514(27)[f]		−0.511(204)	
B_e	0.349 764 0(7)	0.349 767 5(3)	0.349 760 6(33)	0.349 764 4(27)
r_e (pm)[g]	141.734 027(130)	141.733 303(71)	141.734 704(677)	141.733 935(549)
r_0 (pm)[g]	141.981 993(19)		141.979 406(58)	

[a] In cm^{-1} except for r values.

[b] From Ref. (*8*)

[c] The constants followed by an asterisk, *, are the constant with the ν_2/ν_4 Coriolis perturbation removed, the so-called deperturbed constants.

[d] Value calculated without inclusion of γ terms.

[e] The uncertainties are two standard deviations. They refer to the last digits and are shown in parentheses.

[f] The sign for this combination is incorrectly given as + in Ref. (8) but the B_e and r_e values listed there are correct.

[g] The *r* values are calculated using NIST Physical Reference Data values of h = 6.62606876(52) $\times10^{-34}$ J s, N_A = 6.02214199(47) $\times10^{23}$ mol^{-1}, and m(^{16}O) = 15.9949146221(15) amu.

since both these α and γ combinations occur explicitly in correcting the B_0 constant to B_e. Of course, only a partial correction is possible since γ_{11} and other γ_{ij} terms are unknown. In fact, within the uncertainties, the B_e values obtained for $^{34}S^{16}O_3$ are the same regardless of whether or not the γ's are included.

Including γ corrections, the B_e values are 0.349 760 6(33) and 0.349 764 0(6) cm^{-1} respectively for the 34 and 32 isotopomers. These values agree within experimental error and they lead to an average SO bond length of 141.734 4(7) pm. This value is slightly larger than the r_e value 141.733 3(1) pm obtained for $^{32}S^{16}O_3$ from C_e, a difference that can be presumed to arise from the neglected γ terms.

To a very good approximation then, the molecular parameters and potential are unaffected by ^{34}S substitution in SO_3. This is likely a consequence of the fact that substitution is at the center of mass so that more subtle effects such as the neglect of electron-nuclear mass corrections are not apparent. Here the idea is that the electrons lag slightly the vibrational and rotational movement of the nuclei and this leads to small additional corrections to the energy level expressions, as observed in diatomic molecules (*14*). Such effects may be important for the off-axis substitution of ^{18}O for ^{16}O in SO_3 and this will be one aspect examined in forthcoming papers on $^{32}S^{18}O_3$ and $^{34}S^{18}O_3$.

4.7. ACKNOWLEDGEMENTS

We acknowledge support by the National Science Foundation and Oregon State University for the CARS work and analysis performed at OSU. The research described in this paper was performed, in part, in the Environmental Molecular Sciences Laboratory, a national scientific user facility sponsored by the Department of Energy's Office of Biological and Environmental Research and located at Pacific Northwest National Laboratory.

4.8. REFERENCES

1. J.B. Milne and A. Ruoff, *J. Mol. Spectrosc.* 23 (1967) 408-415.

2. A. Kaldor and A.G. Maki, *J. Mol. Struct.* 15 (1973) 123-130.

3. A. Kaldor, A.G. Maki, A.J. Dorney, and I.M. Mills, *J. Mol. Spectrosc.* 45 (1973) 247-252.

4. N.F. Henfrey and B.A. Thrush, *Chem. Phys. Lett.* 102 (1983) 135-138.

5. J. Ortigoso, R. Escribano, and A.G. Maki, *J. Mol. Spectrosc.* 138 (1989) 602-613.

6. E.t.H. Chrysostom, N. Vulpanovici, T. Masiello, J. Barber, J.W. Nibler, A. Weber, A.G. Maki, and T.A. Blake, *J. Mol. Spectrosc.* 210 (2001) 233-239.

7. A. Maki, T.A. Blake, R.L.Sams, N. Vulpanovici, J. Barber, E.t.H. Chrysostom, T. Masiello, J.W. Nibler, and A. Weber, *J. Mol. Spectrosc.* 210 (2001) 240-249.

8. J. Barber, E.t.H. Chrysostom, T. Masiello, J.W. Nibler, A. Maki, A Weber, T.A. Blake and R.L. Sams, *J. Mol. Spectrosc.* 216 (2002) 105-112

9. J. Barber, T. Masiello, E.t.H. Chrysostom, J.W. Nibler, A. Maki, A Weber, T.A. Blake and R.L. Sams, *J. Mol. Spectrosc.* (In press. This reference includes a supplementary file containing all $^{34}S^{16}O_3$ parameters and transitions, including those of the present paper.)

10. J.M.L. Martin, *Spectrochim. Acta. Part A* 55 (2000) 709-718, and private communication.

11. M.L. Orlov, J.F. Ogilvie, and J.W. Nibler, *J. Mol. Spectrosc.* 185 (1997) 128-141.

12. L. Hedberg and I.M. Mills, *J, Mol. Spectrosc.* 160 (1993) 117-142; 203 (2000) 82-95.

13. A.J. Dorney, A.R. Hoy, and I.M. Mills, *J. Mol. Spectrosc.* 45 (1973) 253-260.

14. J. F. Ogilvie, "The Vibrational and Rotational Spectrometry of Diatomic Molecules", Academic press, New York (1998).

5. CONCLUSION

5.1. SUMMARY

In this work, the understanding of the spectroscopy of sulfur trioxide has been furthered. The complex spectrum of the symmetric stretching mode of SO_3, ν_1, has been shown to be due to subtle mixing with the other nearby states of $2\nu_2$, $\nu_2+\nu_4$ and $2\nu_4$. By analyzing infrared-active hot-band transitions to these states from the ν_2 and ν_4 fundamentals, we are able to correctly model the CARS spectrum of ν_1 without the use of any CARS transition values but with the pattern serving as an essential check on the infrared assignments. This has been done successfully for both $^{32}S^{16}O_3$ and $^{34}S^{16}O_3$. With the parameters now available for the first time, parameters for the equilibrium structure of SO_3 can be determined, and it has been shown that the SO bond length is the same for both isotopomers within the uncertainty. Much of the discussion of these results is given in Chapters 2-4, which are copies of papers that have now been published. Below, we offer a few other comparisons of results for the two isotopomers.

Table 5.1 lists the band centers of the bands discussed in this work. The ν_1 band centers for $^{32}S^{16}O_3$ and $^{34}S^{16}O_3$ are identical within the uncertainty of the experiment. This is expected as the isotopic substitution takes place at the center of mass, leaving the motion of the symmetric stretch unchanged. Other band centers show the effects of isotopic substitution by decreasing on replacement of ^{32}S by the heavier ^{34}S atom. Those levels with a component of ν_2 show the greatest decrease as expected since this mode has the greatest amplitude of sulfur motion.

Table 5.2 lists the rotational parameters for the equilibrium and ground states of the two isotopomers. The B_0 values are slightly different for the two isotopomers due to the isotope effect. The C_0 constant has not been determined for $^{34}S^{16}O_3$ but was available for $^{32}S^{16}O_3$ from microwave observations of transitions in centrifugally-distorted states (which have a very small dipole

Table 5.1. Vibrational Band Centers in cm^{-1} for $^{32}S^{16}O_3$ and $^{34}S^{16}O_3$

Band	$^{32}S^{16}O_3$	$^{34}S^{16}O_3$
ν_1	1064.924(11)	1064.920(84)
ν_2	497.567 736(16)	488.799 189(17)
$2\nu_2$	995.018(12)	977.584(86)
$\nu_2+\nu_4$	1027.902 357(21)	1016.732 783(65)
ν_4	530.086 424(14)	527.681 547(13)
$2\nu_4$ (l=0)	1059.814 0(11)	1055.001 1(71)
$2\nu_4$ (l=2)	1060.452 702(28)	1055.636 902(65)

Table 5.2. Rotational Constants[a] for $^{32}S^{16}O_3$ and $^{34}S^{16}O_3$

	$^{32}S^{16}O_3$		$^{34}S^{16}O_3$	
constant[b]	*C* constants	*C* constants[c]	*C* constants	*C* constants[c]
C_0	0.173 988 13(3)[d]			
$\alpha_1\times10^3$	0.418 19(58)	0.418 19(58)	0.410 40(1123)	0.410 40(1123)
$\alpha_2^*\times10^3$	–0.131 84(42)	–0.127 78(4)	–0.128 55(293)	–0.125 69(11)
$\alpha_3\times10^3$	0.597 48(22)	0.599 25(7)	0.584 15(26)	0.585 61(7)
$\alpha_4^*\times10^3$	0.154 64(21)	0.157 29(3)	0.159 40(157)	0.161 79(6)
$(\frac{1}{2}\alpha_2^*+\alpha_4^*)\times10^3$	0.088 72(33)	0.093 39(4)	0.095 12(303)	0.098 94(11)
$\gamma_{22}\times10^5$	–0.143(21)		–0.098(75)	
$\gamma_{33}\times10^5$	–0.059(6)		–0.049(7)	
$\gamma_{44}\times10^5$	–0.068(4)		–0.065(29)	
$\gamma_{24}\times10^5$	–0.119(20)		–0.090(143)	
$(\frac{1}{4}\gamma_{22}+\gamma_{44}+\frac{1}{2}\gamma_{24})\times10^5$	–0.164(13)		–0.134(119)	
constant[c]	*B* constants	*B* constants[c]	*B* constants	*B* constants[c]
B_0	0.348 543 33(5)		0.348 556 03(28)	
$\alpha_1\times10^3$	0.840 93(64)	0.840 93(64)	0.834 47(539)	0.834 47(539)
$\alpha_2^*\times10^3$	–0.811 44(3854)	–0.803 96(493)	–0.803 66(30382)	–0.769 10(2213)
$\alpha_3\times10^3$	1.127 11(36)	1.130 48(9)	1.109 02(33)	1.112 59(6)
$\alpha_4^*\times10^3$	0.072 52(1902)	0.075 24(245)	0.073 87(15113)	0.063 11(1101)
$(\frac{1}{2}\alpha_2^*+\alpha_4^*)\times10^3$	–0.333 20(34)	–0.326 74(5)	–0.327 96(88)	–0.321 44(7)
$\gamma_{22}\times10^5$	0.417(1513)		–0.678(11963)	
$\gamma_{33}\times10^5$	–0.112(10)		–0.119(10)	
$\gamma_{44}\times10^5$	0.173(747)		0.709(6023)	
$\gamma_{24}\times10^5$	–1.583(762)		–2.100(6256)	
$(\frac{1}{4}\gamma_{22}+\gamma_{44}+\frac{1}{2}\gamma_{24})\times10^5$	–0.514(27)		–0.511(204)	
B_e	0.349 764 0(7)	0.349 767 5(3)	0.349 760 6(33)	0.349 764 4(27)
r_e (pm)[e]	141.734 027(130)	141.733 303(71)	141.734 704(677)	141.733 935(549)
r_0 (pm)[e]	141.981 993(19)		141.979 406(58)	

[a] In cm^{-1} except for r values.

[b] The constants followed by an asterisk, *, are the constant with the ν_2/ν_4 Coriolis perturbation removed, the so-called deperturbed constants.

[c] Value calculated without inclusion of γ terms.

[d] The uncertainties are two standard deviations. They refer to the last digits and are shown in parentheses.

[e] The *r* values are calculated using NIST Physical Reference Data values of $h = 6.62606876(52)\times10^{-34}$ J s, $N_A = 6.02214199(47)\times10^{23}$ mol^{-1}, and m(^{16}O) = 15.9949146221(15) amu.

moment). As shown in Eqn. 2.10, the data now available permit extrapolation from B_0 to B_e, the rotational constant of the equilibrium structure. Differences in B_e values when only the α corrections are used indicates that higher order corrections are necessary. When the γ corrections are included, both the B_e and r_e values for the two isotopomers agree within the uncertainty (two standard deviations) given in parentheses.

Additionally, we have analyzed the intensity perturbations that are present in the ν_2, ν_4 fundamentals arising from Coriolis and *l*-resonance interactions. These have been used to determine the relative magnitudes and signs of the dipole derivatives for these modes, again for both isotopomers. Such information is difficult to obtain for most molecules and gives insight into the charge movement in the SO_3 molecules as the atoms move. The average dipole derivative ratio $(\partial\mu^x/\partial Q_{4x})/(\partial\mu^z/\partial Q_2)$ is found to be $\pm 0.62(8)$ for SO_3, and the product $(\zeta^y_{24})(\partial\mu^z/\partial Q_2)(\partial\mu^x/\partial Q_{4x})$ is deduced from the overall band contours to have a positive value. This result indicates that the effective charge movement in the molecular *xz* plane has the same sense of rotation as the atom motion arising from Q_2 and Q_{4x}, producing a p_y vibrational angular momentum component, motion which agrees with charge flow we deduce from *ab initio* calculations. A picture representing this result is given in Fig. 3.4.

Table 5.3 compares the equilibrium bond distances of some selected molecules in pm as compiled in Ref. (*1-2*). The first portion of this table compares the SO bond length for various sulfur oxides. Here, it can be seen that the SO bond distance decreases as additional oxygen atoms are bonded to sulfur, indicating an increase in bond order. As suggested in Ref. (*1*), such a trend can be explained by a contribution of *d*-orbitals on sulfur in the bonding in these molecules. The second portion of the table shows the bond lengths for some nonlinear polyatomics as compiled in Ref. (*2*). The equilibrium bond length for SO_3 determined in this work has a value that is an order of magnitude more certain than those listed in Table 5.3, indicating that SO_3 indeed has one of the most accurately determined configurations of any nonlinear polyatomic molecule.

Table 5.3. Equilibrium Bond Lengths of Selected Molecules.

Molecule	r_e (pm)
SO[a]	148.108 7
SO_2[a]	143.078
SO_3	141.734 0
CH_4[b]	108.70
H_2O[b]	95.843
O_3[b]	127.16
BF_3[b]	130.70

[a]From Ref. (*1*)
[b]From Ref. (*2*)

5.2. REFERENCES

1. E.t.H. Chrysostom, N. Vulpanovici, T. Masiello, J. Barber, J. W. Nibler, A. Weber, A. Maki, and T.A. Blake, *J. Mol. Spectrosc.* **210**, 233-239 (2001).

2. K. Kuchitsu (Ed.), "Structure of Free Polyatomic Molecules – Basic Data", Springer-Verlag, Berlin (1998)

BIBLIOGRAPHY

1. H.C. Allen, Jr. and P.C. Cross, "Molecular Vib-Rotors", John Wiley and Sons, Inc., New York (1963)

2. J. Barber, E.t.H. Chrysostom, T. Masiello, J.W. Nibler, A. Maki, A Weber, T.A. Blake and R.L. Sams, *J. Mol. Spectrosc.* **216**, 105-112 (2002)

3. J. Barber, T. Masiello, E.t.H. Chrysostom, J.W. Nibler, A. Maki, A Weber, T.A. Blake and R.L. Sams, *J. Mol. Spectrosc.* **218**, 197-203 (2003)

4. P.F. Bernath, "Spectra of Atoms and Molecules", Oxford University Press, New York (1995)

5. E.t.H. Chrysostom, "Applications of High Resolution Coherent Anti-Stokes Raman Scattering Spectroscopy", Ph.D. Thesis, Oregon State University (2001)

6. E.t.H. Chrysostom, N. Vulpanovici, T. Masiello, J. Barber, J. W. Nibler, A. Weber, A. Maki, and T.A. Blake, *J. Mol. Spectrosc.* **210**, 233-239 (2001).

7. C. DiLauro and I.M. Mills, *J. Mol. Spectrosc.* **21**, 386-413 (1966).

8. A.J. Dorney, A.R. Hoy, and I.M. Mills, *J. Mol. Spectrosc.* **45**, 253-260 (1973)

9. Gaussian 98, Revision A.9, M. J. Frisch, G. W. Trucks, H. B. Schlegel, G. E. Scuseria, M. A. Robb, J. R. Cheeseman, V. G. Zakrzewski, J. A. Montgomery, Jr., R. E. Stratmann, J. C. Burant, S. Dapprich, J. M. Millam, A. D. Daniels, K. N. Kudin, M. C. Strain, O. Farkas, J. Tomasi, V. Barone, M. Cossi, R. Cammi, B. Mennucci, C. Pomelli, C. Adamo, S. Clifford, J. Ochterski, G. A. Petersson, P. Y. Ayala, Q. Cui, K. Morokuma, D. K. Malick, A. D. Rabuck, K. Raghavachari, J. B. Foresman, J. Cioslowski, J. V. Ortiz, A. G. Baboul, B. B. Stefanov, G. Liu, A. Liashenko, P. Piskorz, I. Komaromi, R. Gomperts, R. L. Martin, D. J. Fox, T. Keith, M. A. Al-Laham, C. Y. Peng, A. Nanayakkara, M. Challacombe, P. M. W. Gill, B. Johnson, W. Chen, M. W. Wong, J. L. Andres, C. Gonzalez, M. Head-Gordon, E. S. Replogle, and J. A. Pople, Gaussian, Inc., Pittsburgh PA, 1998.

10. L. Hedberg and I.M. Mills, *J. Mol. Spectrosc.* **160**, 117-142 (1993); **203**, 82-95 (2000).

11. N.F. Henfrey and B.A. Thrush, *Chem. Phys. Lett.* **102**, 135-138 (1983).

12. L.H. Jones, *Acta. Chem. Scand.* **23**, 335 (1969).

13. A. Kaldor and A.G. Maki, *J. Mol. Struct.* **15**, 123-130 (1973).

14. A. Kaldor, A.G. Maki, A.J. Dorney, and I.M. Mills, *J. Mol. Spectrosc.* **45**, 247-252 (1973)

15. A. Kaldor, A.G. Maki, A.J. Dorney, and I.M. Mills, *J. Mol. Spectrosc.* **45**, 247-252 (1973); N.F. Henfrey and B.A. Thrush, *Chem. Phys. Lett.* **102**, 135-138 (1983).

16. K. Kuchitsu (Ed.), "Structure of Free Polyatomic Molecules – Basic Data", Springer-Verlag, Berlin (1998)

17. A. Maki, T.A. Blake, R.L. Sams, N. Vulpanovici, J. Barber, E.t.H. Chrysostom, T. Masiello, J.W. Nibler, and A. Weber, *J. Mol. Spectrosc.* **210**, 240-249 (2001).

18. J.M.L. Martin, *Spectrochim. Acta Part A* **55**, 709-718 (2000), and private communication.

19. V. Meyer, D.H. Sutter, and H. Dreizler, *Z. Naturforsch. A* **46**, 710-714 (1991).

20. J.B. Milne and A. Ruoff, *J. Mol. Spectrosc.* **23**, 408-415 (1967).

21. J. F. Ogilvie, "The Vibrational and Rotational Spectrometry of Diatomic Molecules", Academic Press, New York (1998).

22. M.L. Orlov, J.F. Ogilvie, and J.W. Nibler, *J. Mol. Spectrosc.* **185**, 128-141 (1997).

23. J. Ortigoso, R. Escribano, and A.G. Maki, *J. Mol. Spectrosc.* **138**, 602-613 (1989).

24. D. Papoušek and M.R. Aliev, "Molecular Vibrational-Rotational Spectra", Elsevier Scientific Publishing Company, Amsterdam (1982)

25. S.-Y. Tang and C.W. Brown, *J. Mol. Spectrosc.* **3**, 387-390 (1975)

26. S.X. Weng, O.S. Binbrek, and A. Anderson, *Spectrosc. Lett.* **24**, 959-973 (1991).

27. E.B. Wilson, Jr., J.C. Decius, and P.C. Cross, "Molecular Vibrations", Dover Publications, Inc., New York (1980)